Computational Fluid Flow Analysis of the Enhanced-Once through Steam generator Auxiliary feedwater system

Vivek Sethapati

Thesis submitted to the faculty of the Virginia Polytechnic Institute and State University in partial fulfillment of the requirements for the degree of

Master of Science
In
Mechanical Engineering

Danesh K. Tafti – Chair
Pavlos P. Vlachos
Francine Battaglia

May 2nd, 2011
Blacksburg, Virginia

Keywords: Leakage flow, Loss coefficient, Auxiliary feedwater, TSP, Bypass flow, Broached holes, OTSG, EOTSG

Computational Fluid Flow Analysis of the Enhanced-Once through Steam generator Auxiliary feedwater system

Vivek Sethapati

ABSTRACT

The once through steam generator (OTSG) is a single pass counter flow heat exchanger in which primary pressurized water from the core is circulated. Main Feedwater is injected in an annular gap on the outer periphery of the steam generator shroud such that it aspirates steam to preheat the feedwater to saturation temperature. An important component of the OTSG and enhanced once through steam generator (EOTSG) is the auxiliary feedwater system (AFW), which is used during accident/transient scenarios to remove residual heat by injecting water through jets along the outer periphery of the heat exchanger core directly on to the tubes at the top of the OTSG. The intention is for the injected water, which is subcooled, to spread into the tube nest and wet as many tubes as possible.

In this project, the main objectives were to use first principles Computational Fluid Dynamics to predict the number of wetted tubes versus flow rate in the EOTSG at the AFW injection location above the top tube support plate. To perform the fluid analysis, the losses in the bypass leakage flow and broached hole leakage flow were first quantified and then used to model a $1/8^{th}$ sector of the EOTSG. Using user defined functions (UDF), the loss coefficients of the leakage flows were implemented on the $1/8^{th}$ sector of the EOTSG computational model to provide boundary conditions at the bypass flow and leakage flow locations With this method, the number of tubes wetted in the sector of EOTSG for various AFW flow rates was found. Results showed that the number of wetted tubes was in very close agreement to that predicted by experimental-analytical methods by the sponsor, AREVA. With the maximum flow rate of 65 l/s a total of 318 tubes were wetted and the percentage of tubes wetted with broached holes was 8.7 %.

The analysis on the bypass leakage flow showed that the loss coefficients was a function of the mass flow rate or the flow Reynolds number through the gap and it increased as the Reynolds number increased from 300 to 1600. The experimental and computational loss coefficients agree to within 15% of each other. In contrast, the constant loss coefficient of 1.3 used by AREVA was much higher than that obtained in this study, particularly in the low Reynolds number range. As the Reynolds number approached 3000, the loss coefficients from this study approached the value of 1.3. This value of the loss coefficient was implemented for the bypass flow leakage in the $1/8^{th}$ sector of the EOTSG model.

The analysis on the broached hole leakage flow was performed using a single hole, five holes, and one, two, four and eight rows of broached holes in order to characterize the loss coefficients. The one hole and five hole computational models were validated with experiments. The computational models showed the presence of voids in the leakage flow through the tube support plate (TSP), which were not observed (visually) in the experiments. The characterization of the broached hole leakage in the one, two and four rows showed that the loss coefficient of the control broached hole increased as the number of rows increased. These results indicated that for the same height of water on the TSP, the resistance to leakage flow increased as the number of tubes increased. They also indicated that leakage flow

through the broached holes was not solely a function of the height of water above the TSP but also the surrounding geometrical topology and the flow characteristics. However, the analysis done for eight rows showed that the loss coefficient became constant after a certain number of rows as the loss coefficient differed by only 5% from the results of the four rows. From these results it was determined that the loss coefficient asymptotes to an estimated value of 4.0 which was implemented in the broached hole leakage flow in the $1/8^{th}$ sector of the EOTSG.

Computational models of the $1/8^{th}$ sector of the EOTSG were implemented with the respective loss coefficients for the bypass and leakage flows. Results showed that as the AFW flow rate increased, the percentage wetted tubes increased. The data matched closely with AREVA's experimental-analytical model for flow rates of 14.5 l/s and higher. It was also deduced that complete wetting of the tubes is not possible at the maximum AFW flow rate of 65 l/s.

Acknowledgement

My Master's thesis has been the most fulfilling achievement in my academic career. It has provided me with the capability to accept difficult challenges and succeed in the engineering field. But without the tremendous help and support of some people I would have not been able to accomplish this thesis.

First and foremost, I would like to thank Dr. Tafti for the continued support, guidance and motivation he has provided through the two year period. After the completion of my under graduate degree, he was the main source who provided me with hope and instilled perseverance in the completion of my masters degree. He has taught me the necessary skills and knowledge needed to complete this project. He has also patiently answered numerous questions that I have posed showing me his commitment and concern. For all that he has done, I am truly in debt to him. I would like to show my appreciation for giving me this opportunity and thanking him for all that he has done.

I also want to thank Dr. Vlachos and Dr. Battaglia, for being my committee members and taking time off to read my thesis and approve it. Dr. Vlachos and his team have put a great deal of effort in the experiment part of this thesis and have provided me with constructive feedback. I would like to thank them for the fast updates and everything else they have done to make this thesis possible.

I would also like to thank AREVA for funding this project for a year and half and providing information needed in a professional and timely manner. I would also like to thank them for their patient and understanding with respect to the nature of this project.

In addition I would like to thank my colleagues in the lab – Sunil Patil, Surya Deb, Kamal Viswanath, Naresh Selvarasu, Nagendra Krishnamurthy, Jonathan Cowan, Sai Shrinivas, Sukhjinder Singh, Kevin Song and Amit Amritkar for their tremendous support and guidance. They have helped me with their extensive technical knowledge to cope with many problems in the completion of my thesis. They have encouraged me to do my best and supported me during the two year period. I thank them, not only for what they have done but for the close bond developed over the course of the years.

Most importantly, I would like to thank my family and my friends for the emotional support provided. My friends in Virginia Tech, in the United States and in Singapore have helped support me during this process. My father, mother and brother have always been a strong support system. They have provided a great deal of encouragement and have given me the courage to embark on this journey. Only with their presence in my life, was I able to believe in myself and complete this accomplishment.

Dedicated to Sethapati Seetharama Raju
Sethapati Savirthri Devi &
Sethapati Venkata Rakesh

Table of Contents

List of Tables

List of Figures

Chapter 1 INTRODUCTION

Pressurized Water reactors constitute the majority of reactors of the 440 nuclear operations around the world. In a PWR, light water is fed to the bottom of the reactor core in the primary circuit where it is heated to a temperature of 315 ^{o}C and pressurized to around 15.5 MPa. This pressurized water is then sent to the secondary circuit where it is used to produce superheated steam for power generation.

The once through steam generator (OTSG) is AREVA's single pass counter flow heat exchanger in which primary pressurized water from the core is circulated from top to bottom in 15,531 tubes of 5/8 inches outside diameter and 52 feet long. Main Feedwater is injected in an annular gap on the outer periphery of the steam generator shroud such that it aspirates steam to preheat the feedwater to saturation temperature. The saturated water enters the bottom of the heat exchanger core, exchanges heat with the primary fluid, boils, evaporates and superheats as it moves from the base to the top of the OTSG where it exits.

An important component of the OTSG and EOTSG is the Auxiliary Feedwater system (AFW), which is used during accident/transient scenarios to remove residual heat by injecting water through jets along the outer periphery of the heat exchanger core directly on to the tubes at the top of the OTSG. The AFW system is also essential as it prevents equipment deterioration in the secondary circuit in accident scenarios. The intention is for the injected water, which is subcooled, to spread into the tube nest and wet as many tubes as possible. The AFW system is highlighted in Figure1.1 which shows the schematic of the EOSTG.

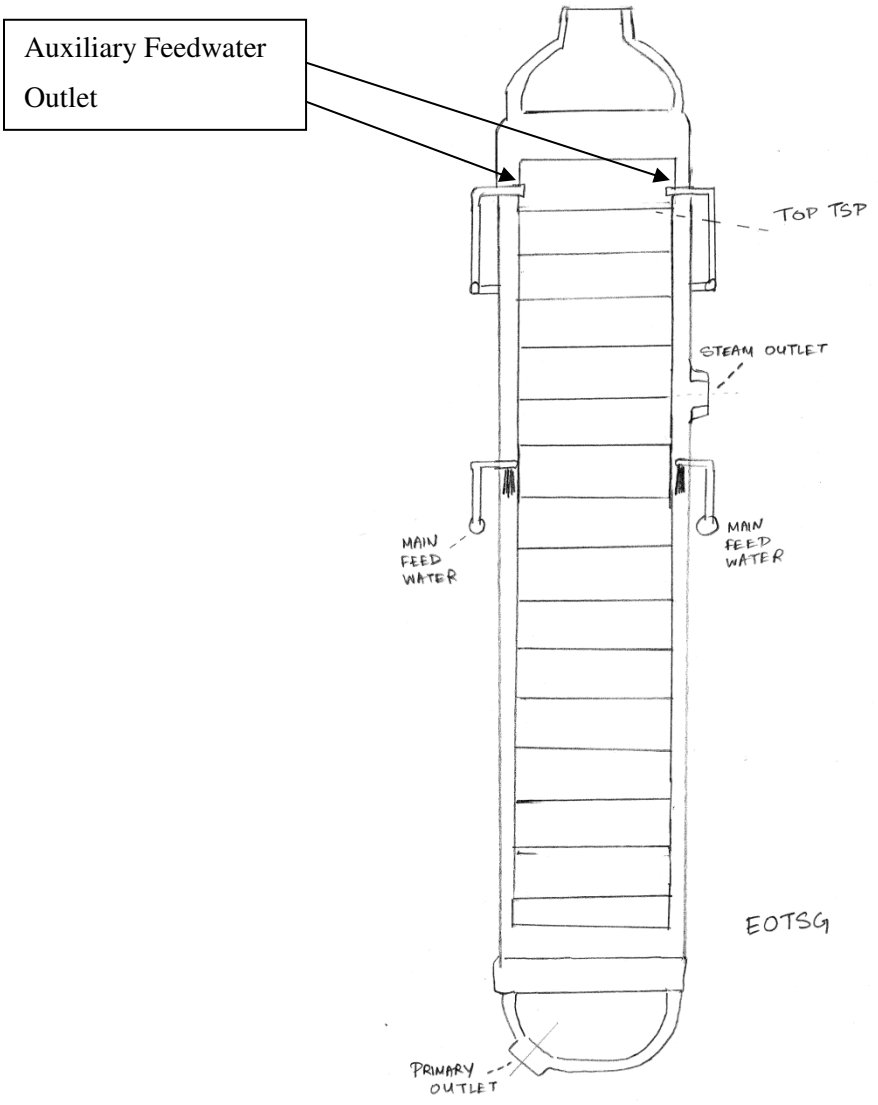

Figure 1.1: Cross section view of the EOTSG highlighting the AFW system

The mechanism of wetting penetration from the AFW is a strong function of the flow rate and the geometry. Previous experimental studies [2] done in a 1/8th sector of the OSTG at Idaho National Labs (INL) in the late 80s show that water impinges on the tube bundle, and under the action of gravity accumulates on the tube support plate (TSP) and forms a layer of finite thickness which flows horizontally into the tube bundle and exits through the broached holes which hold the tubes in place. The water flows as a film or as rivulets down

the tubes, evaporating and removing residual heat. This flow through the broached holes is counteracted by the steam in the upward direction as well. In addition, water also escapes or "bypasses" the tube bundle through the gap between the TSP and the shroud. The bypass flow does not participate in wetting or direct cooling of the tubes but drains down to the bottom of the EOTSG.

The industry's practice for modeling the OTSG and EOTSG uses the one-dimensional code RELAP5 [3]. In modeling the AFW flow, different empirical inputs are used primarily derived from experiments done in a $1/8^{th}$ sector of the OTSG at Idaho National Labs with 625 tubes [2]. The main data used from the INL study is the number of tubes wetted or penetration versus AFW flow rate and the average pool height versus AFW flow rate. This data together with derived form loss coefficients for the bypass flow and broached holes is used to generate a 1-D model to estimate the number of tubes wetted.

The objective of this thesis is to predict the number of wetted tubes versus flow rate in the EOTSG at the AFW injection location above the top tube support plate using first principles Computational Fluid Dynamics (CFD). The computational model neglects the condensation of steam and feedwater boiling. In addition, no heat transfer has been considered so as to avoid over complication of the computational models. In order to perform the fluid flow analysis, the first task focuses on model building and validation of the bypass flow. In Chapter 2, the characterization of loss coefficient versus water column height for the bypass flow is carried out to quantify the leakage flow. Chapter 3 deals with model building and validation of the broached hole leakage flow on the top TSP. In this Chapter, the leakage flow through various number of rows of broached holes is characterized under different conditions of column height and input flow rate. Chapter 4 uses information from the previous two chapters on the leakage flows and applies them using user defined functions in a computational model that simulates a $1/8^{th}$ sector of the EOTSG-AFW system. A map of wetted tubes versus flow rate is derived and compared to correlations derived from the INL study [2]. Chapter 5 presents the summary and conclusions from the fluid flow analysis.

Chapter 2. COMPUTATIONAL INVESTIGATION OF BYPASS FLOW

The bypass flow ("leakage flows") plays a key role in determining the number of wetted tubes, and hence it is important to ascertain that these flows are modeled with accuracy. In these studies, the annular opening between the TSP and the shroud have been investigated under controlled conditions to obtain the loss coefficient under different heads. This has served two purposes: it has validated the grid required to adequately resolve these small spaces in a large computational domain (if required), and it has validated the physical attributes (including turbulence models) of the model required to adequately represent the flow. In addition, it has also validated the values used by AREVA in their current model. The chapter proceeds in the following manner: description of the computational geometry, the input conditions of the model, description of the computational model, implementation of the method in FLUENT, explanation on the procedure for data extraction, results and analysis, and finally the surface tension on the bypass flow and grid sensitivity study on the bypass flow model.

2.1 Geometry of Computational Model

The geometry of the computational model comprised of two tanks that are connected by the bypass gap. Figure 2.1 shows the schematic of the model geometry. The top chamber contains water which enters through an inlet at the side and flows through the bypass gap and is collected in the bottom chamber. The thickness of the TSP is 1.18 inches. The gap was designed with a curvature radius of 4.45 inches and the nominal width of the gap is 0.104 inches. The dimensions of the computational geometry are shown in Table 2.1. At the velocity inlet boundary condition, water is injected at a given rate. In addition, the vent boundary condition controls the intake or outtake of air depending on the height of water in the top chamber. The vent located below the TSP, lets displaced air flow out as water fills the bottom chamber.

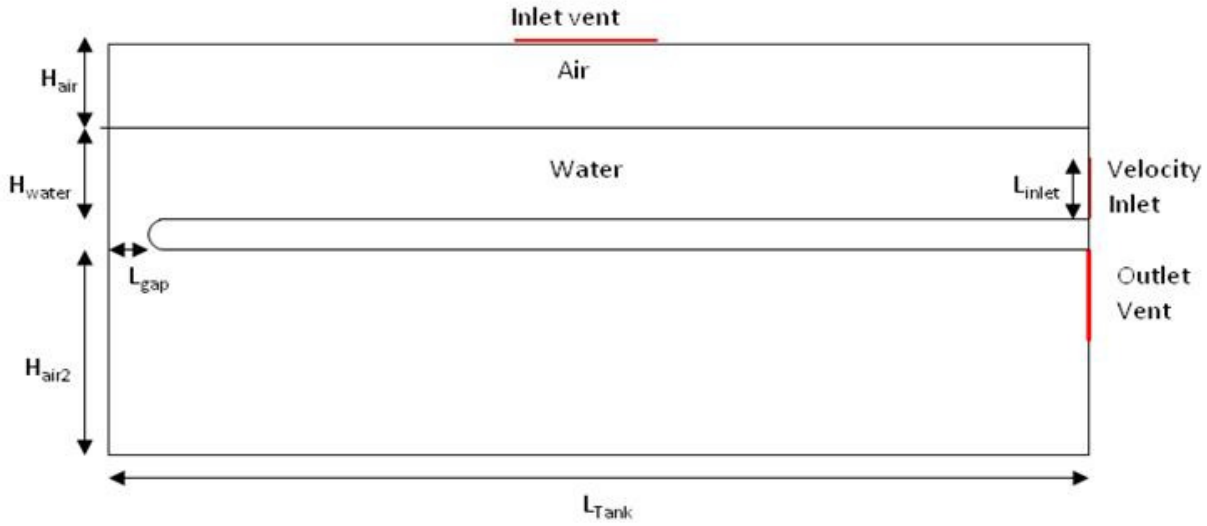

Figure 2.1: Schematic of geometry for computational model

Table 2.1: Dimensions of geometry for computational model

L_{gap} (nominal gap width)	0.104 inches = 0.0026416 m
L_{Tank}	0. 875 m
H_{air2}	0.5720 m
H_{water}	0.0786 m – 0.007335 m
H_{air}	0.0714m – 0.1427m
L_{inlet}	0.01m

2.2 Computational Model Input Conditions

This section highlights the data that was used for the analysis of the bypass flow area. Table 2.2 summarizes the data extracted from Table 5-23 in [3]. It contains the estimated bypass flow rate calculated based on the average pool height over the drilled holes. The average pool height was calculated based on flow into the broached holes region. It was noted in [3] that the loss coefficient was determined to be 1.3 and that it is expected to be

approximately constant for any reasonable bypass area. The value as mentioned in [3] is the summation of the loss coefficients for sudden contraction and expansion of the bypass flows. In order to relate the data provided by [3] to our computational model, the Reynolds number of the bypass flows was calculated as given in equation 1:

$$\mathrm{Re} = \frac{V_{bypass} \times L_{bypass}}{\nu} \tag{1}$$

Where V_{bypass} is the bypass flow velocity,
L_{bypass} is the characteristic length of the nominal bypass gap which is 0.104 inches,
and ν is the kinematic viscosity of water which is $1 \times 10^{-6} m^2 / s$.

The bypass flow velocity, V_{bypass} was calculated by dividing the flow rates with the bypass region area for a 1/8th section of the EOTSG which is 0.033466 ft^2 (0.0031093m^2). The nominal bypass gap width was calculated based on the three flow bypass regions in the periphery of the TSP which have been extracted from [3]. The first being the flow area between the outer diameter of the TSP and filler plates which is 3.9007 in^2. Second being the gaps at the eight alignment slots which add up to a flow area of 19.456 in^2. Third being the gaps at the two keyways which sum up to a total flow area of 11.0382 in^2. In addition, the effects of the change in thermal expansion at hot operating conditions contribute to an estimated increase of flow area by 11.0382 in^2. Therefore, using the total flow area of 38.5523 in^2 and a hot TSP outer diameter of 117.8747 inches and a nominal gap width of 0.104 inches (0.0026416 meters) is calculated. Having all the variables, equation 1 was used to calculate the Reynolds number for each of the flow rates related to the respective nozzles flows. The Reynolds numbers for each flow are listed in Table 2.2 in the last column. The Reynolds numbers along with the corresponding heights served as a guide for the input conditions of the computational model.

Table 2.2: Data summarizing the calculated Reynolds number and average heights corresponding to each nozzle flow rate and estimated bypass flow rate[3]

Nozzle Flow (l/s)	Estimated Bypass flow rate (ft^3/s)	Estimated Bypass flow rate (m^3/s)	Average Height (feet)	Average Height (m)	Calculated Reynolds No.
1.68	0.0686	0.00194	0.0850	0.0259	1650
1.80	0.0704	0.00199	0.0895	0.0273	1690
2.50	0.0768	0.00218	0.107	0.0325	1850
3.50	0.0831	0.00235	0.125	0.0380	2000
5.00	0.0903	0.00256	0.147	0.0449	2170
5.65	0.0930	0.00263	0.156	0.0476	2240
7.60	0.0999	0.00283	0.180	0.0550	2410

2.3 Computational Model

The mesh of the model was generated using Gridgen. The total number of elements for the two-dimensional mesh is 70,000. There were 440 elements in the bypass gap. For resolving the dynamic air-water interfaces to an accurate level, a fine grid was used in the vicinity of the walls close to the bypass gap. The fine grid was also incorporated at the interface of the phases

2.3.1 Implementation of method in Fluent

An unsteady calculation procedure based on the volume of fluid (VOF) method was used in the commercial software Fluent on the computational model. The VOF method is used for interface tracking, where it solves a supplementary transport equation for the volume fraction of one of the phases by assigning a binary state of 0 and 1 to the two phases. In the explicit scheme employed in the VOF model, phase reconstruction is carried out in the computational elements at each time step or iteration in which the volume fraction is between 0 and 1. In order to capture the water and air interface, the geometric reconstruction was enabled for the volume fraction. In addition, a variable time step was employed to ensure that the CFL number was maintained at 1.5. The time steps for the cases were between 1E-04 to

1E-06. In all the cases, the momentum and continuity equations converged to a residual of 1E-05 within the allowed 50 iterations per time step. The cases were run with an unsteady calculation until they reached a steady state. Wall adhesion was enabled for the phase interaction, and all of the contact angles were set to 90 degrees. The k-ε model with standard wall functions was selected as the turbulence model. This model is well known for its robustness, economy and reasonable accuracy for a wide range of turbulent flows as mentioned in [6].

2.4 Procedure for Data Extraction

With the computational model set up in Fluent the initial conditions had to be implemented for the model to start calculation. The Reynolds number and the respective heights given in Table 2.2 were a good initiating point. For each case, the specific height of water was patched in the top chamber and in the bypass gap. The velocity at the inlet was calculated to replicate the various Reynolds number in the gap using the basic continuity equation (2) as shown:

$$V_{inlet} = \frac{V_{bypass} L_{bypass}}{L_{inlet}} \tag{2}$$

Where V_{inlet} is the inlet velocity,

L_{inlet} is the length of the velocity inlet which is 0.01 m,

V_{bypass} is the velocity in the bypass gap

and L_{bypass} is the characteristic length of the nominal bypass gap which is 2.6416E-03 m

Starting from these initial conditions, the flow in the bypass gap goes through a transient before it reaches a steady state when the height of water on top of the TSP is such that the mass flowing into the top chamber from the inlet is exactly balanced by the mass flow through the bypass gap. To monitor the height of the water, two line surfaces were made. The first surface was located close to the bypass gap and the second was located 2.6146E-02 m away from it. Each of the line surfaces measures the mass fraction of water at

the location as shown in Figure 2.2. In addition, the mass flow of water in the bypass gap was monitored.

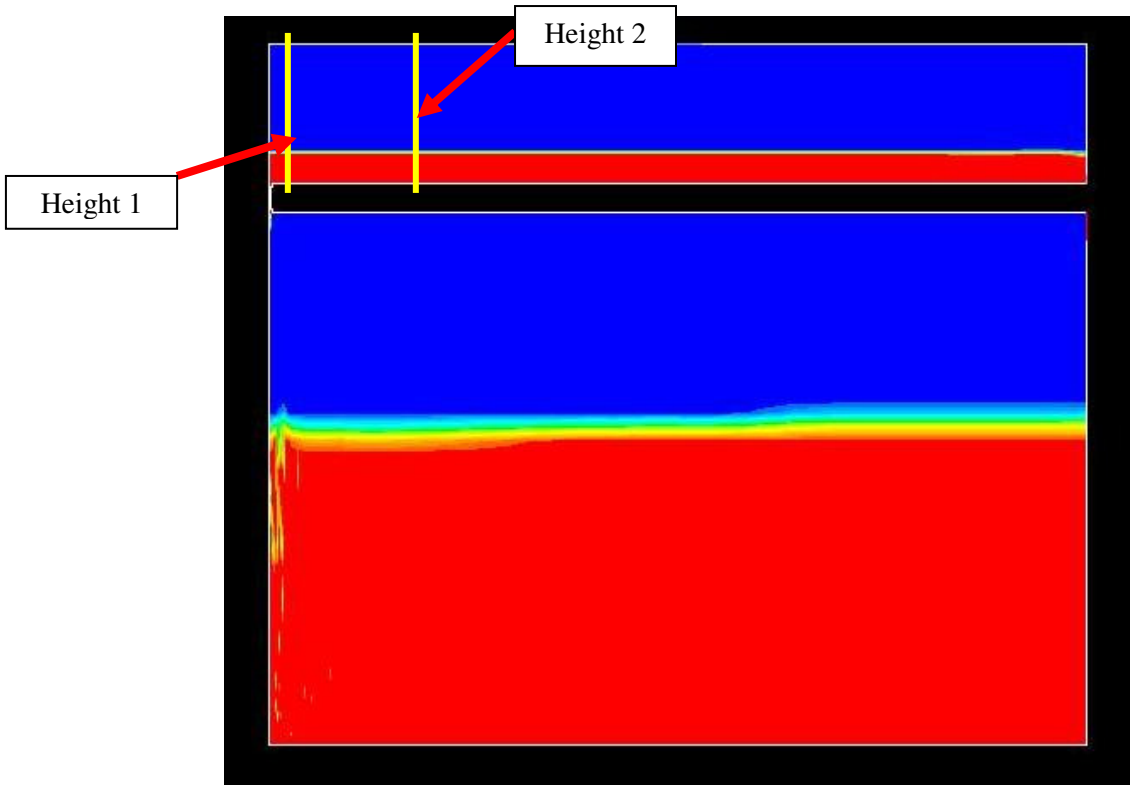

Figure 2.2: Diagram of Computational model highlighting the location of the two heights

With the geometry of the model tied together with the initial and boundary conditions, the first simulation case examined was a flow Reynolds number of 2238. In order to monitor the dynamics of the system, the simulation was run for a fluid flow time of ten seconds. This simulation took about eight hours on three processors. Figure 2.3 shows the plot of the mass flow through the bypass gap during the first 10 seconds. It is evident that there is fluctuation in the mass flow of fluid from 2.2 kg/s to 2.5 kg/s. Similarly, height 1 and height 2 of the water are plotted as shown in Figure 2.4 and 2.5, respectively. Examining the three graphs shows that the oscillations in the water height follow a pattern in conjunction with the change in the bypass gap mass flow rate. This variation indicates that the system has not reached equilibrium so the case was resumed and run till a flow time of 70 seconds. Figure 2.6 summarizes the plot for the bypass gap mass flow during the 70 seconds. It can be

surmised that the variation in mass flow has reduced but has not reached equilibrium. Similar fluctuations in the height of water could also be detected. Therefore, the case was run for an additional 60 seconds and the mass flow finally reached close to a steady state at 2.233 kg/s as shown in Figure 2.7. In addition, Figure 2.8 and 2.9 show the plots of height 1 and 2 which have also reached steady state. The total computational time for the case took 120 hours. The same monitoring procedure was used for each of the Reynolds number given in Table 2.2 to establish a steady state. The results are summarized in the next section.

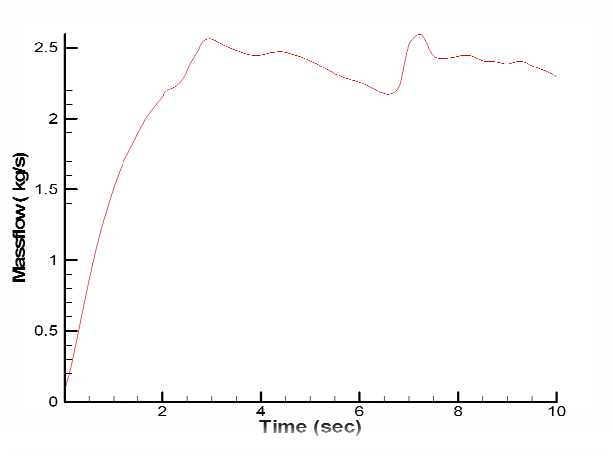

Figure 2.3: Plot of mass flow for flow time of 10 seconds and fluid flow of Re = 2238

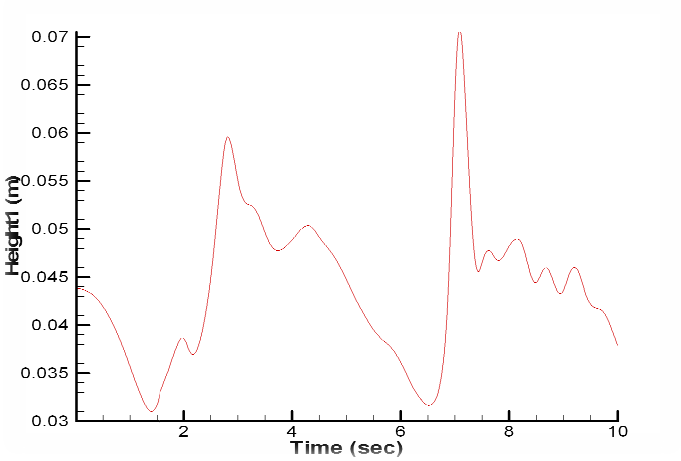

Figure 2.4: Plot of height 1 for flow time of 10 seconds and fluid flow of Re = 2238

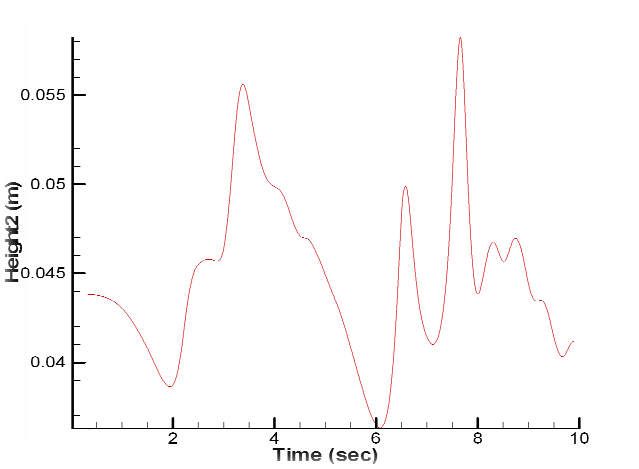

Figure 2.5: Plot of height 2 for flow time of 10 seconds and fluid flow of Re = 2238

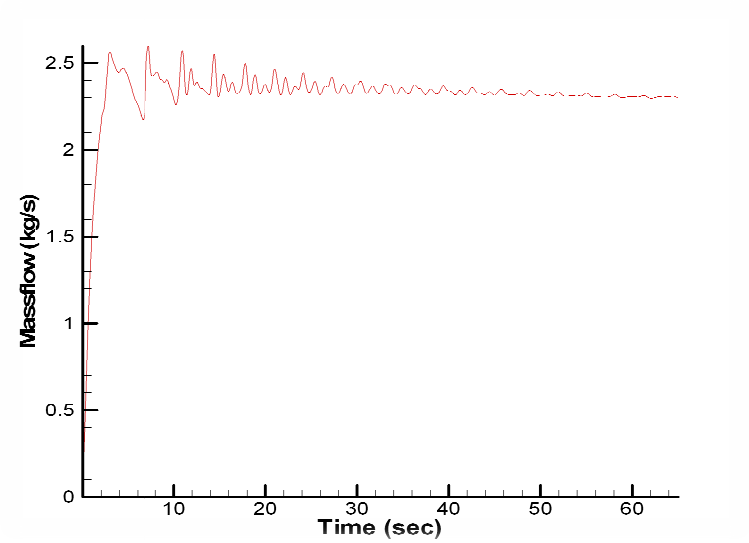

Figure 2.6: Plot of mass flow for flow time of 70 seconds and fluid flow of Re= 2238

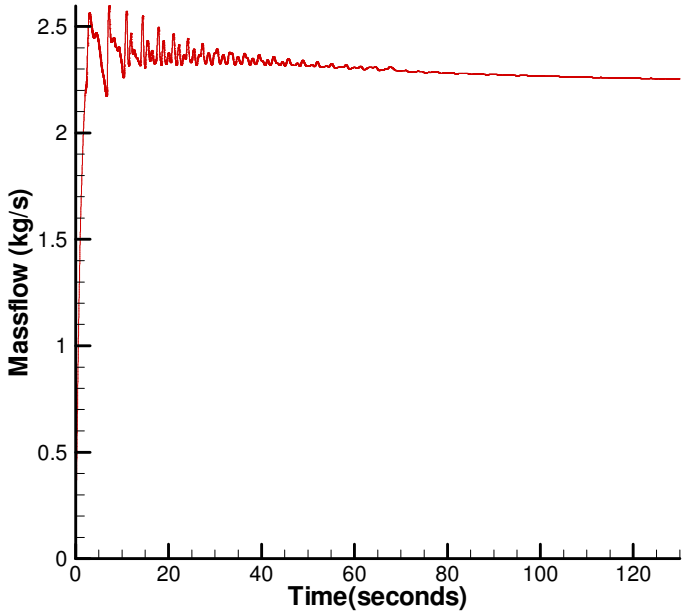

Figure 2.7: Plot of mass flow for flow time of 130 seconds and fluid flow of Re= 2238

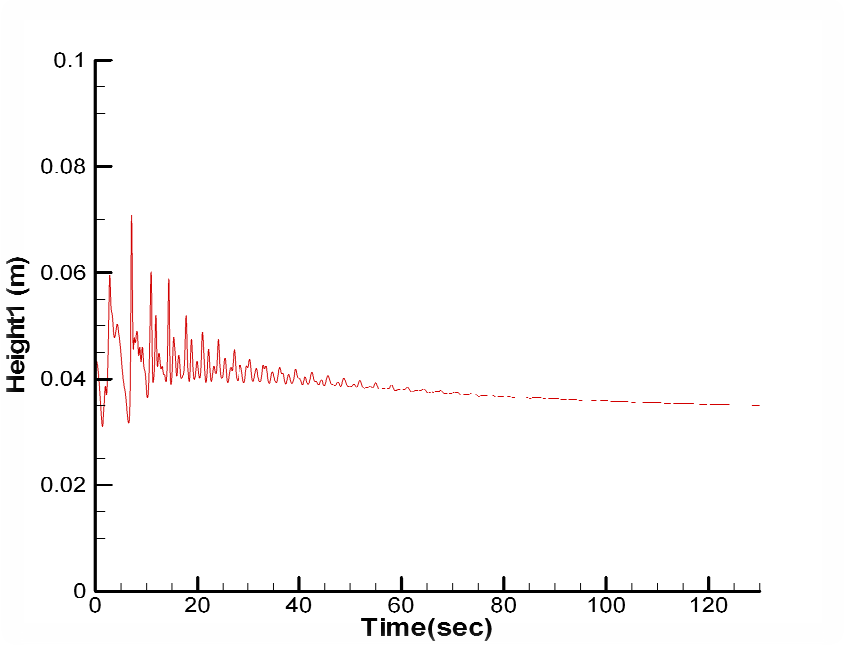

Figure 2.8: Plot of height 1 for flow time of 130 seconds and fluid flow of Re= 2238

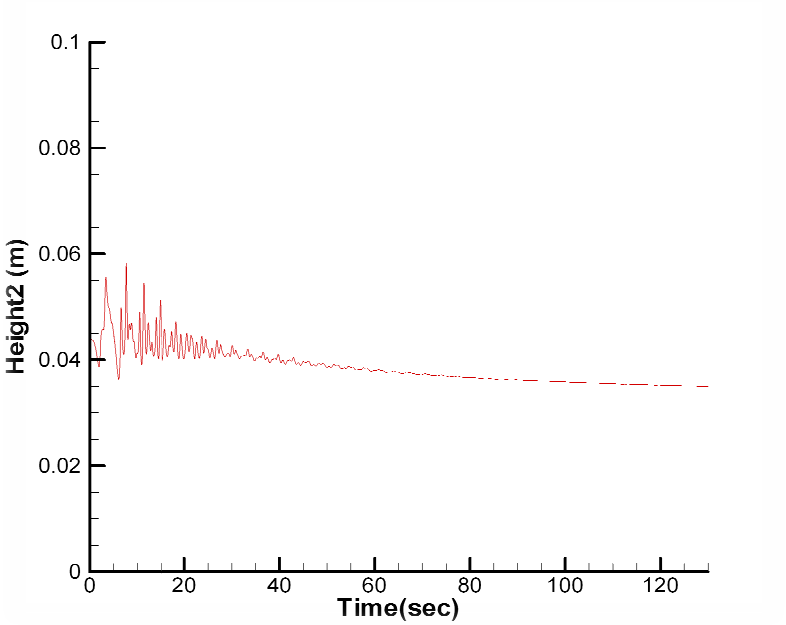

Figure 2.9: Plot of height 2 for flow time of 130 seconds and fluid flow of Re = 2238

2.5 Results and Analysis

A total of 9 simulations were carried out, each matching the respective Reynolds number. To meet the objectives, the bypass loss coefficient for each case was calculated using equation 3 given in [3]:

$$k_{bypass} = \frac{2gh_0}{(V_{bypass})^2} \tag{3}$$

Where k_{bypass} is the loss coefficient,

h_0 is the average of height 1 and height 2

and V_{bypass} is the velocity in the bypass gap

Table 2.3 summarizes the values for height 1, height 2 and the loss coefficients for the corresponding Reynolds number. The trend from the data shows that as the heights

increase so does the loss coefficient of the bypass gap. Figure 2.10 shows pictures of the computational model for the fluid flow with Reynolds number 3000, 2500 and 2238 at steady state. The pictures show that there is no separation in the flow through the bypass gap and that the height of water in the top chamber is uniform. Likewise, Figure 2.11 shows the pictures of the computational model for the fluid flow with Reynolds number 1848, 1750 and 1650. In these cases, as the Reynolds number decreases, there are some variations in the height of water on the TSP. In fact, for the fluid with a Reynolds number of 1650, when the height of fluid on the TSP is small with respect to the gap width, a convex free surface forms as the water flows into the bypass gap. In this case, height 2 is 62.5 % larger than height 1 and the validity of equation (3) to calculate a loss coefficient is suspect. In spite of this, the data point is included in the analysis, but should be used with some caution.

Table 2.3: Data from Computational model for respective Reynolds number

Reynolds No.	Mass flow (kg/s)	Height 1 (m)	Height 2 (m)	Loss Coefficient
1650	1.6477	0.0056	0.0091	0.3684
1750	1.7505	0.0102	0.0102	0.4523
1848	1.8647	0.0136	0.0136	0.5340
2000	2.0170	0.0216	0.0214	0.7202
2100	2.1470	0.0283	0.0281	0.8339
2238	2.2330	0.0350	0.0350	0.9574
2500	2.4910	0.0490	0.0490	1.0765
3000	2.9380	0.0786	0.0786	1.2413

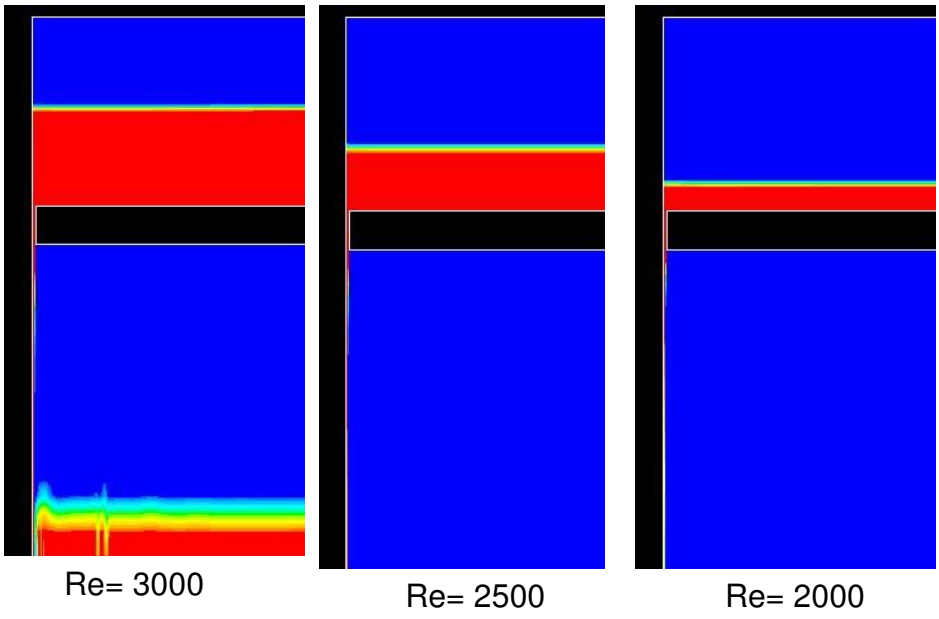

Figure 2.10: CFD Snap shots of flow in the bypass gap for Reynolds number 3000, 2500 and 2000

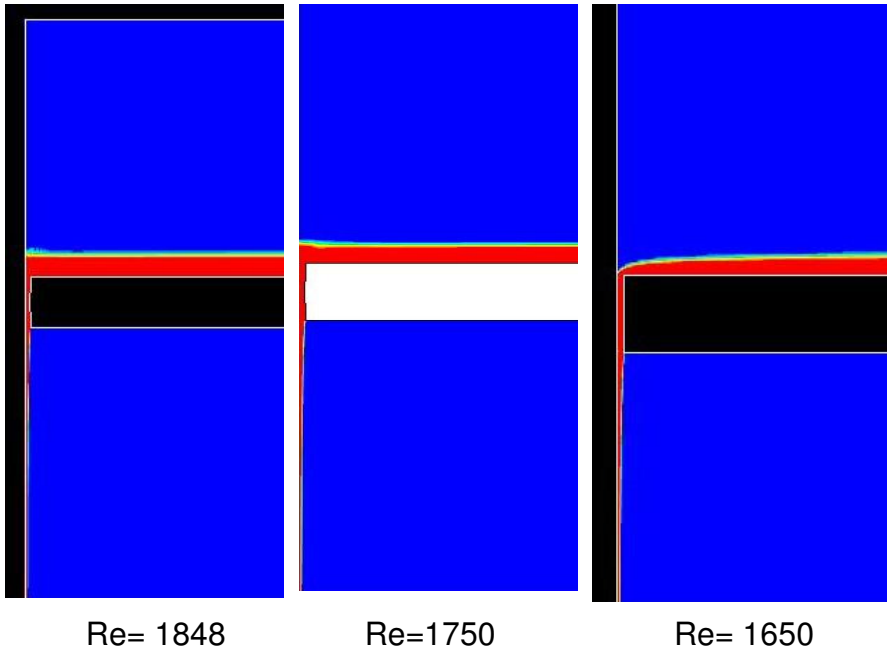

Figure 2.11: CFD Snap shots of flow in the bypass gap for Reynolds number 1848, 1750 and 1650

The calculated loss coefficient is plotted against Reynolds number in Figure 2.12. The calculated loss coefficient increases with Reynolds number and seems to be leveling off at a value close to 1.3 used in Relap5 [3]. The Relap5 loss coefficient of 1.3 was calculated from the addition of the loss coefficients for sudden expansion and contraction, which typically are calculated at high Reynolds numbers at which there is no Reynolds number dependence.

Since the Reynolds number ranges from 1600-3000 in the calculation, the flow through the bypass gap could be laminar, turbulent or transitional. To establish the sensitivity of the loss coefficient to this factor, additional laminar calculations were performed in the low Reynolds range. For each of these simulations the computational time for the mass flow to reach steady state was approximately 192 hours with three processors. The results show that at the low end of the Reynolds number range there is a 26% difference in the loss coefficient calculated by the laminar model but as the Reynolds number increases to 2100, the laminar and turbulent model results only differ by 3.32 %.

The experimental model results have also been incorporated into Figure 2.12. In comparison, the experiment results also show that as the Reynolds number of the fluid increases so does the loss coefficient. But they underpredict the loss coefficients of the bypass flow compared to the computational results by 1.04 % to 13.1 %.

Figure 2.13 shows the distribution of the loss coefficient with average height of the water level for the two models compared to the Relap5 model. The computational results suggest that beyond a height of approximately 10 cm, the loss coefficient would approach the value used in Relap5. The results indicate that the current predictions in Relap5 would overpredict the number of tubes wetted by underpredicting the bypass leakage flow.

Figure 2.14 further compares the height of water on the TSP to the flow Reynolds number (or mass flow rate) in the bypass gap. It is seen that for the same height of water on the TSP, the Relap5 model underpredicts the bypass flow by 10 to 20 % compared to the computational results.

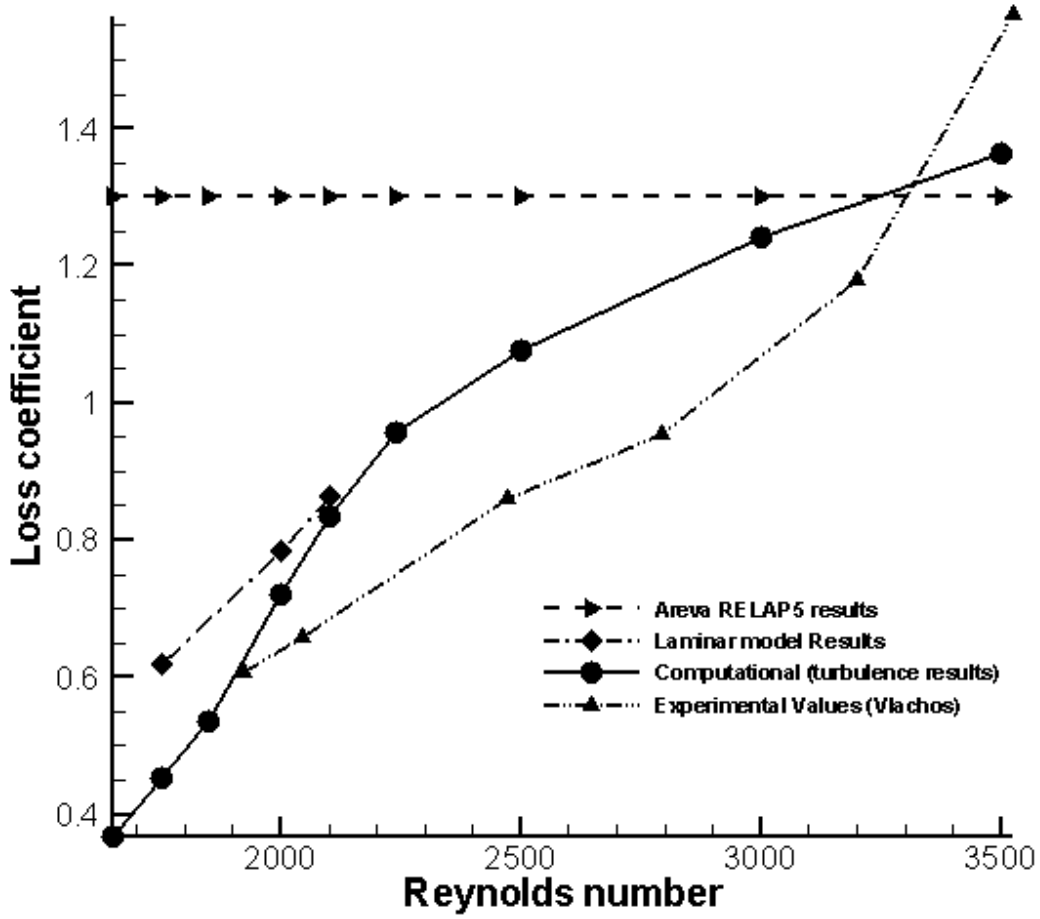

Figure 2.12: Data comparing loss coefficient versus Reynolds number of computational results with Areva RELAP5 results.

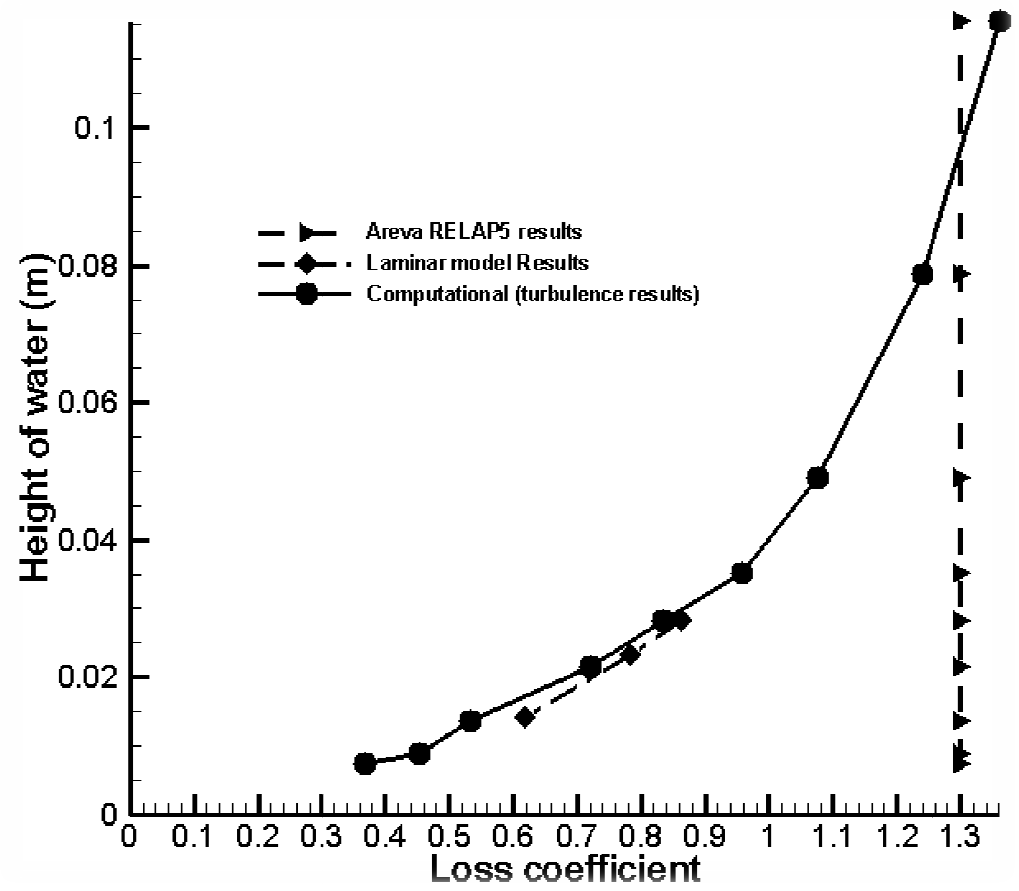

Figure 2.13: Data comparing height of fluid versus loss coefficient of computational results with Areva Relap5 results.

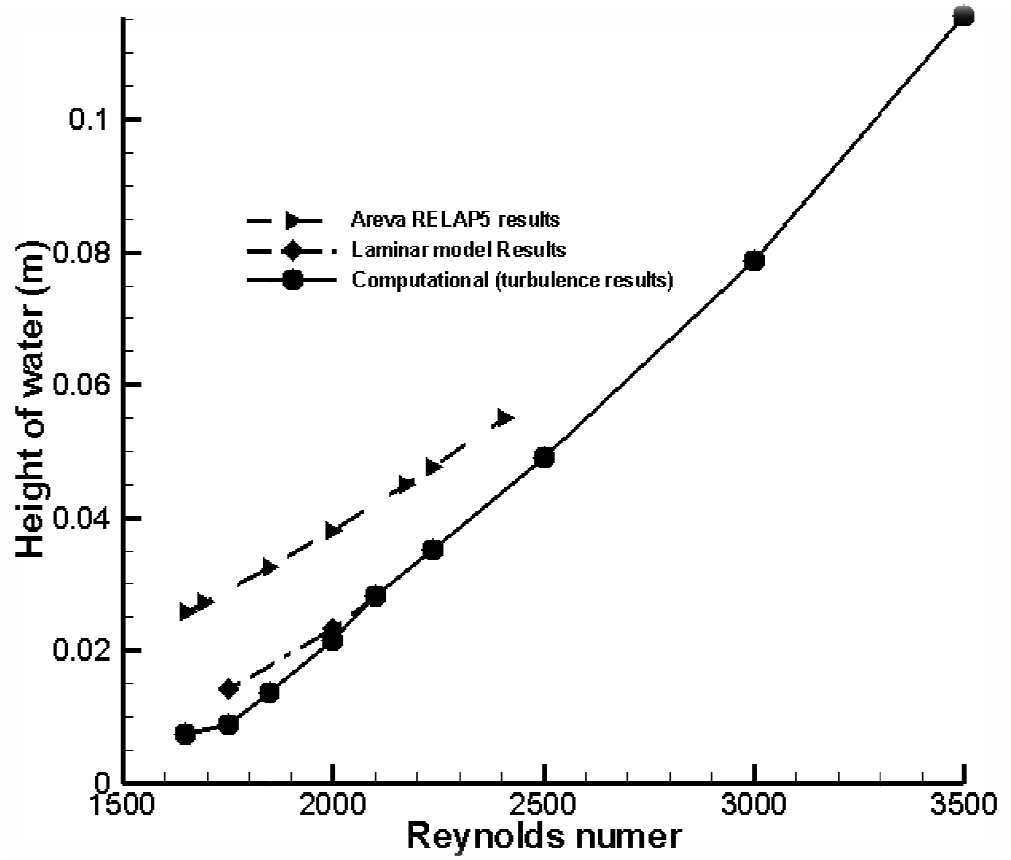

Figure 2.14: Data comparing water height versus Reynolds number of computational results with Areva Relap5 results.

2.6 Surface Tension Analysis

This study was done to evaluate if the surface tension plays an important role in the bypass flow. The Weber number is the ratio of the inertial force to the surface tension force acting on a fluid element [4]. It is described in equation 4 with each of the given components:

$$We = \frac{\rho V^2 \ell}{\sigma} \tag{4}$$

Where ρ is the density of water at room temperature = 998.2 kg/m^2,

V is the velocity of the fluid,

ℓ is the characteristic length,

and σ is the surface tension of water with air at room temperature = 0.00728 N/m.

To carry out the calculations, the velocities of the fluids in the bypass gap were extracted from the computational model calculations shown in Table 2.3. The characteristic length in this case is obviously the width of the bypass gap, 0.0026416 m or 0.104 inches. The calculations of the Weber number are reflected in Table 2.4. The results show that the Weber number for the lowest Reynolds number is 141 which is much higher than the value 1. This signifies that the bypass flow is not significantly affected by surface tension and inertial effects are dominant.

Table 2.4: Data summarizing the calculated Weber number corresponding to each Reynolds number of the bypass flow rate

Reynolds No.	Velocity (m/s)	Weber Number
1650	0.625	141
1750	0.671	163
1848	0.707	181
2000	0.766	212
2100	0.814	240
2238	0.847	260
2500	0.945	323
3000	1.115	450
3500	1.291	604

2.7 Grid Sensitivity Study

A grid sensitivity study was done to evaluate the effect of the grid resolution on the calculation of the loss coefficient. In order to accomplish this, two more meshes comprising of 15,000 cells (very coarse) and 40,000 cells (coarse) were tested with the same geometry as the 70,258 mesh size. Similar to the cases above, the standard k-ε turbulence model was applied to the computational model. Table 2.5 summarizes the data obtained for each of the cases. The data shows that the increment of the calculated loss coefficient between the 15,000 cells and 40,000 cells is 23 % while the difference between the 40,000 cells and

70,258 cells is 5%. It was assumed that the value obtained on a 70,000 cell grid was close to the converged solution and this grid was used for the bypass flow calculations.

Table 2.5 Data summarizing results for grid sensitivity test

Total no. of cells	No. of cells in gap	Reynolds no.	Loss coefficient
70,258	440	2129	0.8424
40,000	150	2128	0.8027
15,000	75	2128	0.6528

Chapter 3 COMPUTATIONAL INVESTIGATION OF BROACHED HOLE FLOW

The aim in this Chapter is to characterize the leakage flow through the broached holes for different conditions of water column height and inlet velocity. The analysis for the broached hole flow was more complicated and computationally intensive compared to the bypass flow. The objective is to correlate flow conditions and height of fluid on the TSP to the leakage flow via a loss coefficient.

The Chapter proceeds in the following manner: methodology for validation cases consisting of a single broached hole and 5 broached holes in staggered fashion in which the description of the geometry, the model input conditions, validation of the computational model and procedure for data extraction are described. It then proceeds to the methodology for multiple broached holes in which the description of the geometry, the model input conditions and the procedure for data extraction are explained. Finally, a thorough description of the results and analysis of these computational models and the impact of surface tension is evaluated.

3.1 Methodology for single broached hole flow and five broached holes flow

The analysis for the broached holes flow was started by validating the computational models with experimental data. It was decided that the most efficient way to validate the computational model with the experiment would be to first evaluate the loss coefficients for a single broached hole. With the success of this model it was decided to expand it to a more complex system of five broached holes in staggered fashion.

3.1.1 Geometry of Computational models

The geometry for the single broached hole model consists of two chambers linked with a broached hole through the TSP plate. Water is channeled through the inlet of the top chamber as shown in Figure 3.1. Since the boundary conditions of the sides are walls the water seeps through the broached hole and flows to the bottom chamber where it leaves the

system through the outlet vent. The inlet and outlet vent also regulate the flow of air as the system reaches steady state. The width of the model was 0.3285 m to match the experimental setup. This length of the model, about fourteen times larger than the width of each flow gap, ensures that the backflow of fluid at the walls do not affect the leakage flow. Table 3.1 shows the dimensions of the computational model.

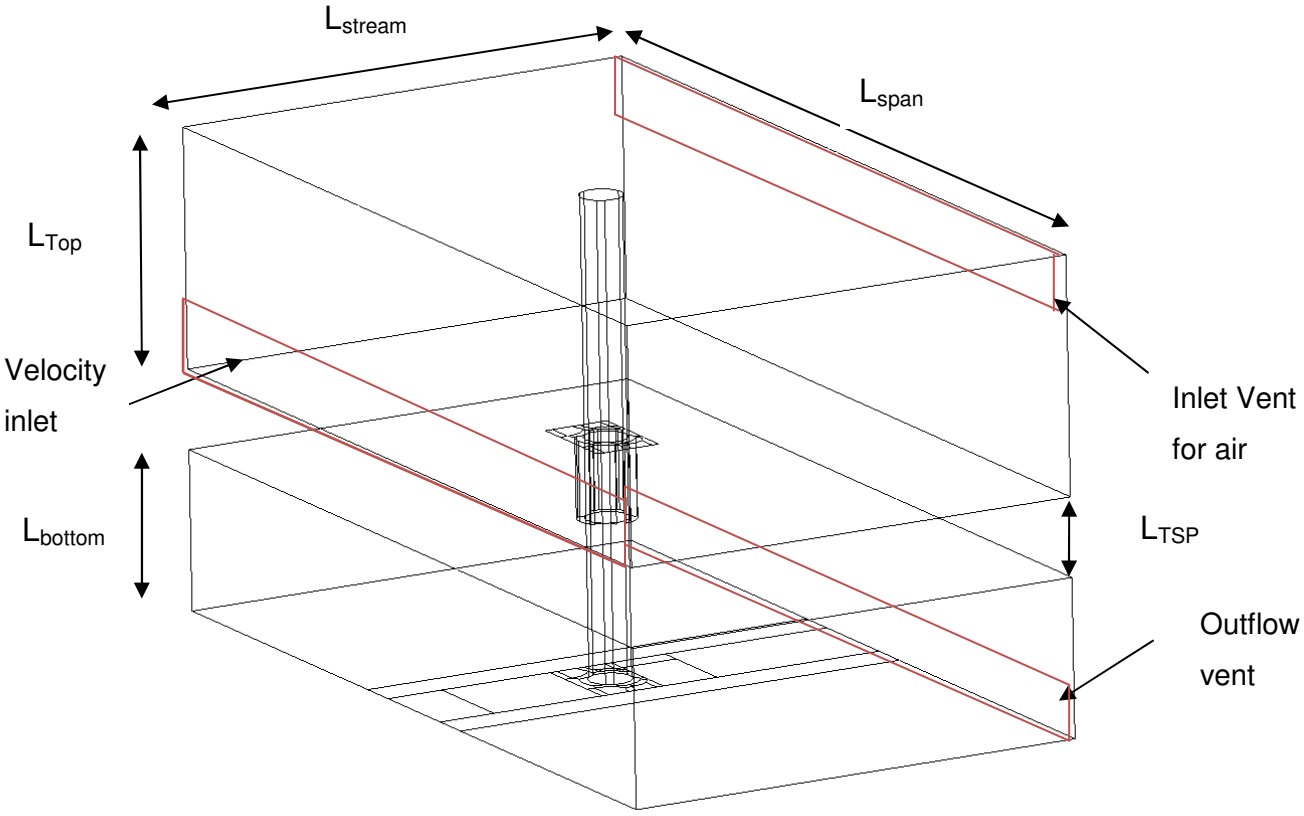

Figure 3.1: Schematic of geometry for computational model (single broached hole)

Table 3.1: Dimensions of geometry for computational model (single broached hole)

L_{Top}	0.09 m
L_{Bottom}	0.06 m
L_{stream}	0.180 m
L_{span}	0.3285 m
L_{TSP}	0.029972 m

The computational model for the five broached holes follows a similar concept to the preceding one. Two chambers are linked with five broached holes through the TSP plate. Water is channeled through the inlet of the top chamber as shown in Figure 3.2 and exits out of the bottom chamber through the outlet vent as it flows through the broached holes. The model shown in Figure 3.2 is a modification of the single hole broached hole and therefore consists of the same boundary conditions. The span wise and stream wise length of the model is 0.3586 meters and 0.231 meters respectively as shown in Table 3.2. The model is made to replicate the experimental conditions and constraints for validation purposes.

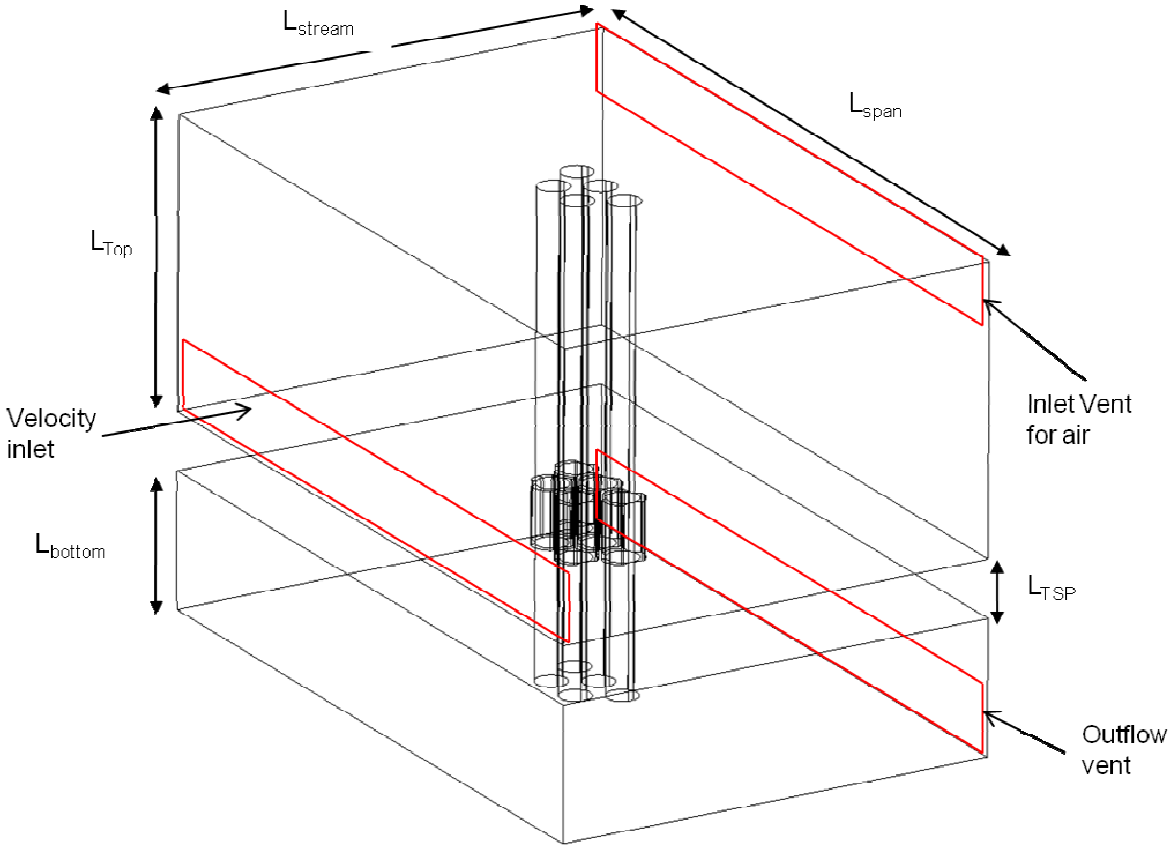

Figure 3.2: Schematic of geometry for computational model (five broached holes)

Table 3.2: Dimensions of geometry for computational model (five broached holes)

L_{Top}	0.150 m
L_{Bottom}	0.090 m
L_{stream}	0.231 m
L_{span}	0.358 m
L_{TSP}	0.029972 m

3.1.2 Computational Model Input Conditions

This section highlights the data that was used for the analysis of the broached flow area. Table 3.3 shows the various broached hole flow rates corresponding to the different nozzle flow rates. The data summarized in Table 3.3 is extracted from information provided in Table 5-24 in [3]. In addition, information on the number of tubes in the broached hole region that are wetted were based on the fit found in Figure 5-1 in [3]. The flow rate divided by the total open area of the broached holes was used to derive the mean velocity through each broached hole with water. These values hold under the assumption that the broached holes are completely filled. Similar to the section above, the Reynolds number was calculated for each hole corresponding to each flow rate using equation 5:

$$\mathrm{Re} = \frac{V_{broached} D_{broached}}{\nu} \tag{5}$$

where $D_{broached}$ is calculated using the hydraulic diameter formula given in equation 6:

$$D_{broached} = \frac{4A_{broached}}{P} \tag{6}$$

where $A_{broached}$ is the leakage flow area through a broached hole surrounding the tube, and P is the total perimeter of the leakage flow area.

The value for $D_{broached}$ was found to be 4.5199504E-3 m and was incorporated in each calculation to find the Reynolds number. The area of the leakage flow through the broached hole was estimated to be 3.770398E-5 m^2 and the perimeter was estimated to be 3.336672E-2 m^2. Using these results and the equations listed above, Reynolds number range from 600 to 8600 was obtained. These values identified the range of Reynolds numbers for the computations.

Table 3.3: Data summarizing the calculated Reynolds number corresponding to the flow rates in the broached holes[3]

Broached hole flow rate(m3/s)	Average Height (m) of water	Wetted tubes	Area of Broached holes(m^2)	Mean Velocity in each hole(m/s)	Reynolds No.
0.001943	0.02589	9	0.001018	1.910	8628
0.001994	0.02728	16	0.001810	1.102	4981
0.002176	0.03247	44	0.004980	0.4372	1976
0.002354	0.03801	73	0.008260	0.2851	1289
0.002558	0.04490	110	0.01240	0.2056	929
0.002634	0.04760	124	0.01403	0.1878	848
0.002831	0.05500	163	0.01844	0.1536	694

3.1.3 Computational Model for validation (single and five broached holes)

The mesh of the models was generated using Gridgen and the total number of elements for the single broached hole and five broached holes model is 3.2 million and 4.9 million cells, respectively. For both models, a fine mesh was used in the vicinity of the broached hole walls so as to capture the dynamics of the fluid and to resolve the air water interface accurately. Most of the mesh was structured but 5% of the mesh was unstructured to reduce the total grid size of the models. Just like the model for the bypass flow, an unsteady calculation procedure supported by the VOF method in the commercial software Fluent was incorporated till the case reached a steady state solution. Similar to the bypass cases, a variable time step was employed to ensure that the CFL number was maintained at 1.5. The time steps for the cases were between 1E-05 to 1E-07. In all the cases, the momentum and continuity equations converged to a residual of 1E-05 within the allowed 50 iterations per time step. The k-ε turbulence model was used for all the calculations to model the high Reynolds number flow through the broached holes. The model provides reasonable accuracy and is robust and economical. Most importantly, despite the large grid size of each type of these models, they provided results within a reasonable time frame. Surface tension effects were assumed to be much smaller than inertial effects, and a contact angle of 90 degrees was

used to model the water-air-solid contact line. In addition, a variable time step was incorporated to maintain the CFL number at 1.5.

3.1.4 Procedure for Data Extraction

With the computational models for the single and five holes setup in Fluent, the initial conditions had to be implemented for the calculations to start. The range of Reynolds numbers available in Table 3.3 provided an estimate of the inlet velocity at the boundary. For each case, the corresponding height of the water was patched in the top chamber and through the broached holes. The velocity at the inlet was calculated to replicate the Reynolds number in the gap using the continuity equation for the three dimensional flow as shown in equation 7:

$$V_{Inlet} = \frac{V_{broached} A_{broached}}{A_{Inlet}} \tag{7}$$

Where V_{inlet} is the inlet velocity,

A_{inlet} is the area of the velocity inlet,

$V_{braoched}$ is the velocity in the broached hole

$A_{braoched}$ is the total respective broached hole open area for respective models

The solution procedure for this case is similar to the bypass flow. Starting from the initial conditions the flow in the broached holes goes through a transient before it reaches a steady state where the height of the water in the top chamber is such that the mass flow flowing through the inlet is balanced out by the mass flow going through the broached holes. To monitor this mass flow, a surface plane was generated at the exit of the broached hole(s) for the single and five broached holes cases. This plane measured the mass flow of water going through. As soon as the mass flow reached a steady state and the model was in equilibrium, the heights were measured. Several surface planes were made in the span wise and stream wise direction to measure the height of the water. Figure 3.3 shows an example of two planes made in the vicinity of the broached holes to measure the height of the water. Plane 1 measures the height of the water in the span wise direction and plane 2 measures the

height of the water in the stream wise direction. Since the heights did not differ by much the average of the heights was used in the calculation of the loss coefficient. This procedure was carried for each of the broached holes in the five holes model and the average height was calibrated.

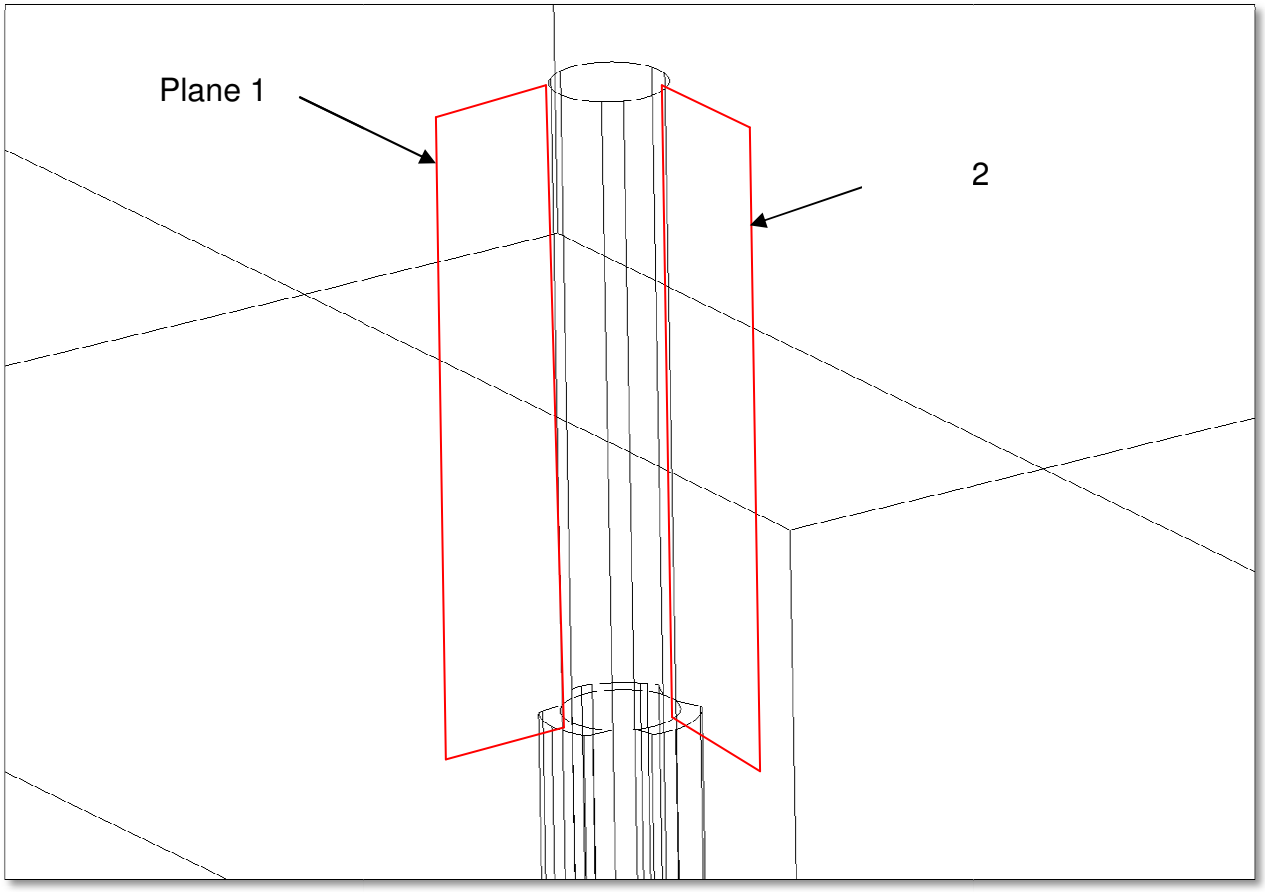

Figure 3.3: Schematic of computational model highlighting the locations of the heights measured

3.2 Methodology for multiple rows of broached holes

It was decided to extend the model to single and multiple rows to characterize leakage flows in these conditions. Since the broached holes were staggered on the tube support plate the influence of neighboring broached holes on the leakage flows had to be evaluated. In order to capture this, computational models for one row, two rows, four rows and eight rows

were built. Since the four row computational model gives a good visual description of the system, it is explained as the representative geometry in this chapter.

3.2.1 Geometry of Computational models for multiple rows of broached holes

The concept of the model for the four rows is similar to the model used for validation. The domain of the model consists of two chambers linked with broached holes. Figure 3.4 shows the schematic of the computational model geometry. The width of the broached hole gap was reported to be 0.1139 inches. The radii of the tubes going through the TSP were designed to be 0.320 inches. The dimensions of the geometry are summarized in Table 3.4. Figures 3.5, 3.6 and 3.7 show the schematic of the geometry of the computational model for the one row, three row and eight row cases, respectively.

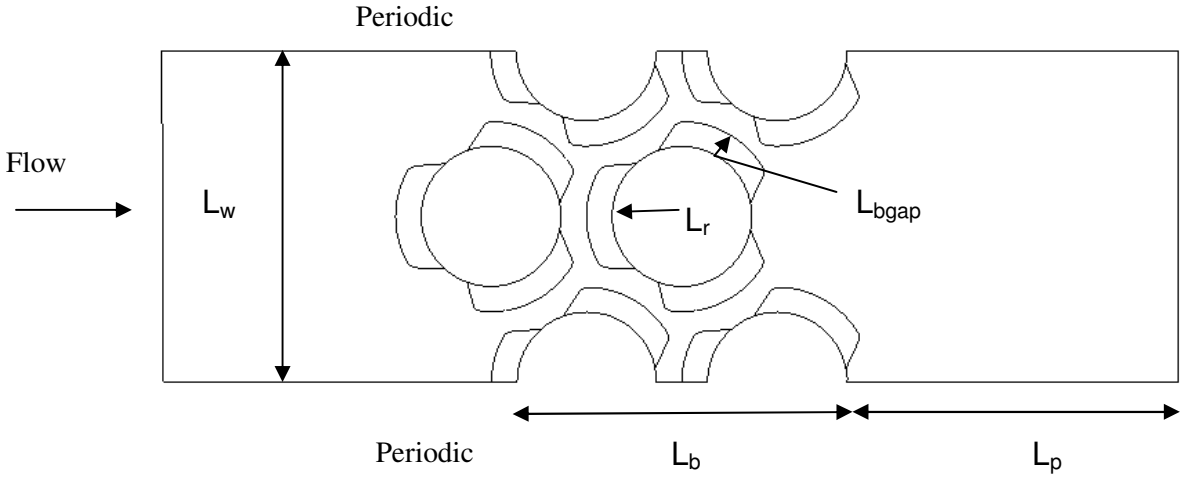

Figure 3.4: Schematic of geometry for computational model of the broached holes (4 Rows) domain

Table 3.4: Dimensions of geometry for computational model

L_b	1.514 inches
L_r (Tube radius)	0.320 inches
L_w	1.515 inches
L_p	1.428 inches
L_{bgap} (broached hole gap)	0.1139 inches

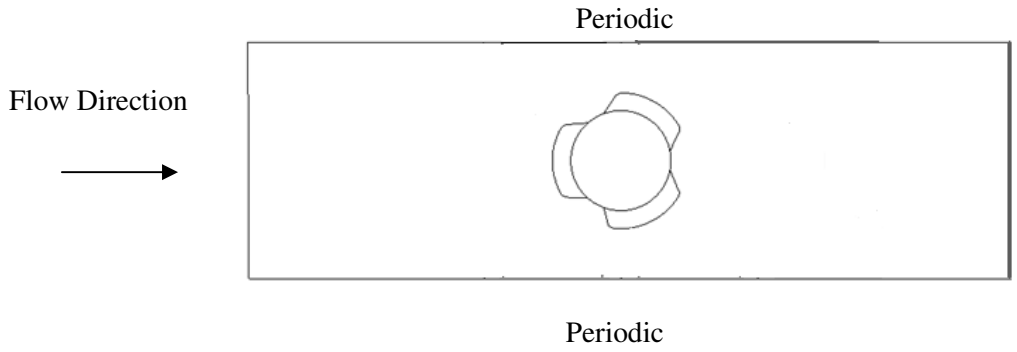

Figure 3.5: Schematic of geometry for computational model for one row of broached holes

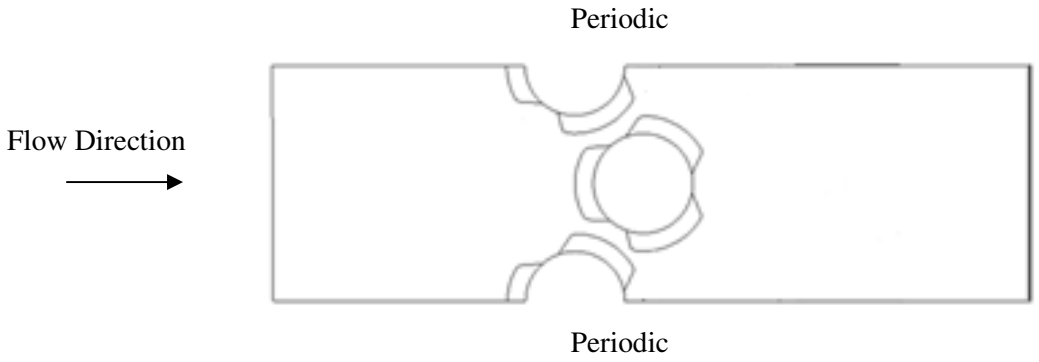

Figure 3.6: Schematic of geometry for computational model for two rows of broached holes

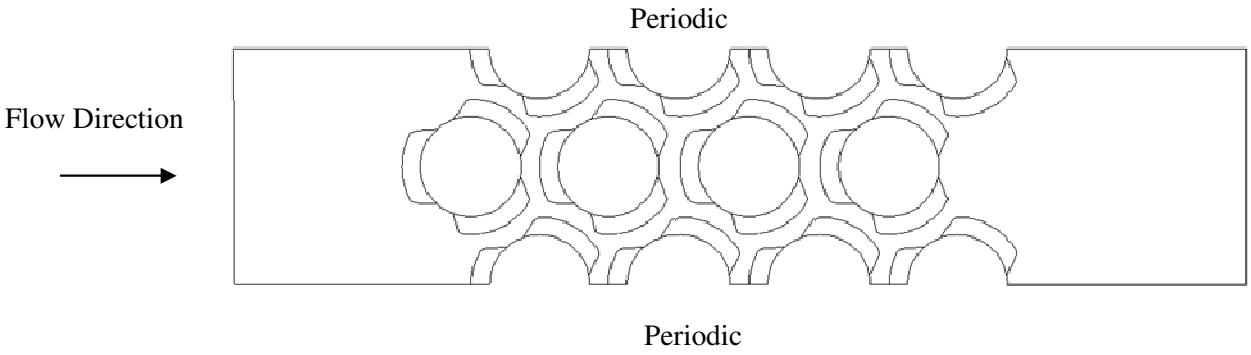

Figure 3.7: Schematic of geometry for computational model for eight rows of broached holes

3.2.2 Computational model for multiple rows of broached holes

The mesh of the model was created using Gridgen. The full computational geometry consists of an upper chamber with a water inlet and air vent connected to the bottom chamber with an air vent via the gaps in the broached hole tube supports. A total of 3 million elements are used to design the mesh for the four row case. Figure 3.8 shows a schematic of the computational model in Gridgen. Similar to the previous analysis, a fine grid was used in the vicinity of the walls and the broached holes. To model an infinite number of broached holes in the span wise direction, periodic boundary conditions were applied at either faces of the domains as shown in Figure 3.8.

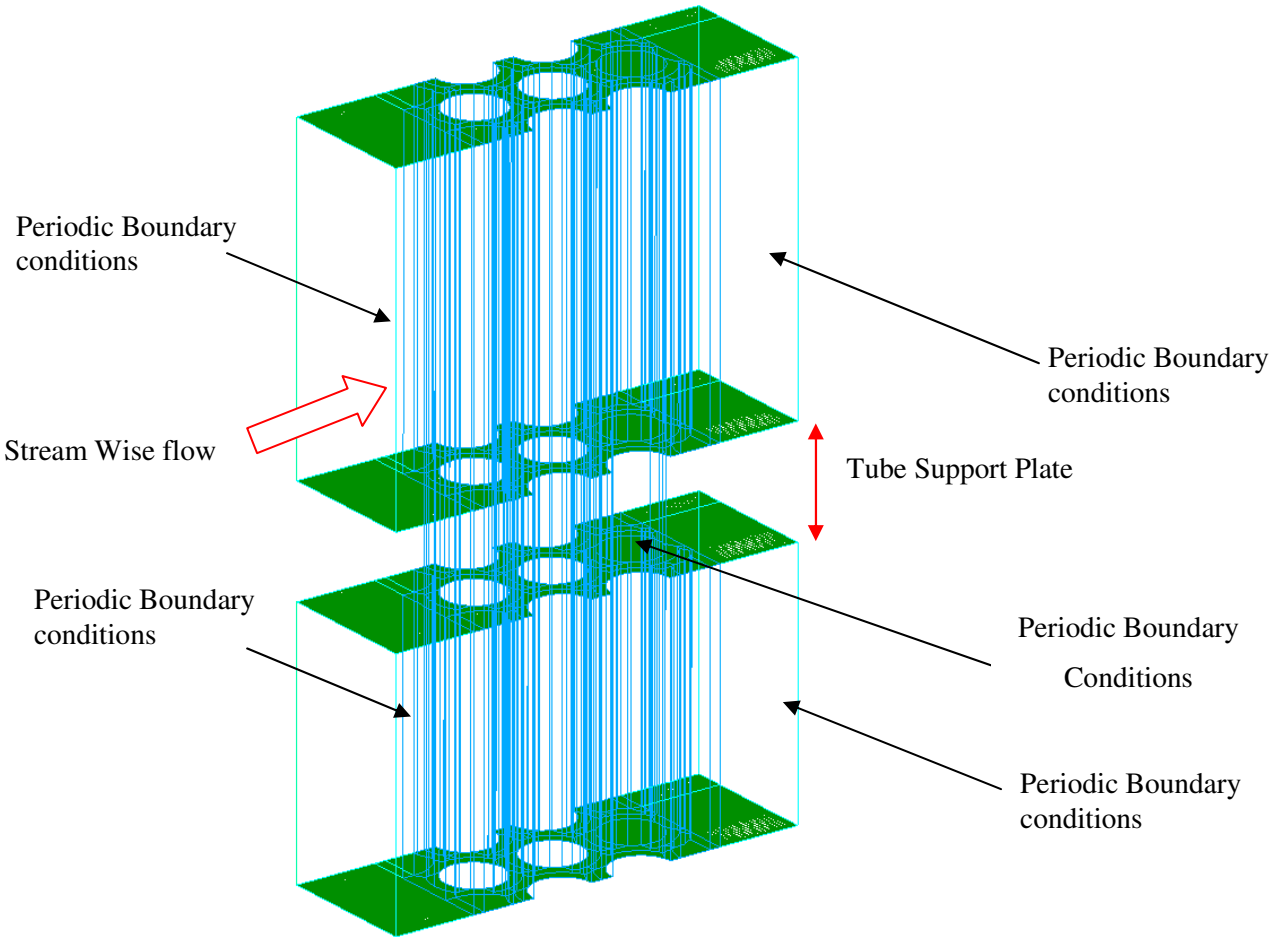

Figure 3.8: Isometric view of the computational model for the Broached holes (4 rows) analysis showing periodic boundary conditions on either side of the span wise faces

3.2.3 Procedure For Data Extraction

The procedure for each of the cases followed a similar process as the validation test. First the velocity at the inlet was calculated to replicate the Reynolds number using the continuity equation and equation 5. The area, $A_{broached}$ for each of the cases corresponded to the total area of the control broached hole leakage flow as shown in Figure 3.9. Surface planes at the outlet of the broached holes were generated to monitor mass flow until steady state was reached. In addition, the heights were measured using several surface planes in the

stream wise and span wise direction. At an average, the simulations took 120 to 168 hours to reach steady state with 7 processors.

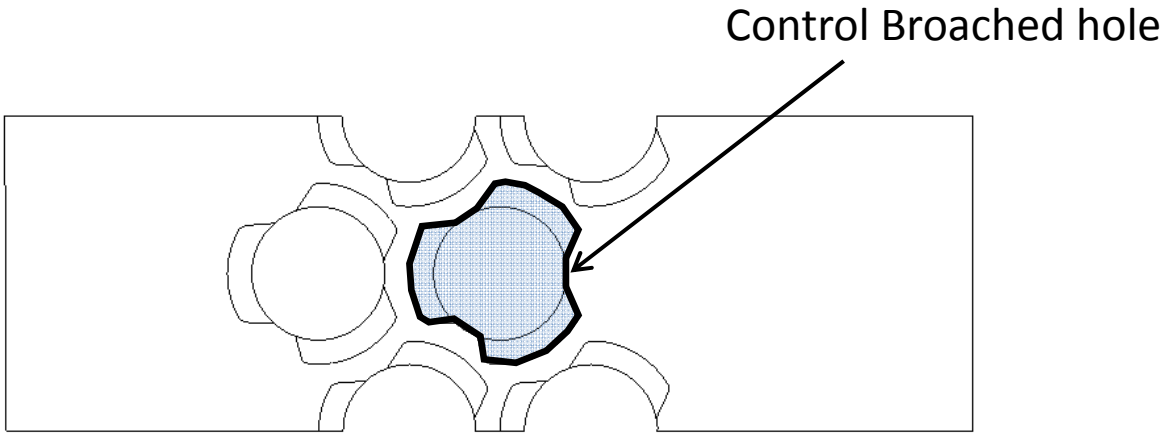

Figure 3.9: Schematic of geometry for computational model for four rows of broached holes highlighting control broached hole

3.3 Results and Analysis

The first two cases were aimed to validate the computational model used in Fluent with the experimental model. This would give sustainable evidence on the robustness and accuracy of the computational models. Validating the models ensured that they could be extended to characterize the leakage flow for a row of broached holes. It was first decided to analyze the loss coefficients for one row of broached holes and then extend to two rows. When it was found that the loss coefficient was increasing with the addition of rows in the computational domain, the analysis on four rows was carried out and ended with the computational analysis on eight rows. The results derived from each of the cases in characterizing the leakage flow for different conditions have been compared and analyzed in this section.

3.3.1 Computational model versus Experimental data Validation (single broached hole)

The first run examined was the flow with a Reynolds number of 3000. Since the geometry of the model was small it was estimated that the flow time to reach a steady state would be within a second. But because of the large grid size it was computationally intensive to run each of the cases. The simulation took 24 hours to reach 0.1 seconds of flow time and about a week (168 hours) to reach steady state at 0.98 seconds flow time with six processors. Figure 3.10 shows the plot of the mass flow of the water with time. It is evident that after 0.9 seconds of flow time the variation in the mass flow of water reduces and the system reaches equilibrium. Expecting the same dynamics of fluid flow as the bypass flow analysis, it was decided to proceed with the calculations and results analysis. But at examining the broached hole closely it was found that it was not being completely filled. There were voids present in the broached hole. The cross sectional planes of the broached holes showed that there was smooth and defined flow of fluid through the broached hole. It was observed that the water flowing through the hole was separated from air by a relatively smooth interface. In addition there was a low pressure circulation of air in the void. Figure 3.11 shows a figure of the contours of volume fraction in the broached hole through the tube support plate. The blue color in the contour plot represents air and the red color represents water. This figure gives a good visual representation of the smooth flow of water in the broached hole. In the void, air from the bottom sector is drawn up into the broached hole in a recirculating pattern. These voids are seen clearly at the broached hole outlet as shown in Figure 3.12. Figure 3.13 shows an isometric view of the contour of volume fraction. The plot shows that the level of water is even at steady state and that there are voids present in the broached holes. In addition, the outlet vent at the bottom tank removes water and therefore the mass fraction at the bottom tank is very low.

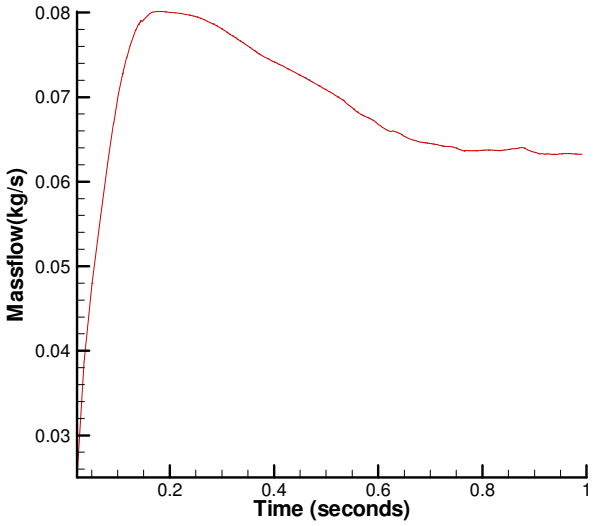

Figure 3.10: Plot of mass flow versus flow time for broached hole case 1(Re=3000)

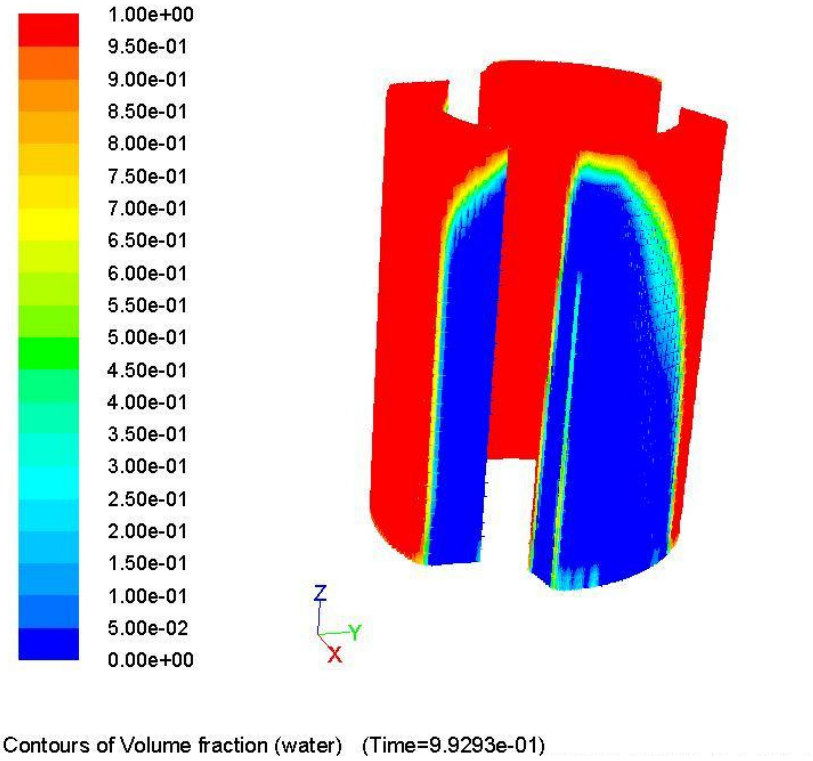

Figure 3.11: Contours of volume fraction plot of broached hole in TSP (Re=3000)

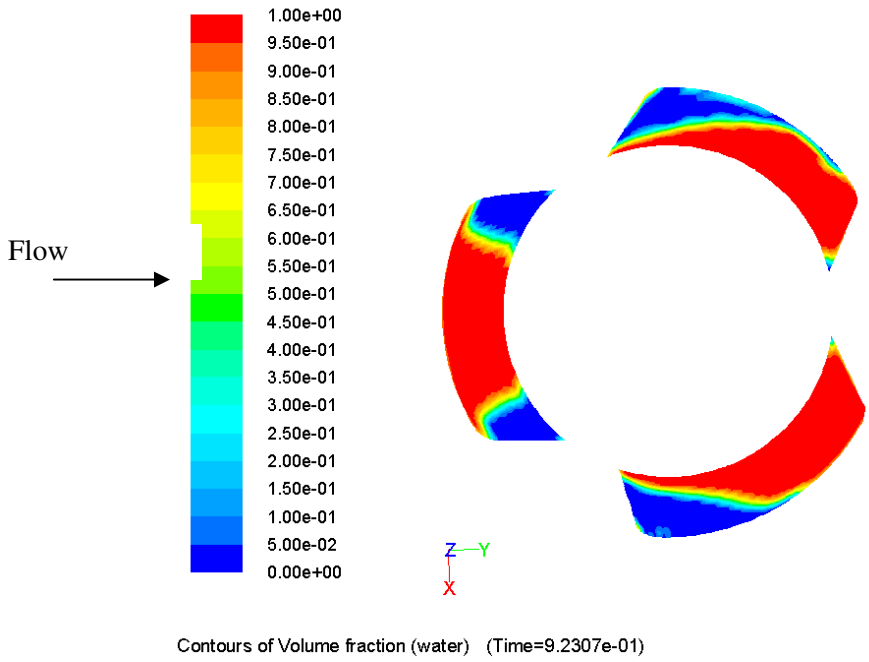

Figure 3.12: Contours of volume fraction plot of broached hole outlet surface plane (Re=5000)

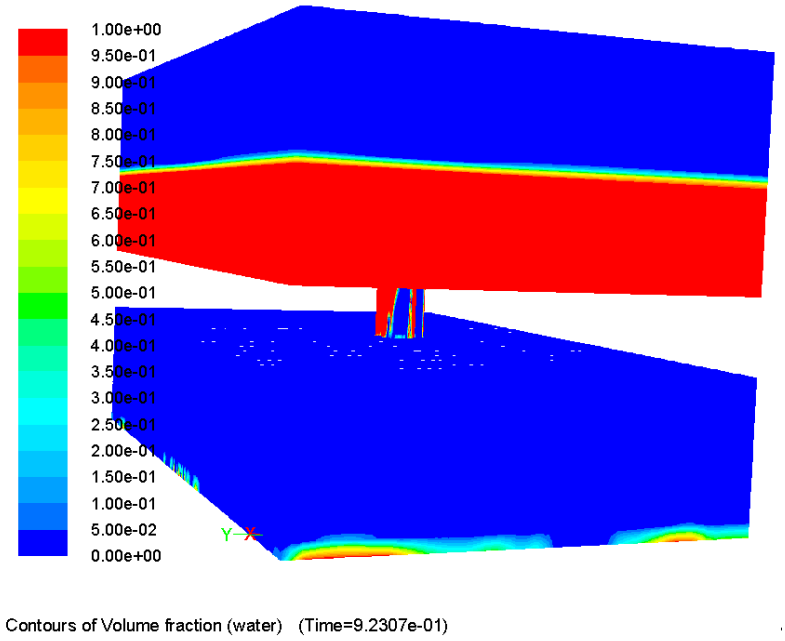

Figure 3.13: Contours of volume fraction plot of the computational model (Re=5000)

From the visualizations shown above it is certain that there are voids present in the broached holes for the range of Reynolds number being examined. To take these voids into consideration two separate calculations have been made in the derivation of the loss coefficients. In the first case the superficial velocity of water in the hole is calculated. This is defined as the velocity of a fluid in a pipe, conduit, column, etc. in the absence of packing or obstruction. The superficial velocity is calculated using equation 8:

$$V_{broached} = \frac{\dot{M}}{\rho A_{broached}} \tag{8}$$

where $\dot{M}$ is the mass flow of water through the mass flow surface plane and ρ is the density of the water which taken as 998 kg/m^3

Here the loss coefficient is calculated using equation 9 as shown:

$$k_{broached} = \frac{2gh_0}{(V_{broached})^2} \tag{9}$$

In the second method, the mass flow rate is adjusted to account for the voidage as in

$$V_{broached} = \frac{\dot{M} / mf_{water}}{\rho A_{broached}} \tag{10}$$

where mf_{water} is the area-weighted mass fraction of water

Table 3.5 summarizes the data obtained from the computational model with the presence of voids. Table 3.6 summarizes data that is adjusted for voids. It is important to note that in the case where the model for broached hole is adjusted for voids, the actual velocity calculated increases and so does the Reynolds number. Thus the loss coefficient calculated reduces because the height remains the same. It is noted that data in Table 3.5 shows the loss coefficient differing by about 5%. Whereas when the loss coefficients are adjusted for voids, they increase as the Reynolds number increases. This trend is similar to the bypass flow analysis.

Table 3.5: Data from computational model for broached with voids

Reynolds No.	Average height(m)	Loss Coefficient
2004	0.0205	2.08
2512	0.0320	2.12
2879	0.0416	2.09
3300	0.0546	2.12
3970	0.0737	1.95

Table 3.6: Data from computational model for broached hole adjusted for voids

Reynolds No.	Average height(m)	Loss Coefficient
3000	0.0205	0.806
3676	0.0320	0.974
4200	0.0416	1.00
4608	0.0546	1.07
5102	0.0737	1.18

For validation purposes, the distribution of the loss coefficients over the Reynolds number range was evaluated along with experimental data. Figure 3.14 shows the distribution of the loss coefficients for both cases compared to the experimental data. For the first case in which no correction is made for voids, the loss coefficient averages out to 2.07. The other values deviate by 0.4% to 5.9% from this average value. Visual inspection in the experimental setup could not identify the presence of voids in the broached holes and therefore the experimental loss coefficients are lower than the computations calculations with voids. The experimental values show that loss coefficient of the broached hole configuration qualitatively stay constant with Re and level off at K=1.2. These values vary by 5 % over a Reynolds number range of 4500 to 6000. The adjusted (correcting for the void fractions) computational loss coefficients are in agreement with the experimental values. Additional computational cases were also run by changing model constants such as the surface tension between water and air, and changing the contact angle of the fluid with respect to the walls in the model. It was found that the results were insensitive to these changes and the voids were present with the loss coefficients remaining the same.

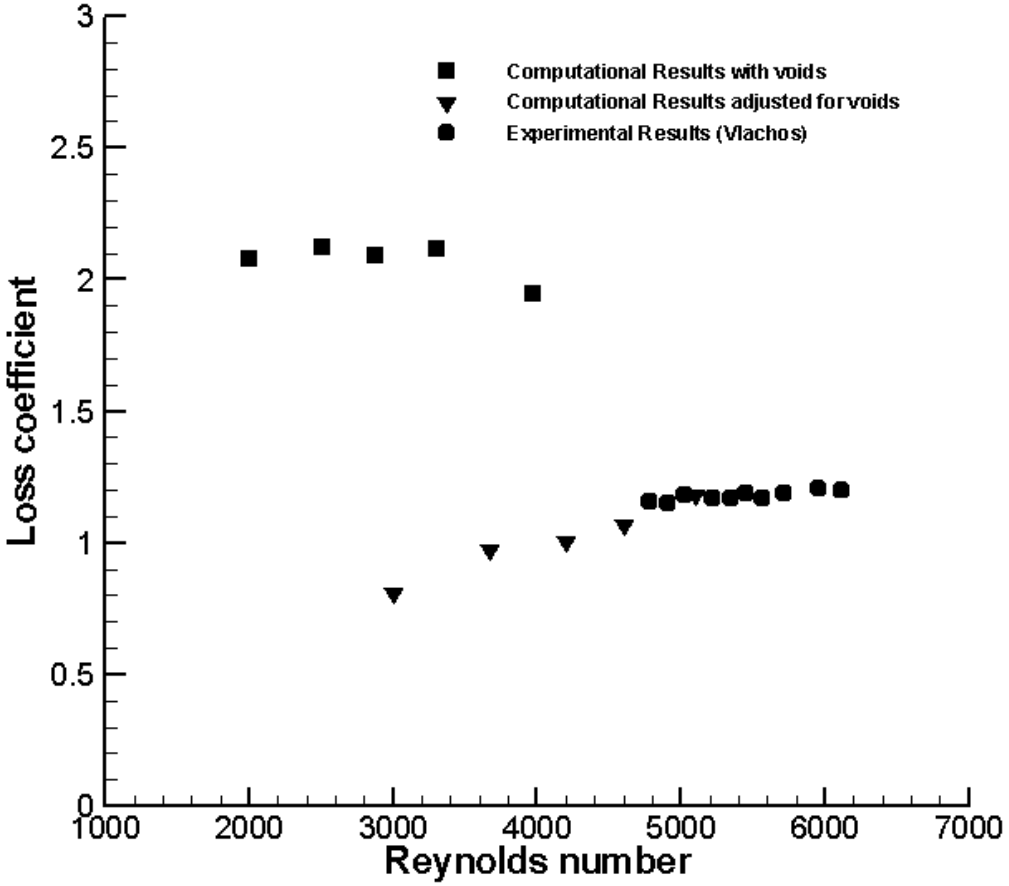

Figure 3.14: Plot of Reynolds number versus loss coefficient for computational results compared with experimental results for one broached hole validation case

3.3.2 Computational model versus Experimental data Validation (Five broached holes)

This computational model was designed for further validation purposes. The geometry of the model was relatively larger than the previous one and therefore took twice the amount of time. Each simulation took about two weeks (336 hours) to reach an estimated steady state flow time of 2 to 5 seconds with 8 processors with about 16 GB of memory. Figure 3.15 shows the plot of the mass flow of the fluid at the outlet of the broached holes with time. The plot shows that after three seconds the fluctuation of the mass flow reduces and the system reaches a steady state. Information from the previous case gave reason to believe that there would be voids in the broached holes. Despite using multiple broached

holes, the voids were present over the range of Reynolds numbers varying from 2000 to 4500. Figure 3.16 shows the contour of volume fraction plots of the five broached holes at the outlet. It was also noted that the volume fraction of the voids reduced as the Reynolds number of the inlet flow increased. This phenomenon is also evident in many of the cases done for the multiple rows and is explained thoroughly in the following chapter sections. Figure 3.17 shows the isometric view of the contour plot of the computational model. It highlights the steadiness of the water level at a steady state and shows the concept of the flow system of fluid from the inlet to the outlet boundary conditions.

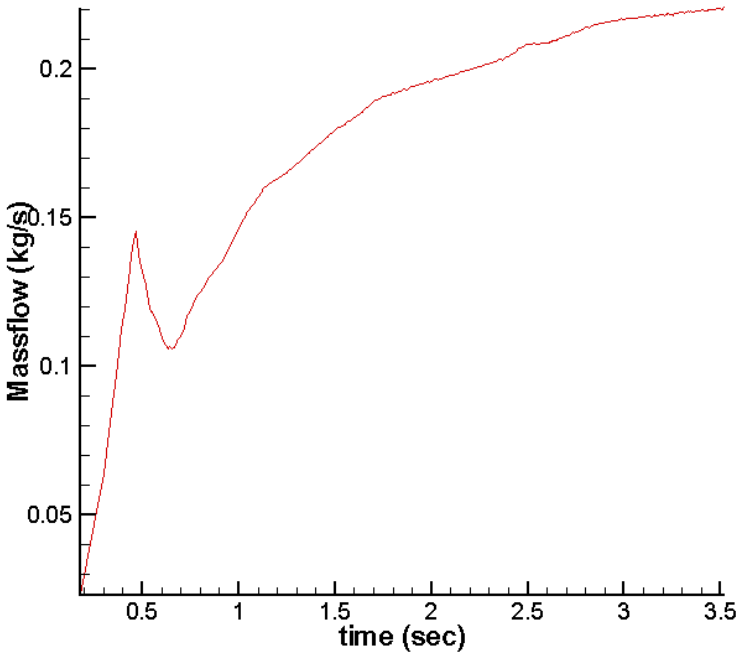

Figure 3.15: Plot of mass flow versus flow time for 5 broached holes case (Re=3000)

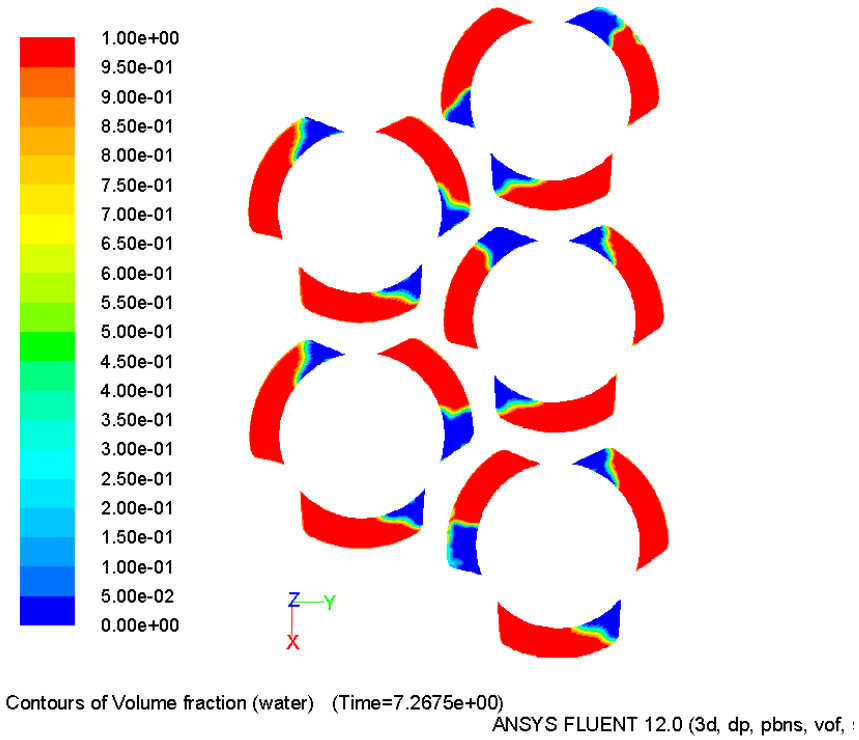

Figure 3.16: Contours of volume fraction plot of five broached holes outlet surface plane (Re=3000)

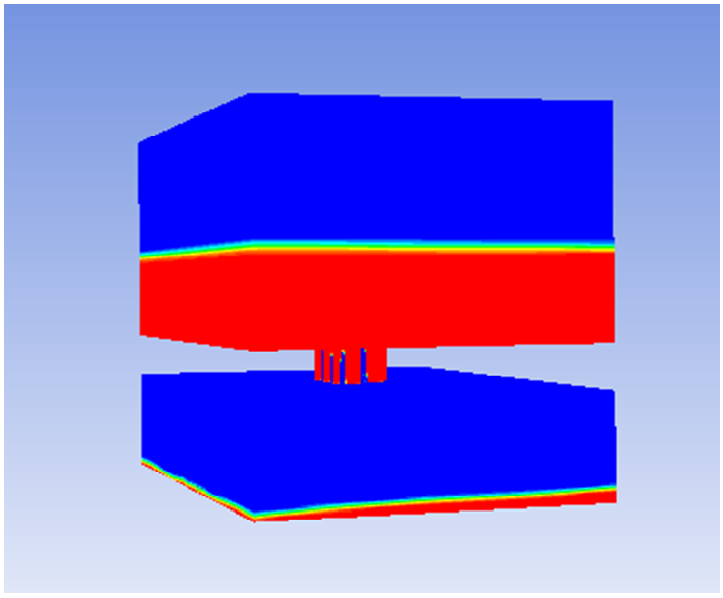

Figure 3.17: Contours of volume fraction plot of the computational model (Re=3000)

To take into consideration the voids present two separate calculations were made in the calculation of the loss coefficient. Equation 8 and 9 were used to calculate the loss coefficient based on voids present and equation 9 and 10 were used to calculate the loss coefficient when adjusted for voids. Table 3.7 summarizes data with the existence of voids and Table 3.8 summarize data that is attuned for voids. It is noticeable that the loss coefficient values in Table 3.8 are lower than those in 3.7 because the voids are considered and the height of the water remains the same. The trend from the data where the calculations have been adjusted for voids show that as the Reynolds number increases so does the loss coefficient.

Table 3.7: Data from computational model for broached holes with voids

Reynolds No.	Average height(m)	Loss Coefficient
1905	0.0270	3.098
2779	0.0454	2.450
3573	0.0625	2.040

Table 3.8: Data from computational model for broached holes adjusted for voids

Reynolds No.	Average height(m)	Loss Coefficient
3043	0.0270	1.215
3781	0.0454	1.323
4384	0.0625	1.355

Similar to the process above, the distribution of loss coefficients from Tables 3.8 and 3.7 were evaluated along with experimental data. Figure 3.18 shows this distribution of data compared with experimental results. The computational results with voids have a similar negative gradient trend like the data in the previous validation model. Again visual inspection of the experiments failed to identify any voids present in the broached holes and therefore experiment values are much lower than the loss coefficients data with voids. However when the calculations for the loss coefficients are adjusted for voids the computation data matches up well with the experiment data. The values shown in Figure 3.17 are within 5% of each

other across the Reynolds number range of 1000 to 5000. These comparisons provide validation and give confidence that these models can be expanded on to find the loss coefficient values of multiple rows of broached holes and that the results attained are accurate and can be implemented for the 1/8th sector of EOTSG computational model.

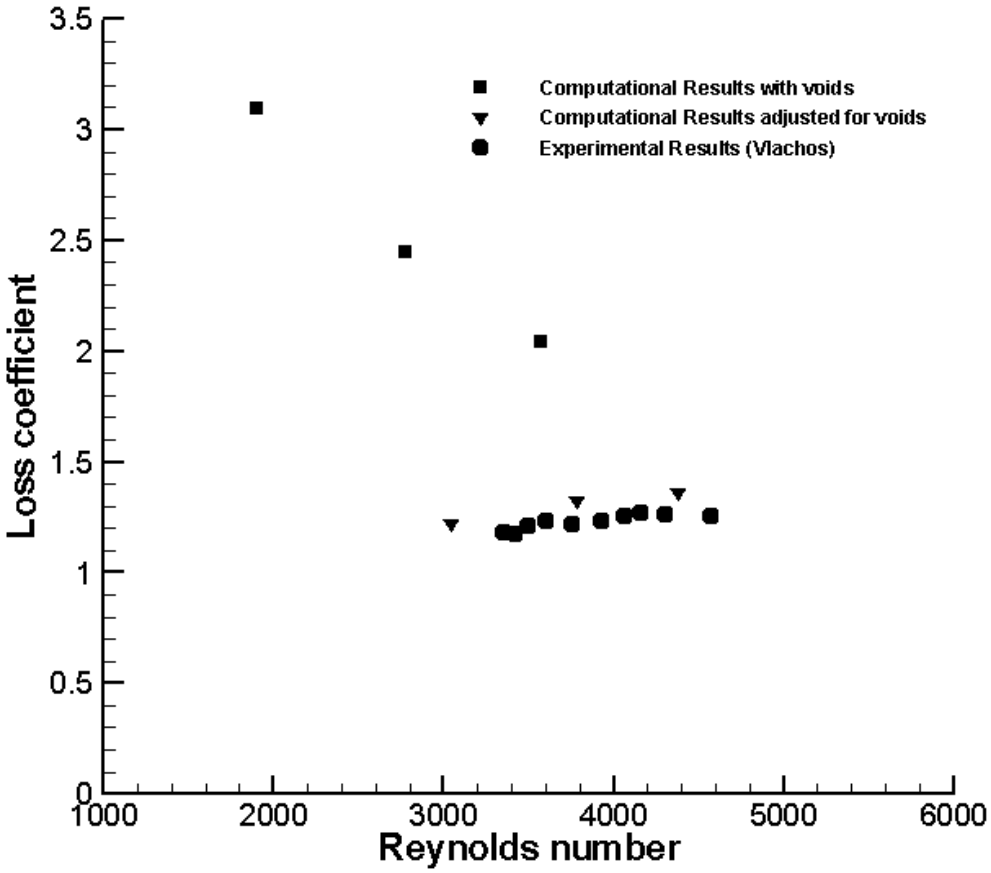

Figure 3.18: Plot of Reynolds number versus loss coefficient for computational results compared with experimental results for five broached holes validation case

3.3.3 Computational Results for one row of broached holes

It was necessary to carry out the computational analysis on a row of an infinite number of broached holes to view the losses and resistance the tube rows would present to the flow. Similar to the validation test, it was decided to calculate two separate loss coefficients using the superficial velocity and actual velocity of water at the broached hole

outlet to account for the voids. Figure 3.19 shows the contours of volume fraction plot at the outlet of one of the broached hole. Calculations showed that for this case (Reynolds number 3265) the void fraction at the outlet of the broached hole is 0.3205. Equations 8 and 9 were used to calculate the loss coefficient using the superficial velocity and equation 8 and 10 were used to calculate the loss coefficient using the actual velocity of water. Table 3.9 summarizes values of the loss coefficient for the computational model with voids and Table 3.10 summarizes data of the model where the broached holes are adjusted for the voids. This test was carried out to view the implications on the loss coefficient and therefore just two Reynolds numbers were considered. Figure 3.20 shows the plot of these two cases and the data from the validation case. It is interesting to note that the loss coefficient values for the computational results adjusted for voids are within 10% of the one hole result. We can conclude from this that putting more holes in the span wise direction does not change the loss coefficient by a large amount. Next we consider the effect of multiple rows.

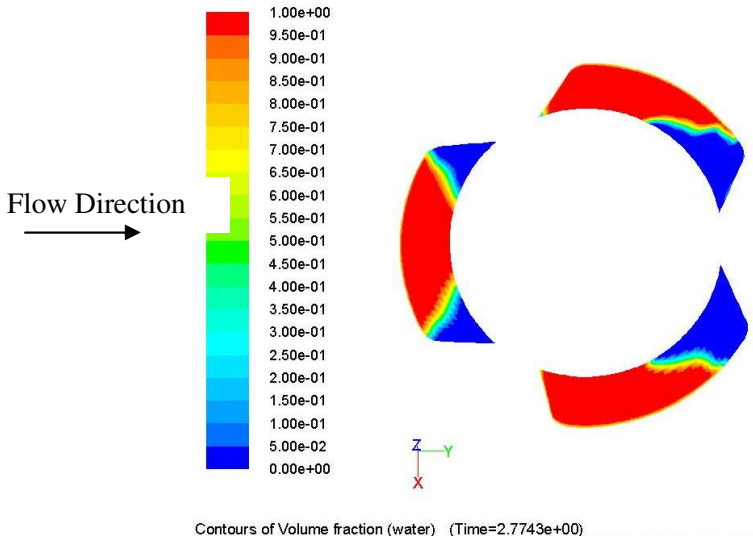

Figure 3.19: Contours of volume fraction plot for 1 row of broached holes(Re=2000)

Table 3.9: Data from computational model for 1 row of broached holes with voids

Reynolds No.	Average Height(m)	Loss coefficient
2000	0.0172	1.8
2500	0.0320	2.12
3250	0.0336	2.26

Table 3.10: Data from computational model for 1 row of broached holes adjusted for voids

Reynolds No.	Average Height(m)	Loss coefficient
3295	0.0172	0.661
4000	0.0320	0.933
4750	0.0336	1.12

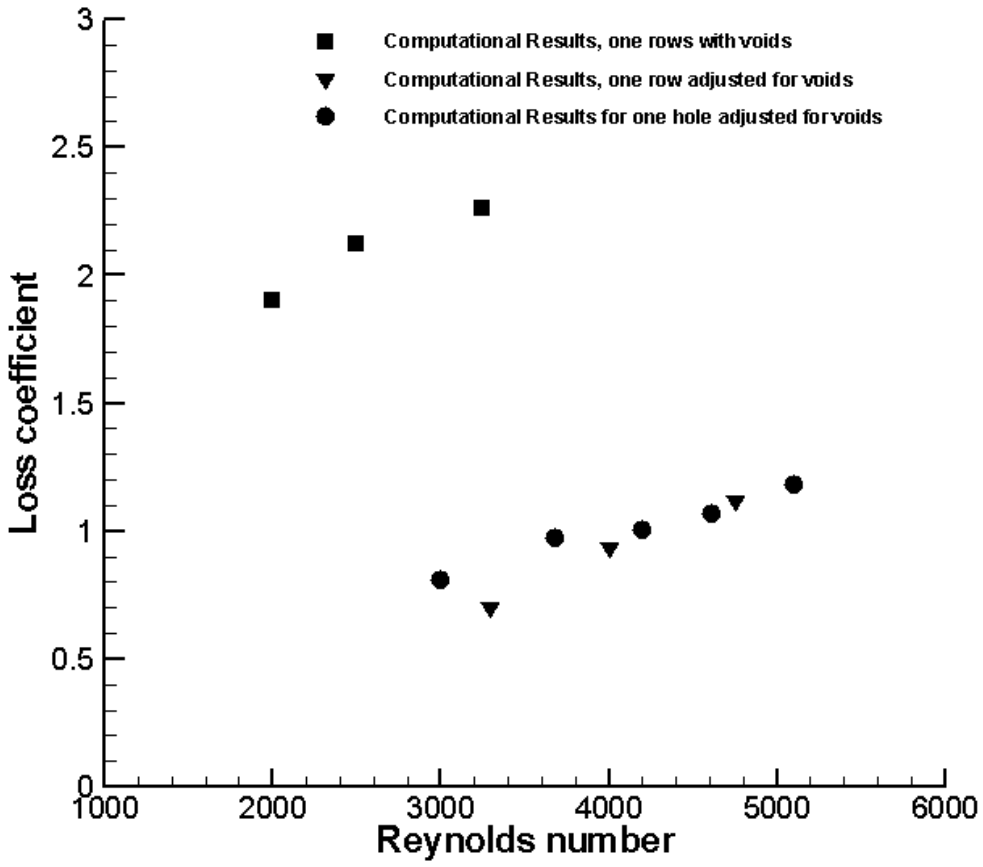

Figure 3.20: Plot comparing computational results for 1 row of broached holes with voids and results adjusted for voids

3.3.4 Computational results for two rows of broached holes

Having derived the losses for one row of broached holes the same procedure was carried out for two rows of broached holes. This case would provide information on the impact of additional rows on the loss coefficient of the control row of the broached holes. Similar to the procedure for the previous cases, two calculations were done to predict the loss coefficients using the superficial velocity and actual velocity of water at the outlet of the broached hole. Figure 3.21 shows the contours of volume fraction plot at the outlet of the broached holes at a Reynolds number of 2000. When compared to Figure 3.19 for one row of broached holes, the void fraction for this case is about 60% less. This observation leads to the conclusion that for the same Reynolds number, the voids reduce as more rows are included in the calculation. Equations 8 and 9 were used to calculate the loss coefficient using the superficial velocity and equation 8 and 10 were used to calculate the loss coefficient using the actual velocity of water. Table 3.11 summarizes data of the loss coefficients for the computational model with voids and Table 3.12 summarizes the values of the model in which the flow is adjusted for voids. It is observed that as the Reynolds number increases, the voids decrease and as a result the loss coefficient between the two methods converge. As shown in Tables 3.11 and 3.12, the values of the loss coefficient at Reynolds number of 6000 only differ by 2.16%. The average loss coefficient of the computational results adjusted for voids is 2.20 and the average value for the results with voids is 2.67. This case showed that the loss coefficient increased by 31.5% with the addition of one row of broached holes. Therefore further investigation on the impact of additional rows on the loss coefficient was performed.

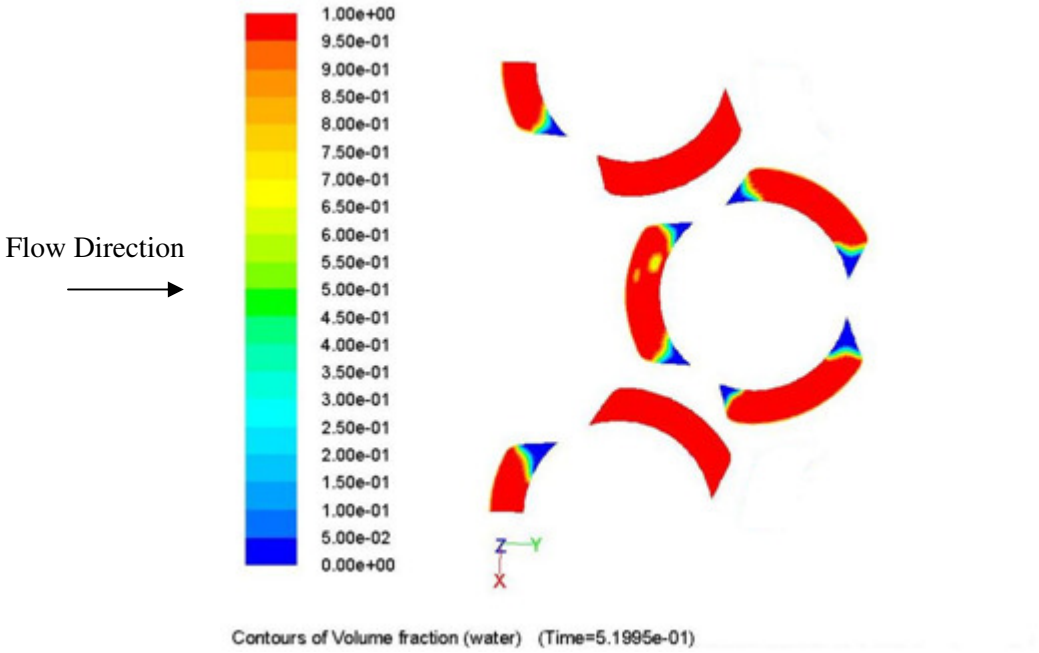

Figure 3.21: Contours of volume fraction plot for two rows of broached holes(Re=2000)

Table 3.11: Data from computational model for 2 rows of broached holes with voids

Reynolds number	Average height(m)	Loss coefficient
2000	0.0246	2.81
2387	0.0430	3.15
4915	0.145	2.50
5975	0.190	2.22

Table 3.12: Data from computational model for 2 rows of broached holes adjusted for voids

Reynolds number	Average height(m)	Loss coefficient
2297	0.0246	1.936
2652	0.0430	2.300
5015	0.145	2.401
6035	0.190	2.172

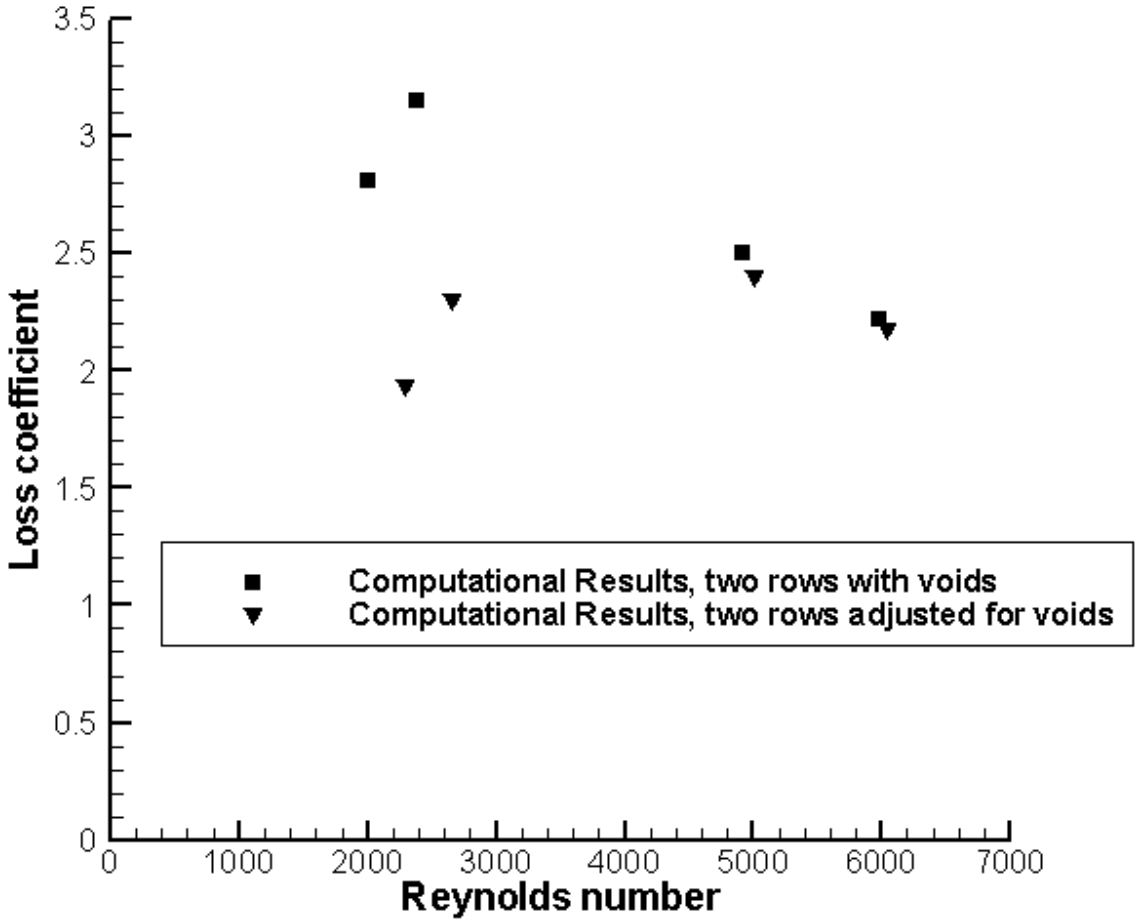

Figure 3.22: Plot comparing computational results for 2 rows of broached holes with voids and results adjusted for voids

3.3.5 Computational Results for four rows of broached holes

Due to the fact that the values of the loss coefficients increased with the number of rows it was decided to create a computational model that would simulate four rows of broached hole, using the flow Reynolds numbers provided in Table 3.3 as a guide. Each of the simulations took 168 hours to 240 hours with 8 processors to reach steady state depending on the speed of the flow. As expected, in most of the cases, the broached holes did not fill up completely with water. However, it was noticed that as the Reynolds number of the flow increased, the void fraction reduced. Figure 3.23 and 3.24 show the contour of volume fraction plot at the outlet of the broached holes for a flow of Reynolds number of

2000 and 4000. It is evident that as the velocity of the fluid increases the void fraction reduces. A possible reason to this behavior could be the increase in hydrostatic pressure with the higher Reynolds number flow that forces the liquid through the holes, preventing voids. Equations 8, 9 and 10 were used to calculate the loss coefficients on the control row, as shown in Figure 3.9, of the broached holes with the superficial velocity and actual velocity. This ensured that the loss coefficients calculated are from the effect of the two preceding rows. Table 3.12 summarizes the data of the loss coefficient for the computational model with voids and Table 3.13 sums up the data of the model where the broached holes are adjusted for the voids. As expected the loss coefficients are higher compared to the models for the one and two rows. This is caused by the introduction of more rows of tubes and broached holes in the system. In this case, the fluid must overcome a larger resistance in the presence of more tubes as the fluid navigates through a more complex geometry than in the previous cases. Figure 3.25 plots these results. It can be seen that the value of the loss coefficients calculated with both models increase to a value ranging from 3.9 to 4.0. In addition the deduction that as the Reynolds number increases, the voids reduce, is evident as the two curves converge to a defined loss coefficient value.

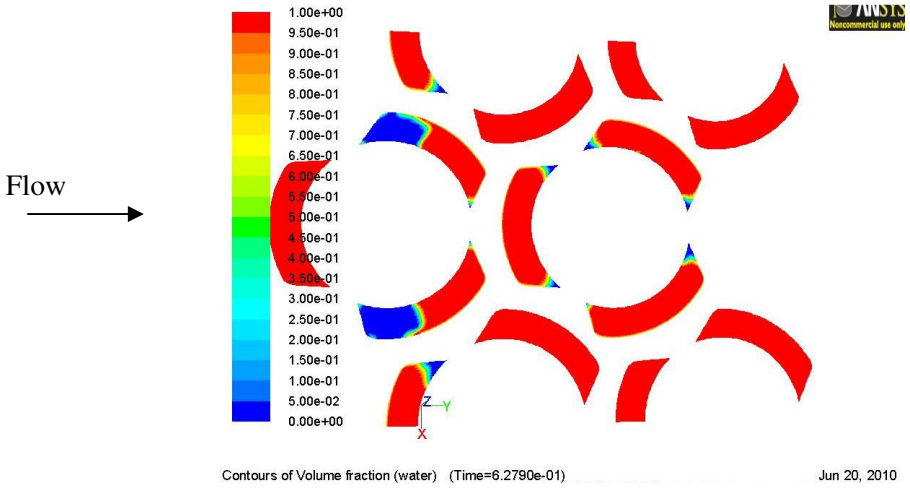

Figure 3.23: Contours of volume fraction plot for 4 rows of broached holes (Re=2000)

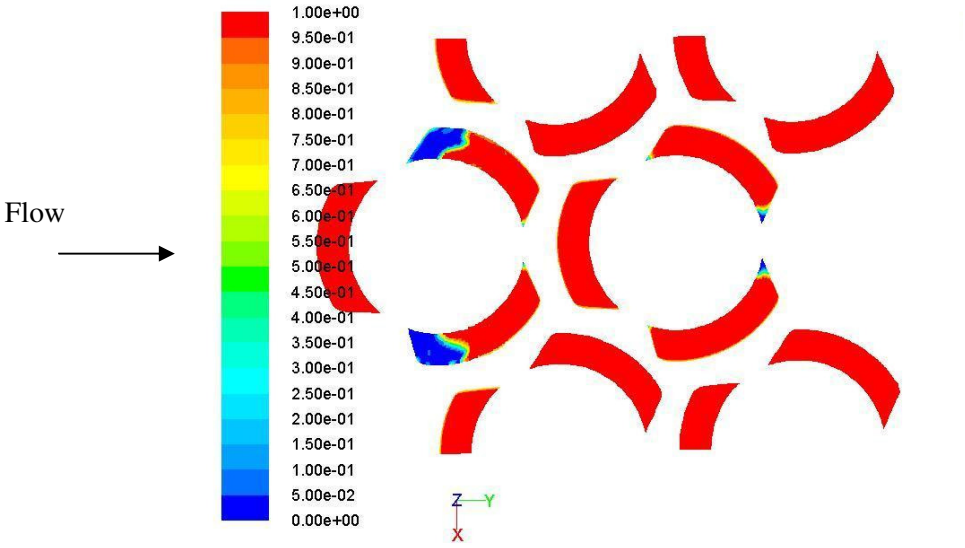

Figure 3.24: Contours of volume fraction plot for 4 rows of broached holes (Re=4000)

Table 3.12: Data from computational model for 4 rows of broached holes with voids

Reynolds number	Average height(m)	Loss coefficient
2414	0.0736	4.30
2891	0.0800	3.99
3478	0.1106	3.81
3981	0.1500	3.94

Table 3.13: Data from computational model for 4 rows of broached holes adjusted for voids

Reynolds number	Average height(m)	Loss coefficient
2500	0.0736	3.60
3000	0.0800	3.67
3600	0.1106	3.90
4020	0.1500	3.45

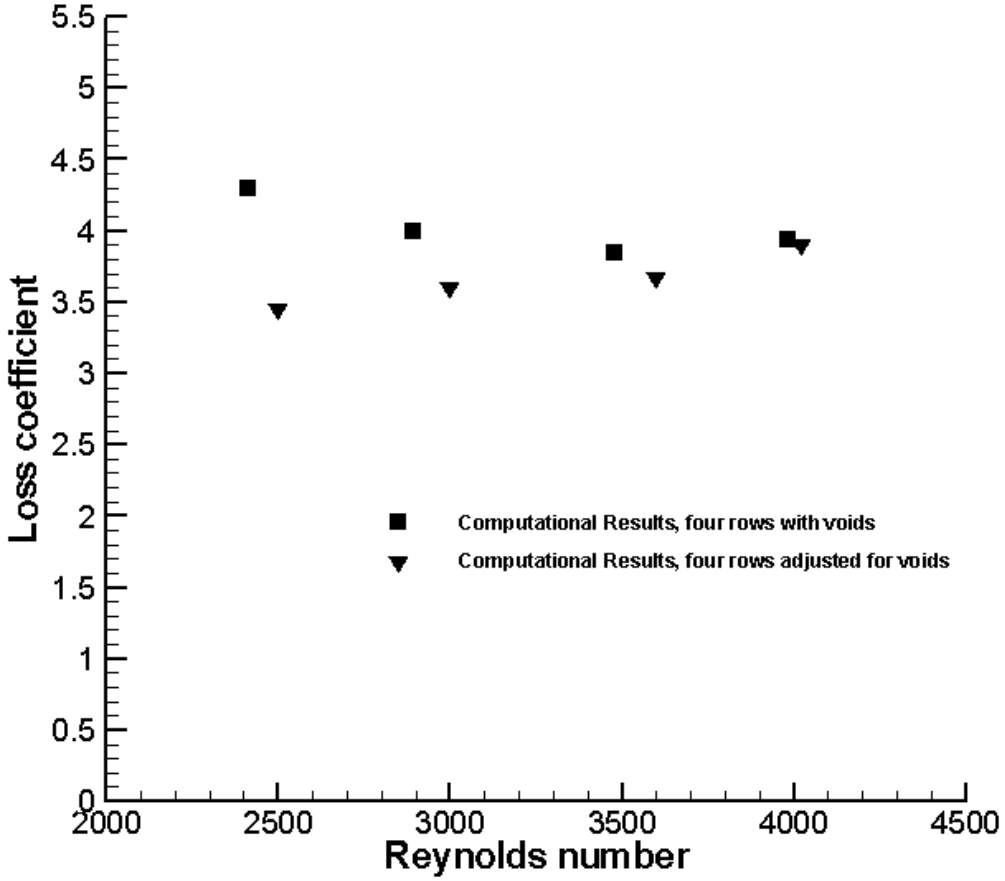

Figure 3.25: Plot comparing computational results for 4 rows of broached holes with voids and results adjusted for voids

3.3.6 Computational results for eight rows of broached holes

The increment of the loss coefficients between the two rows and four rows was approximately 60%. This gave motivation to run additional cases on eight rows of broached holes. Calculations on this case helped evaluate the impact of additional rows on the loss coefficient. Due to the larger number of rows in these cases, the computational model consisted of 6 million elements. Each of the simulations took 336 hours to 504 hours with 8 processors to reach steady state depending on the velocity of the flow. Since the cases were computationally expensive, the three cases examined were of Reynolds number flow of 1084, 3318 and 4599. This range of cases was sufficient for comparison purposes with results from

the other rows. The results have the same trend as previous cases; there were voids present in the broached holes and the voids reduced as the velocity of the flow increased. As the Reynolds number of the inlet flow increases so does the hydrostatic pressure of the fluid, causing the fluid to be forced through the holes reducing voids. This is evident by comparing Figures 3.26 and 3.27. It can be seen in Figure 3.26 that when the Reynolds number flow is close to 1000, the voids are prominent in most locations. But with the increase in Reynolds number these voids are much weaker as shown in Figure 3.27. Equations 8, 9 and 10 were used to calculate the loss coefficients on the control row of the broached holes as highlighted in Figure 3.26. The calculations assured that the loss coefficient values resulted from the effects of the preceding six rows. Table 3.14 summarizes data of the loss coefficient with voids and Table 3.15 highlights data of the model where the broached holes are adjusted for the voids. Figure 3.28 shows the plot of these data. It is evident that the values of the loss coefficients calculated with both models increases to a value ranging from 3.9 to 4.2. These results are similar to the loss coefficients from the four rows but are much higher than the two and one rows.

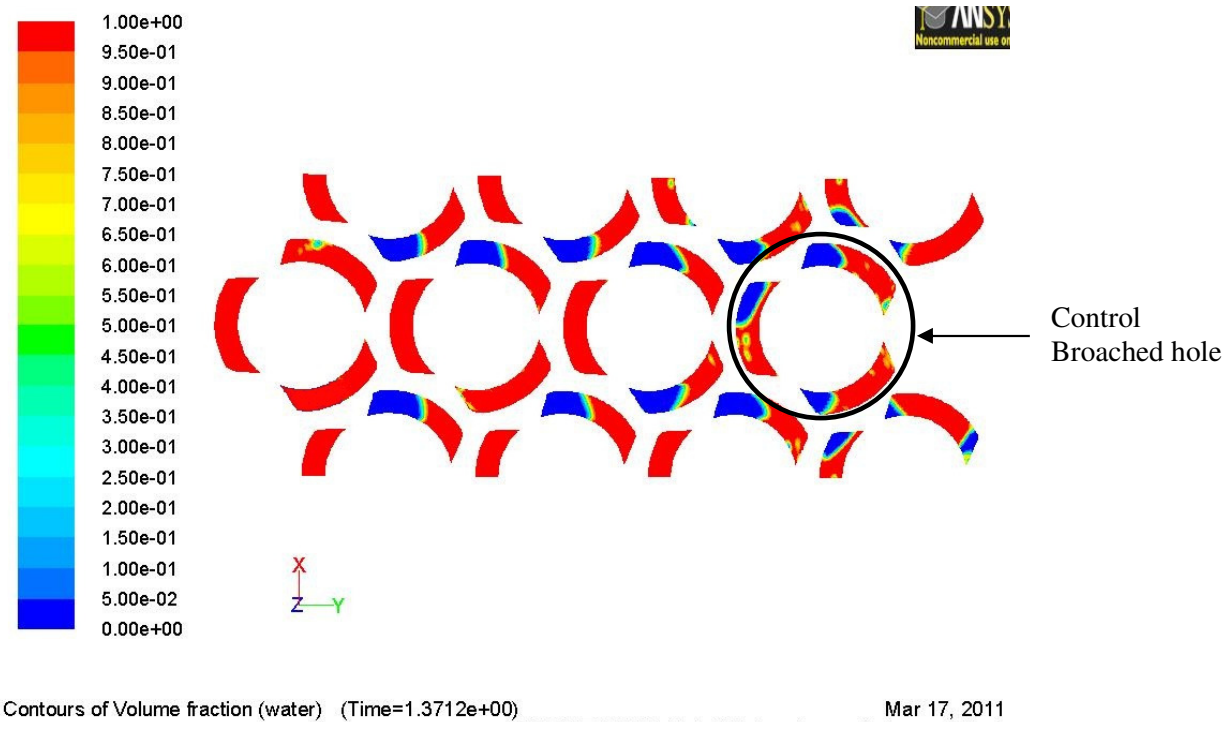

Figure 3.26: Contour of volume fraction plot for 8 rows of broached holes (Re=1084)

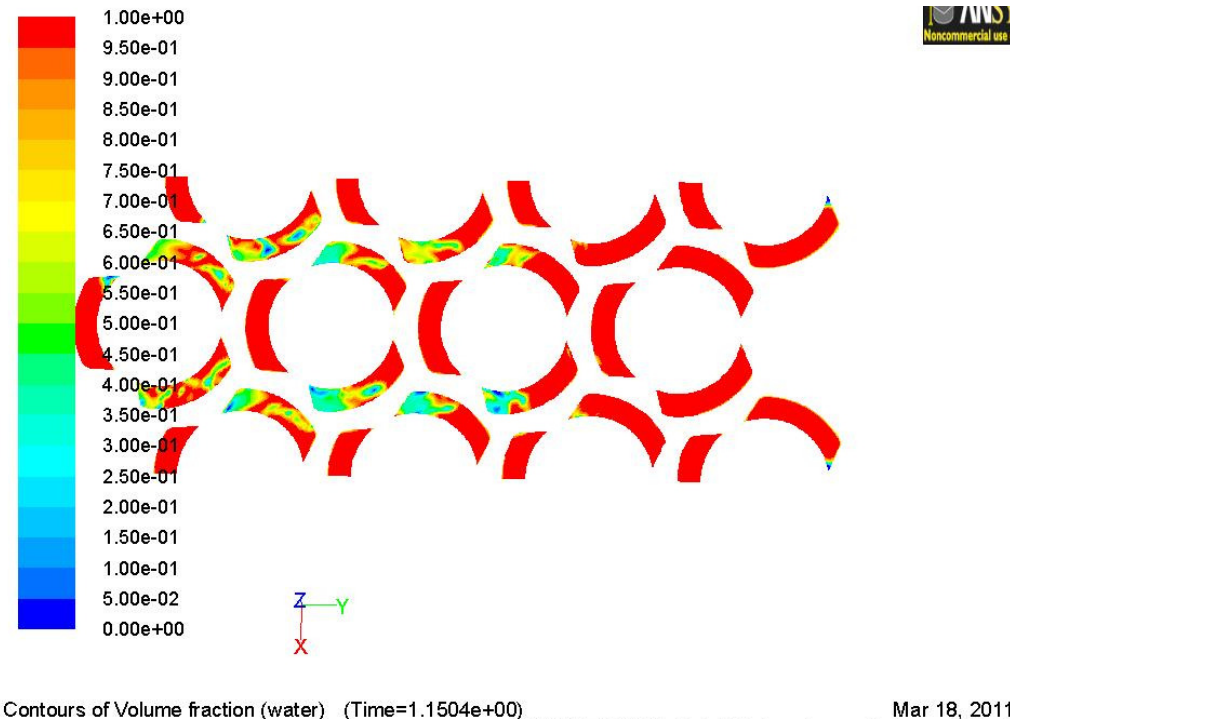

Figure 3.27: Contour of volume fraction plot for 8 rows of broached holes (Re=4599)

Table 3.14: Data from computational model for 8 rows of broached holes with voids

Reynolds number	Average height(m)	Loss coefficient
1084	0.0118	4.18
3318	0.1005	3.80
4600	0.1034	4.12

Table 3.15: Data from computational model for 8 rows of broached holes adjusted for voids

Reynolds number	Average height(m)	Loss coefficient
1550	0.0118	3.47
3320	0.1005	3.79
4590	0.1034	4.11

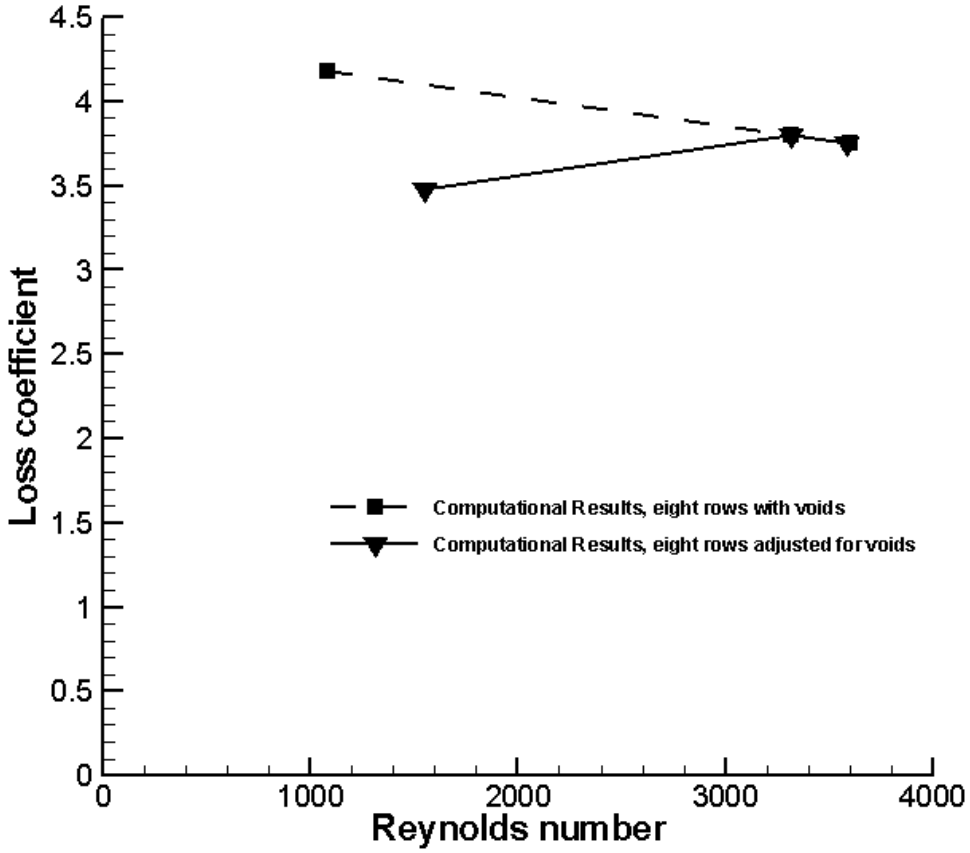

Figure 3.28: Plot comparing computational results for 8 rows of broached holes with voids and results adjusted for voids

3.4 Significance of Results for broached holes

This section of the chapter addresses the results from the analysis done on multiple rows of broached holes and arrives at a solution for the loss coefficient that needs to be implemented in the $1/8^{th}$ sector of EOTSG computational model. The average loss coefficients when adjusted for voids for the first and second row of broached holes differ by 100 % and the average loss coefficient between the two rows and four rows is 60 %. However this was not the case when the loss coefficient results for 8 rows were calculated. The results of the loss coefficients when adjusted for voids between the eight rows and four rows only differed by 5 % to 10 %. The 8 row case showed evidence that after four rows the loss coefficient converged to a definite value. A reasonable explanation is that the after four rows the fluid flow is fully developed. Figure 3.29 shows the plot of the results for the multiple rows of broached holes. From the figure it can be determined that the loss coefficient asymptotes to an average value of 4.0. Since the $1/8^{th}$ sector of the EOTSG contains multiple rows, this loss coefficient is employed for further calculations in the $1/8^{th}$ sector for each broached hole.

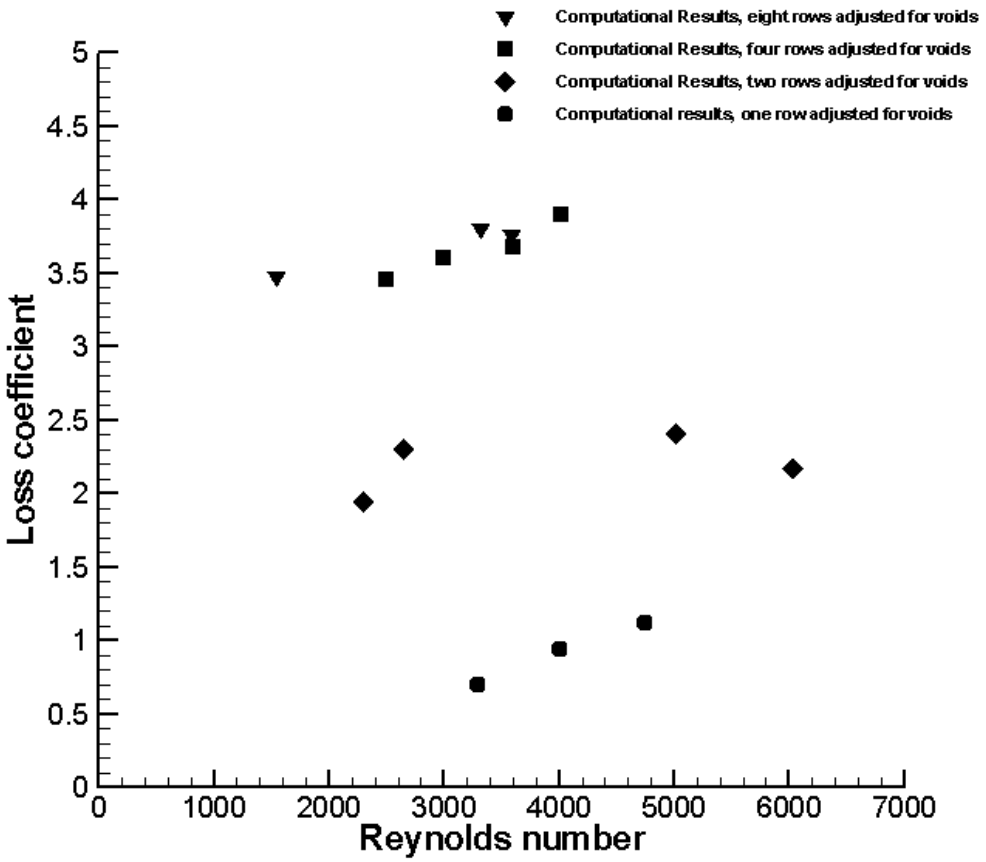

Figure 3.29: Plot comparing results of the various configurations of broached holes when adjusted for voids

3.5 Surface Tension Analysis

Similar to the study done in Chapter 2, the surface tension analysis was carried out for the broached holes. Using equation 4, the Weber number was calculated for each of the flows in the validation and various rows of broached holes cases. The characteristic length in this computation is the hydraulic diameter of the broached hole. The calculation for the hydraulic diameter is given in the previous section of this chapter in equation 6 as being 4.5199504e-3 m. The value of the Weber number for the various cases is summarized in Table 3.16. The majority of the Weber numbers are much larger than unity. This indicates that surface tension does not play a considerable role in the flow dynamics through the broached holes.

Table 3.16: Data summarizing Weber numbers for entire broached holes cases

Type of Broached holes case	Re No.	Velocity(m^2)	Weber Number
One hole validation	3000	0.66	160
	3676	0.81	240
	4200	0.93	313
	4608	1.02	376
	5103	1.13	462
Five holes Validation	3043	0.41	62
	3781	0.60	132
	4384	0.78	218
One row (adjusted for voids)	3295	0.44	71
	4000	0.55	111
	4750	0.72	400
Two rows (adjusted for voids)	2297	0.50	90
	2652	0.58	120
	5016	1.09	429
	6036	1.31	621
Four rows (adjusted for voids)	2500	0.65	151
	3000	0.65	155
	3600	0.77	215
	4020	0.87	276
Eight rows (adjusted for voids)	1549	0.34	41
	3320	0.72	188
	4590	1.02	373

Chapter 4 INVESTIGATION OF AFW SYSTEM IN 1/8th SECTOR OF THE EOTSG

In this chapter, using results derived in the previous chapters, the fluid mechanics analysis of the auxiliary feed water system in the tube bundle of the EOTSG is carried out. This analysis finds the number of tubes wetted with a given AFW flow rate in the EOTSG. The computational results are compared with data derived from the INL study and appropriate conclusions of the AFW system are made. The chapter proceeds in the following manner: an explanation of the methodology of AFW system in which the geometry of the 1/8th sector of the EOTSG, the computational model, input conditions, the implementation of correlations in the model and procedure for data extraction are described. From there it proceeds to results and analysis of the AFW flow rates versus tubes wetted and conclusions drawn based on computational data compared with industrial data.

4.1 Geometry of Computational model

The concept of this model is based on capturing the flow rate from the AFW system in a section of the EOTSG. As shown in Figure 4.1 there are 7 AFW assemblies around the periphery of the top TSP in the EOTSG spaced at 45 degrees from each other. It should be noted that there is no AFW connection at the 12 o'clock position as shown in the figure. This placement of the AFW systems allows the division of the EOTSG into 8 symmetric sectors of which seven are exposed to an AFW system. Since the AFW flow rate versus number of tubes wetted is of interest, assuming that each of the AFW system affects each sector correspondingly, only one of the seven sectors as highlighted in Figure 4.1 was modeled. Previous tests carried out in the INEL reports [2] showed that the maximum water penetration from the AFW system did not exceed more than 20 rows into the tube bundle. This information influenced the generation of the model by limiting it to 24 rows of tubes as shown in Figure 4.2, which is the schematic of the geometry for the computational model of 1/8th sector of EOTSG. The length of the sector in the stream wise direction is 0.481 meters and the outer circumference or the section shroud is 1.172 meters in length. The dimensions

are summarized in Table 4.1. The scoped view gives a more defined representation of the bypass flow whose width is also summarized in Table 4.1. This view also shows that the broached hole areas have been represented by circular areas around the tubes. Since the loss coefficient of the broached holes flow have been derived the actual geometry of the broached holes do not need to be resolved in the model. This helped reduce grid generation and computational cost.

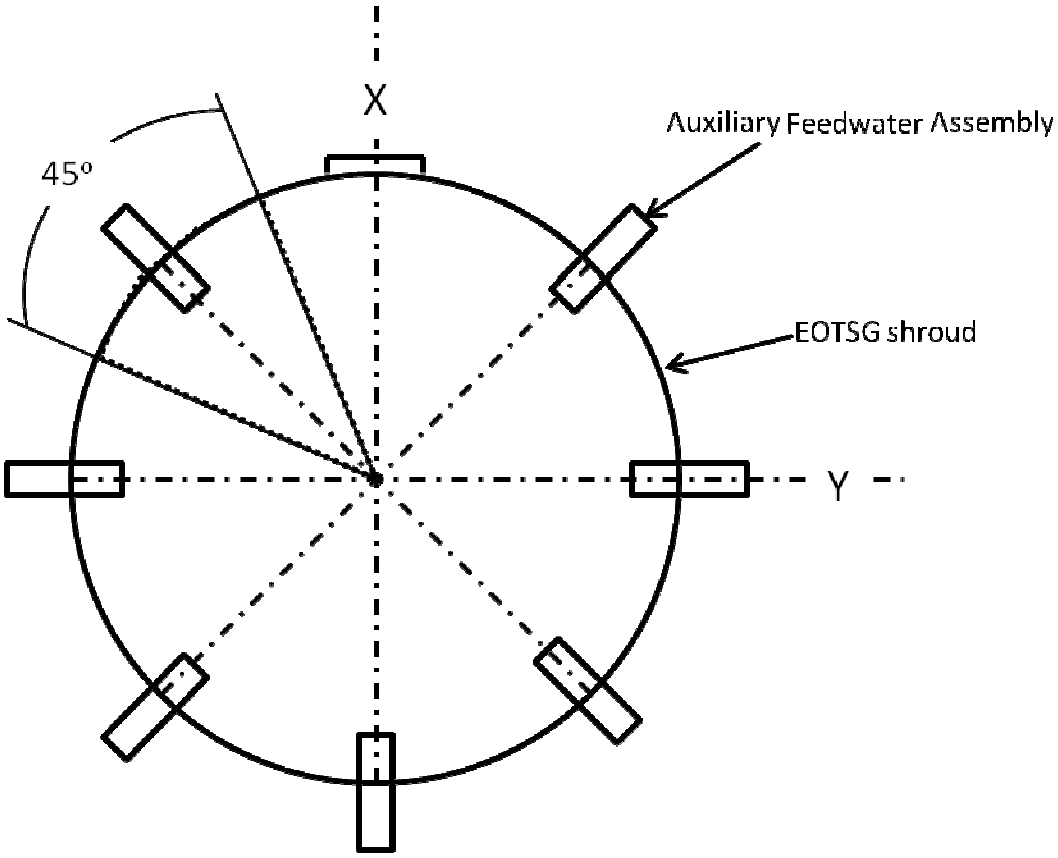

Figure 4.1: Top view of the schematic of the geometry of the EOTSG

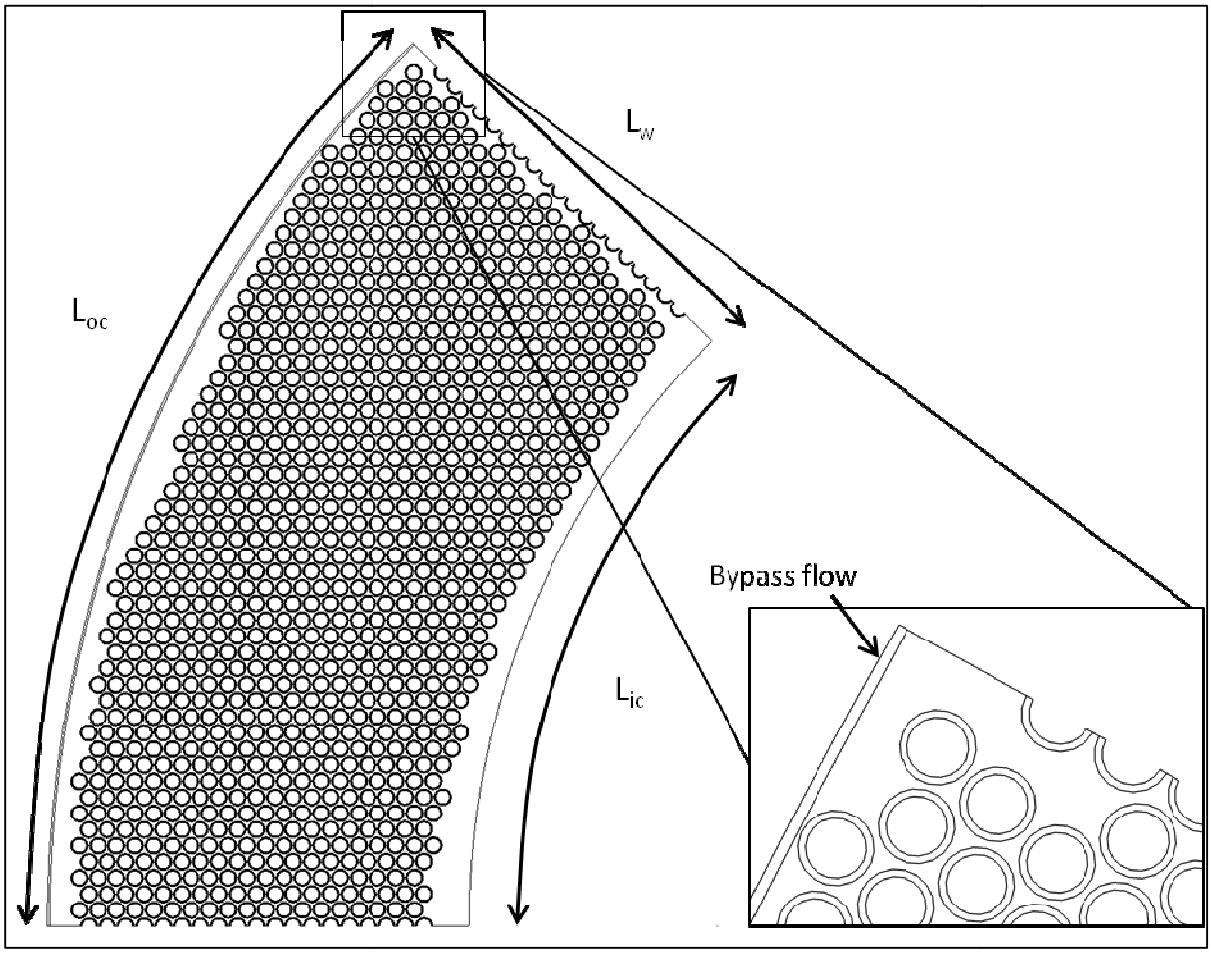

Figure 4.2: Schematic of the geometry for computational model of 1/8th sector of the EOTSG

Table 4.1: Dimensions of geometry for computational model of 1/8th sector of EOTSG

L_{oc}	1.172 m
L_{ic}	0.793 m
L_w	0.481 m
Bypass Flow gap width	0.104 inches

4.2 Computational model of 1/8th sector of the EOTSG

Similar to previous chapters, the model was created using Gridgen. The complete model comprises of just the upper chamber of the top support plate in the EOTSG. Figure 4.3 shows a schematic of the computational model in Gridgen. The mesh of the model is constructed with 2.5 million elements. The computational model is a combination of structured and unstructured mesh. The structured mesh was used in the bypass flow, broached hole flow and boundary condition areas. The unstructured mesh was implemented around the flow areas. The mesh was designed to be finer in the vicinity of the model's walls. There are a total of 1016 broached holes and 2023 fluid zones spanning across the 24 rows. In addition to the broached holes, there are also "drilled" holes on the first two rows of the model. The drilled holes are designed not to let flow through and are modeled as such. The inlet velocity represents the face of the AFW pipe from which water is injected into the EOTSG. It is designed to match the inlet area of the AFW system which is a 4-Inch Sch 40 pipe with an internal diameter of 4.026 inches and total area of 0.0082194 m^2. The height of the computational domain is 0.20 meters which from the previous cases was decided to be sufficient. The top and the right hand face of the model are kept as inlet and outlet vent conditions so as to let either of the phases flow in and out as the model reaches a steady state. Periodic boundary conditions are applied on the faces of the span wise directions of the model. In addition, the TSP plate is shown in Figure 4.3 to give good visual representation of the computational domain. As the calculations on the model proceed, water would flow out of the velocity inlet into the domain and either seep out through the modeled broached holes or through the outlet and inlet vent conditions.

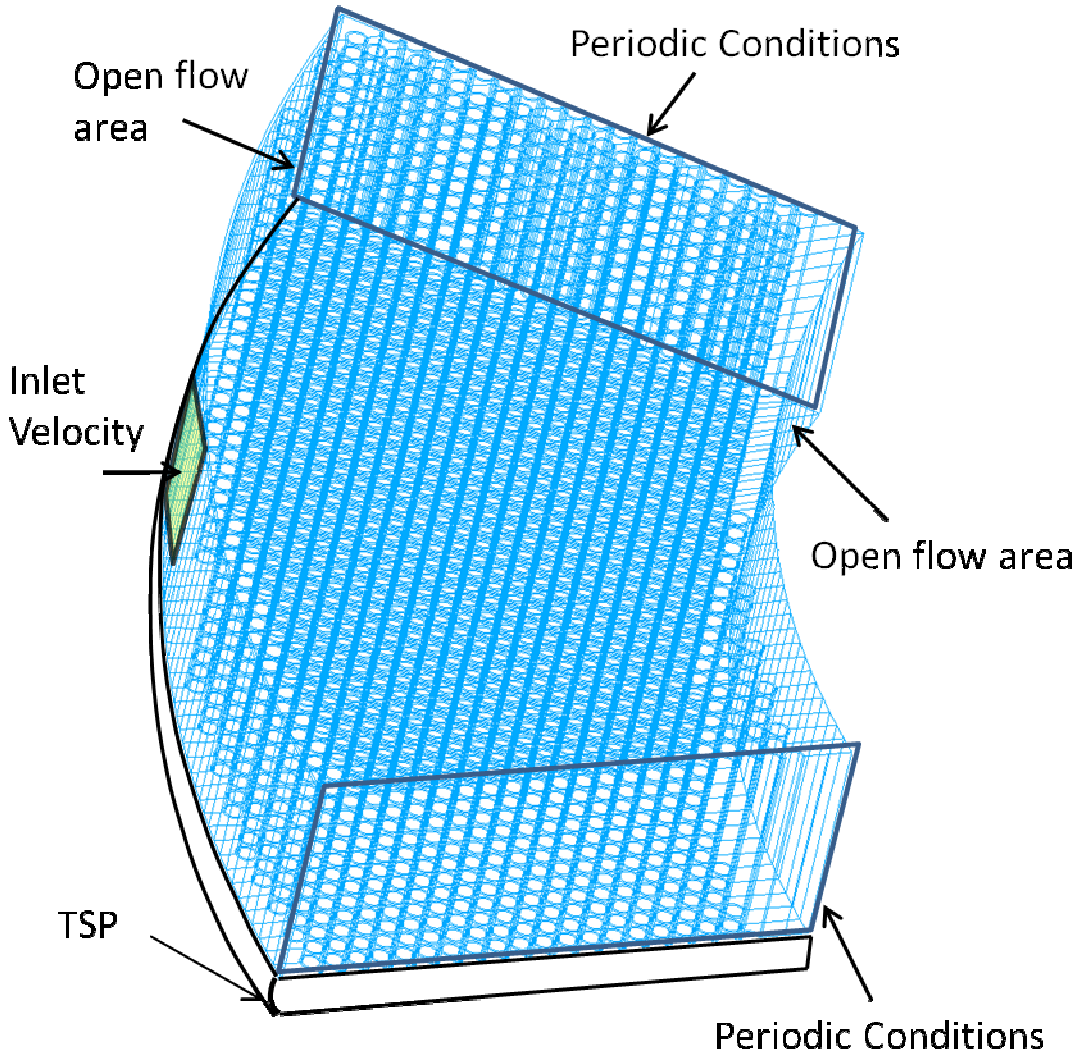

Figure 4.3: Computational model of 1/8th sector of the EOTSG showing boundary conditions

4.3 Input conditions for Computational model

This section of the chapter highlights input data used for the 1/8th sector of the EOTSG computational model. The data in Table 4.2 shows the various number of tubes wetted on the top TSP corresponding to the different AFW flow rates for the steam generator (EOTSG). The data provided is derived from Table 6-2 in [3]. The percentage of the tubes wetted at the top TSP is also present for better quantification purposes. It is important to note that these results are based on calculations conducted by AREVA in [3] using INEL test

results given in Reference [2]. The calculation method is claimed to take the bypass flow into consideration. It is also explained that the number of tubes wetted at the top TSP includes only the wetted tubes in the broached holes location (i.e. the wetting in the drilled hole locations on the top TSP is not considered). The calculation results are noted to be highly dependent on characteristics of the EOTSG design, such as the bypass flow area, the loss coefficient through the broached holes in the top TSP and the number of tubes. The data provided a range of values for the inlet condition of the computational model so the results may be compared. In order to cover this range the following AFW flow rates mainly, 7 l/s, 22.5 l/s, 40 l/s and 65 l/s were employed as the inlet condition for the computational model. As an initial guess the upper chamber of the computational domain was almost filled with water (0.1875 m) before the calculations were started.

Table 4.2: Data from AREVA summarizing tubes wetted versus AFW Flow rate for the EOTSG[3]

AFW Flow rate (gpm)	AFW Flow rate (l/s)	Number of Wetted Tubes at Top TSP	Percentage of Tubes Wetted at Top TSP(%)
186.4	11.7	63	0.40
200	12.6	112	0.72
277	14.3	308	1.97
389	24.5	511	3.28
555	35.0	770	4.94
627	39.5	868	5.57
844	53.2	1141	7.32

4.4 Implementation of correlations data in computational model

The main concept behind the computational model for the 1/8th sector of the EOTSG is to model the leakage flows with boundary conditions instead of resolving them. Resolving each of the leakage flows would increase computational cost to a point where the calculations

would not be feasible. The loss coefficients derived in Chapter 2 and 3 for the bypass flow and broached holes leakage flow had to be implemented in the computational model as explained in section 4.2. The quantification of the leakage flow for the two flow areas come from the losses that occur in these geometries. The loss coefficient values that captured the losses in the broached holes and bypass flow were initially defined to be 4.0 and 1.3, respectively. Cases with other loss coefficients for the leakage flows have also been investigated to check the sensitivity of the computational model.

In order to use these correlations data in FLUENT, a User Defined Function (UDF) is written. The purpose of a UDF is to let the user use features and functions that are not originally included in FLUENT by default. The UDF file used to implement the loss coefficients is taken from ANSYS Online Technical Support and is included in Appendix D. The concept of the UDF is to first calculate the height of the water present in either the bypass flow or broached holes fluid zone. Figure 4.4 shows the zone of the broached flow in which the height is measured by the UDF. The macro in the UDF is designed to look up the required fluid zone and loop over all the cells as it detects the fluid thread pointers for water. It then calculates the volume occupied by water in that zone by multiplying the cell count to the volume of the cells. Eventually by dividing this amount with the cross sectional area of the zone, the height of water is obtained. This height is then inserted in the loss coefficient equation to evaluate the leakage velocity required to be implemented in the domain of the broached hole as show in the scoped image in Figure 4.4. The implementation is done through a DEFINE_PROFILE function that is applied as a boundary condition to the broached hole. This procedure is applied to each of the 1016 broached holes that have respective zone numbers and boundary names. A similar concept is applied to the bypass flow as shown in Figure 4.5. The height of water is measured throughout the computational domain above the bypass flow area using the UDF and the corresponding velocity is executed as a boundary condition at the bypass flow area. However this UDF is not applied to the drilled holes (first two rows) to restrict water from flowing through them.

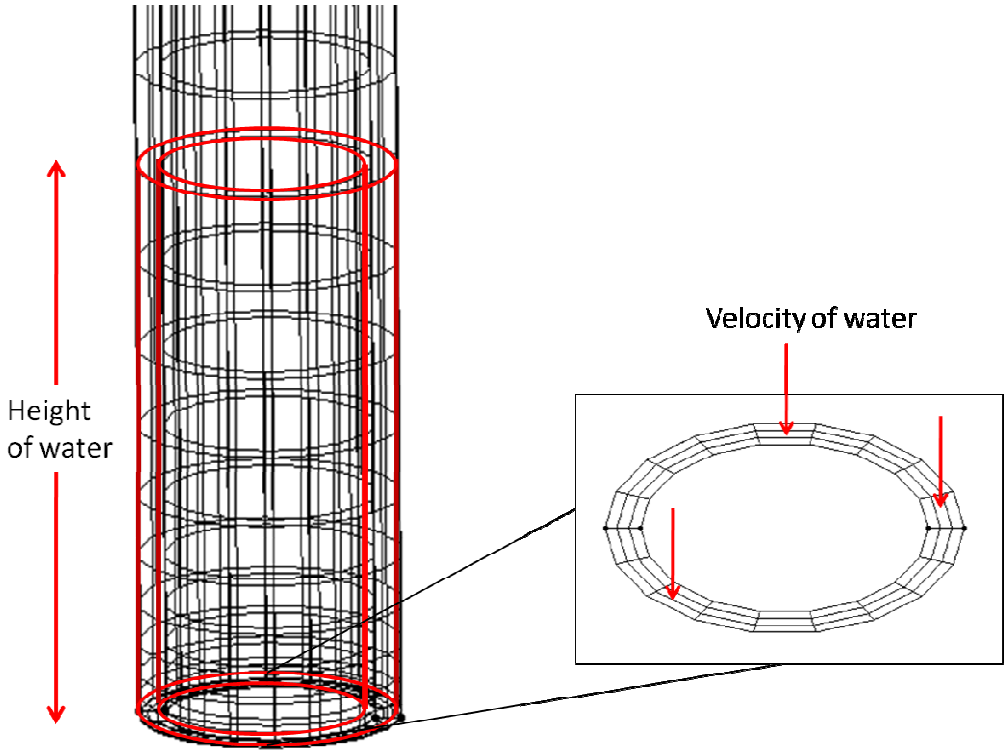

Figure 4.4: Computational Model showing UDF concept for broached hole

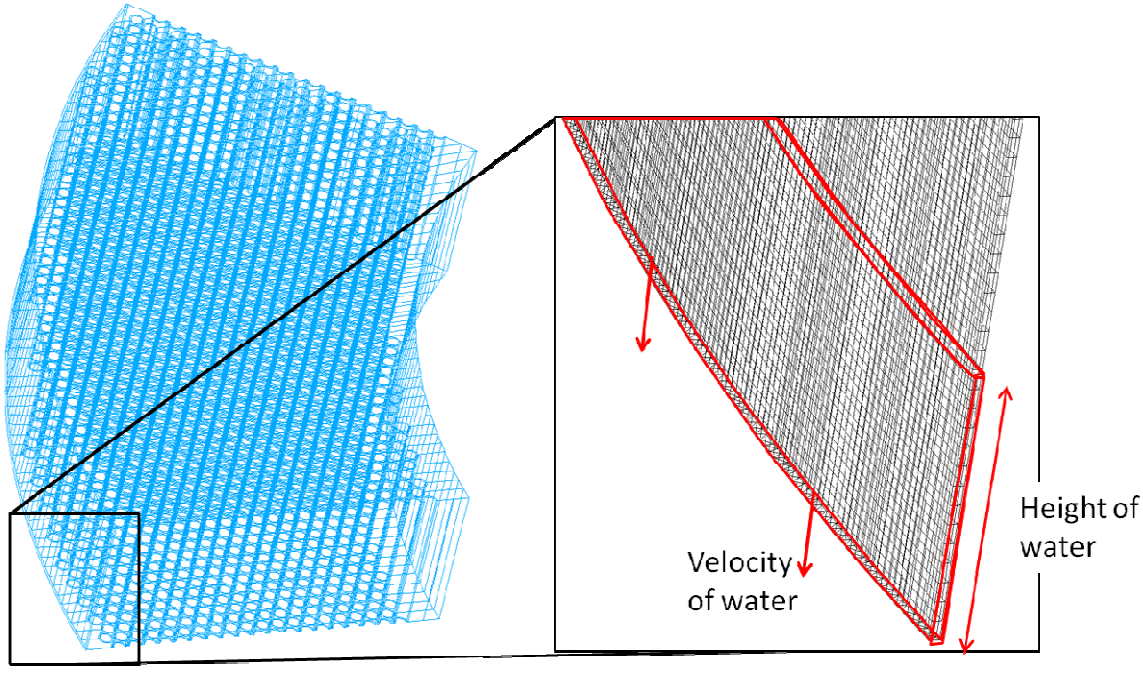

Figure 4.5: Computational Model showing UDF concept for bypass flow

4.5 Procedure for Data Extraction

The UDF functions along with the necessary input and boundary conditions, were used for each calculation. For the initial starting cases consisting of 22.5 l/s and 65 l/s inlet velocities, the upper chamber of the 1/8th sector of EOTSG was filled to a height of 0.1875m with water. It was decided that the other two cases 7 l/s and 40 l/s could be started from the previous case restart files by altering the inlet velocity so as to save computational cost. For further investigation it was also decided to vary the loss coefficient of the broached holes from 4.0 to 6.0, 2.0 and 0.5. These initial conditions would give a range of results that could be compared with data from AREVA.

Before initiating the calculation, the velocity through the leakage flows and the height of the liquid in the computational domain had to be monitored. In order to do this, surface monitors were set up that output height data of water in the fluid zones at locations highlighted in Figure 4.6. The heights were measured to indentify when the system would reach equilibrium. The velocity data at the leakage flow boundary conditions that corresponded to the fluid zones were also monitored (locations are shown in Figure 4.6). This process helped validate the functionality of the UDF. All the cases were run as unsteady calculations to a steady state in which the residuals converged to values of 1E-05.

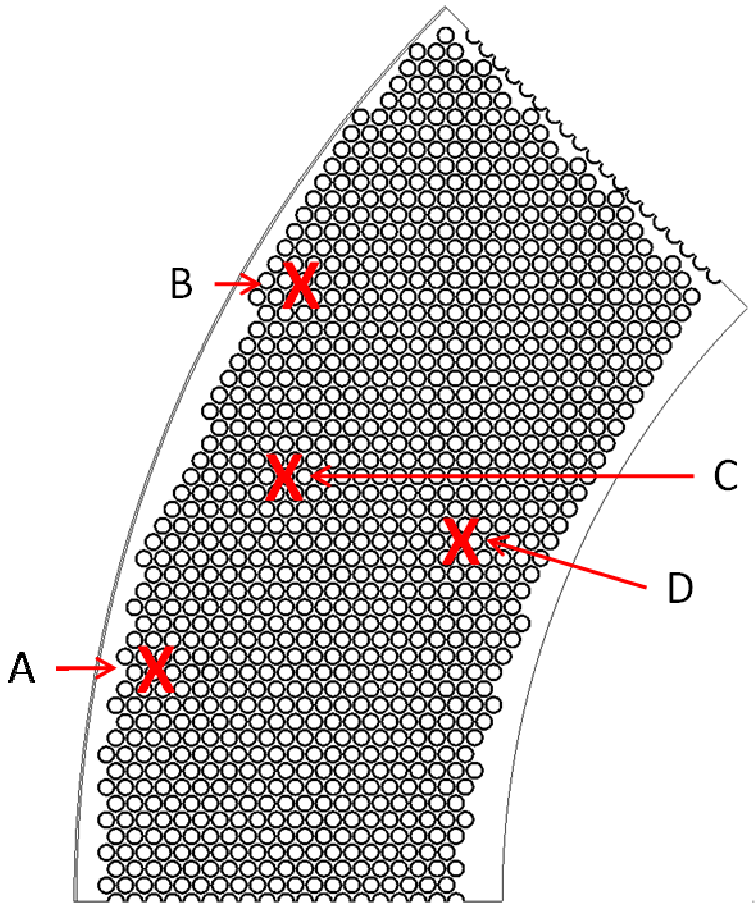

Figure 4.6: Top view of Computational model highlighting locations of surface monitors for measurements of velocity and height

4.6 Results and Analysis

The literature analysis from reports of the INEL tests done in the 80's gave reason to start off with the cases consisting of 22 l/s and 65 l/s as the inlet conditions. Due to the implementation of UDFs, each case had to be run using one processor. The simulations for the first two cases took four weeks (672 hours) to complete with 4GB of memory each. The surface monitors at the four locations as shown in Figure 4.6 were constantly monitored until the heights reached a steady state. The system with the inlet condition of 65 l/s took 0.95 seconds of flow time to reach a steady state. Figure 4.7 and 4.8 show the height of the water at locations A and B as shown in Figure 4.6. It is evident that because this flow is very high

the height of the water retained at these locations close to the outer periphery of the EOTSG dropped by only 2 cm each. The slope of the curves are smooth and the gradual decrease to a steady state can be seen clearly. The result from the surface monitor at location C, close to the middle of the computational model is highlighted in Figure 4.9. The height drop here is 5.5cm as the location is further away from the periphery of the EOTSG and there is more flow out of the broached holes. As in the previous two figures, the height curve is smooth and it reaches a steady state close to the one second mark. The last surface monitor is at location D and this is shown in Figure 4.10. The height in this case drops smoothly with no fluctuations and goes to zero. This figure shows that the fluid around location D was completely drained and the tubes are not wetted at the given flow rate. The leakage flow rate at these locations was also monitored to ensure the correct functionality of the UDF. Figure 4.11 shows the velocity flow at the outlet of the broached hole at location A. It is seen that the shape follows the same pattern as the height curve in Figure 4.7 and the velocity values correspond to that given by equation 11 validating the correct implementation of the UDF.

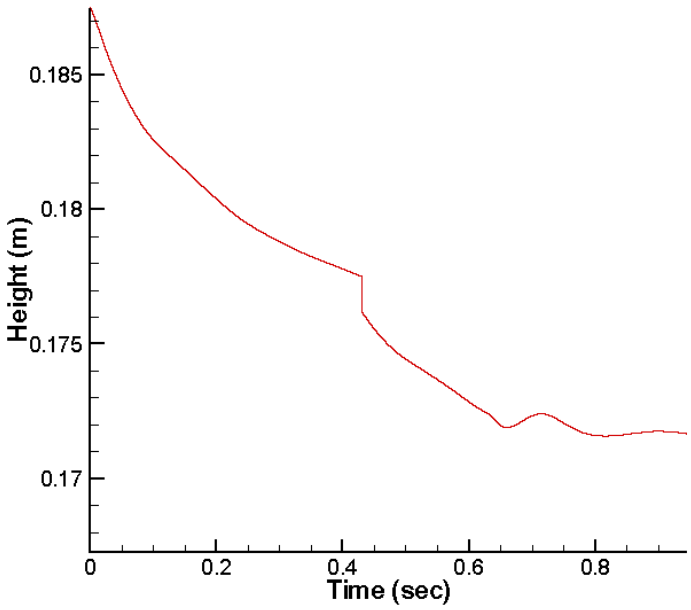

Figure 4.7: Plot of height of fluid in the EOTSG computational model (location A)

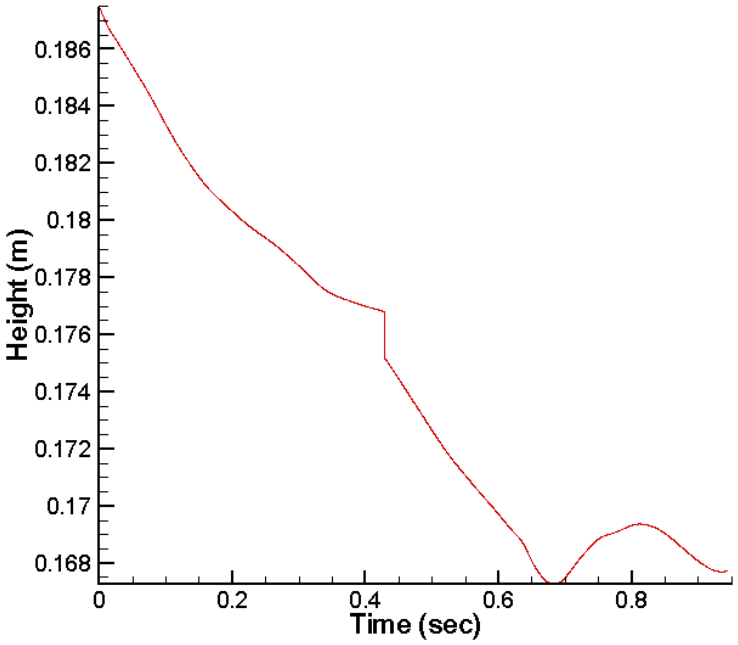

Figure 4.8: Plot of height of fluid in the EOTSG computational model (location B)

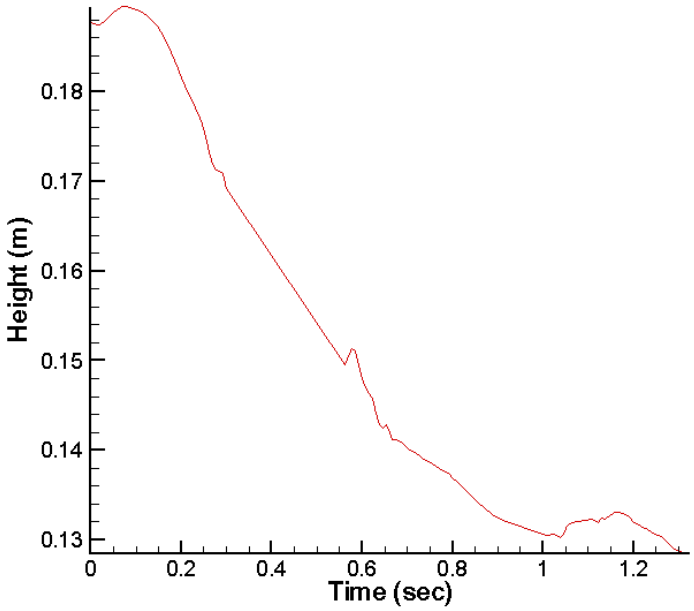

Figure 4.9: Plot of height of fluid in the EOTSG computational model (location C, this surface monitor was ran till 1.2 seconds to reach convergence)

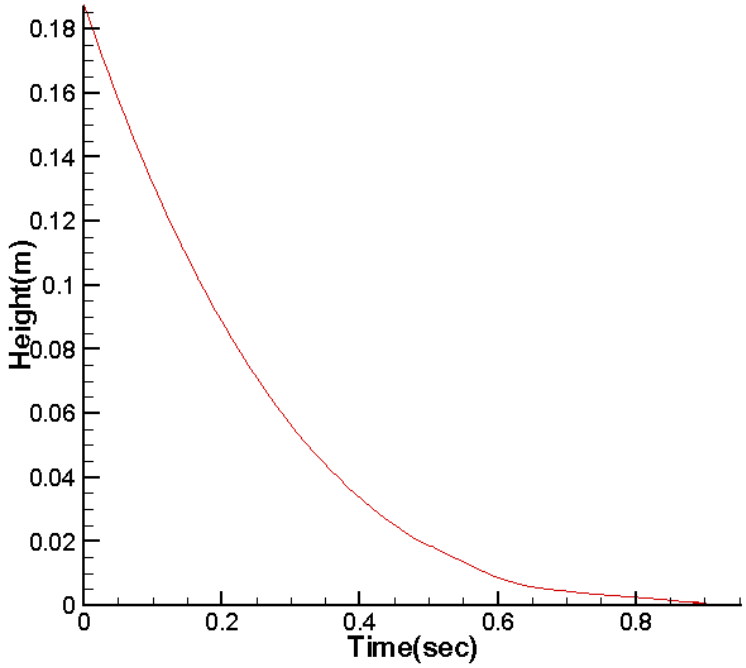

Figure 4.10: Plot of height of fluid in the EOTSG computational model (location D)

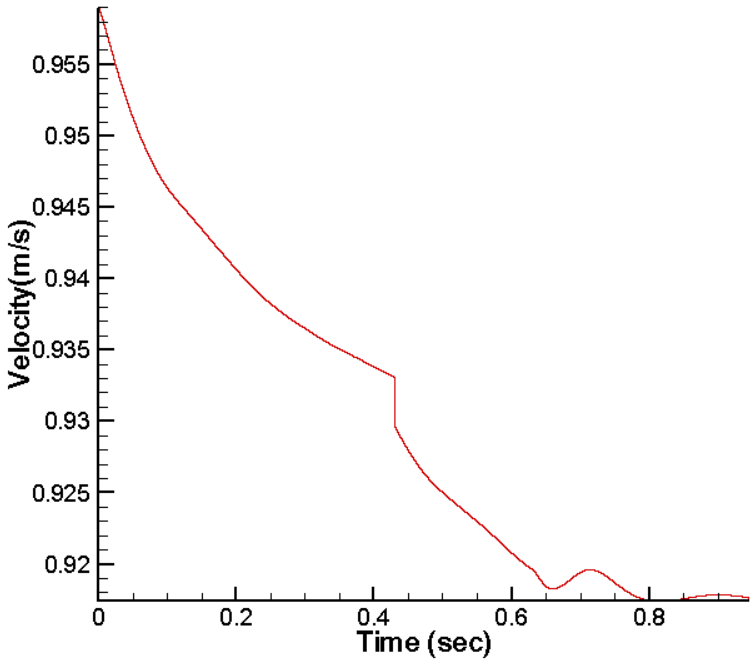

Figure 4.11: Plot of velocity of fluid in the EOTSG computational model (location A)

$$V_{broached} = \sqrt{\frac{2gh_0}{k_{broached}}} \tag{11}$$

where h_0 is the height of the water surrounding each broached hole,
$V_{broached}$ is the velocity of the water to be implemented at each broached hole,
and $k_{broached}$ is the loss coefficient value of the broached hole

As the computational model went though the flow transient, the cross sectional VOF plot of the model was also monitored to evaluate the flow analysis. This was done to ensure that the flow was physical and that the inlet and outlet vents did not pose problems. Figure 4.12 shows the top view cross sectional VOF plot located 1cm above the TSP plate during the transient state (0.6 seconds of flow time). Figure 4.13 shows the same plot at steady state (0.95 seconds of flow time). The red and blue colors represent water and air, respectively. The symmetric azimuthal distribution of the AFW is evident in Figure 4.13. There is more penetration of water in the middle of the EOTSG because of the central location of the AFW inlet in the system. By visual inspection it was found that 316 tubes were wetted at this flow rate.

Similar to this procedure, an investigation was done for the other three cases. Figure 4.14, 4.15 and 4.16 show the contours of VOF for the AFW rate of 22.5 l/s, 7 l/s and 40 l/s respectively. The results of number of tubes wetted and the percentage of tubes wetted are summarized in Table 4.3. From the data in the table and figures it is apparent that when the AFW flow rate increases so does the wetting penetration of tubes in the EOTSG sector. Table 4.3 highlights both the percentage of tubes wetted in the whole (broached and drilled holes) region as well as in the broached hole region. This is done for comparison purposes with previous industrial data. A plot of the data from Table 4.3 is shown Figure 4.17. The slope of the computational results clearly show the trend that as the flow rate increases so does the number of wetted tubes. Without taking the drilled holes into consideration, the computational results agree with AREVA's data at flow rates of 14.5 l/s and more. AREVA's data is more conservative as the computational data predicts more wetting of tubes in the

range of 0.5 % to 0.6% (5 to 6 tubes) at flow rates lower than 20 l/s. The percentage difference becomes larger with flow rates below 14.5 l/s because the number of rows of wetted tubes at the broached hole locations becomes less than 4. Previous studies in the earlier chapters show that the applying a loss coefficient of 4.0 with these number of rows wetted would not yield accurate results. Therefore a lower loss coefficient should be applied to capture the wetting of tubes at AFW flow rates that are lower than 14.5 l/s.

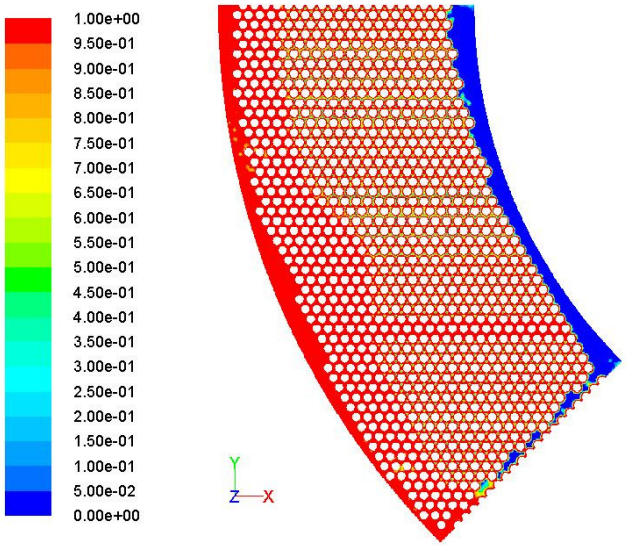

Figure 4.12: Contour of volume fraction plot of 1/8th sector of EOTSG at 0.6 sec (AFW= 65l/s)

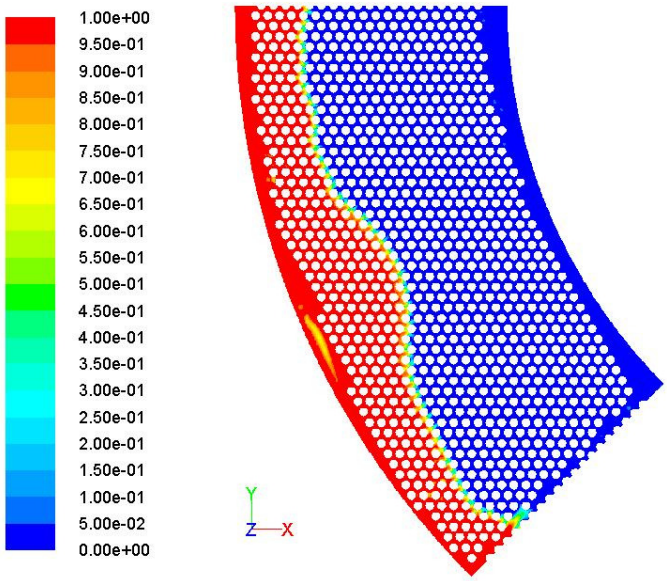

Figure 4.13: Contour of volume fraction plot of 1/8th sector of EOTSG at 0.95 sec (AFW= 65 l/s)

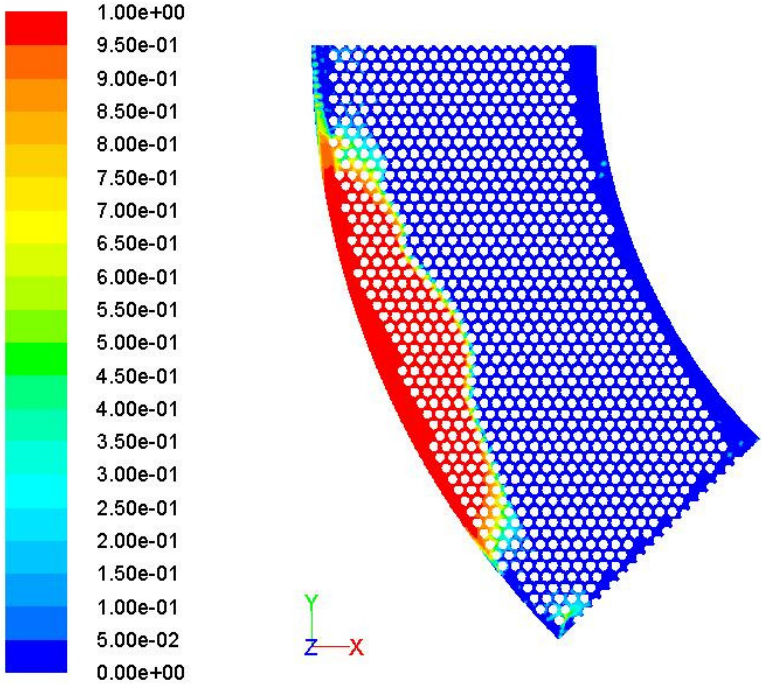

Figure 4.14: Contour of volume fraction plot of 1/8th sector of EOTSG (AFW= 22 l/s)

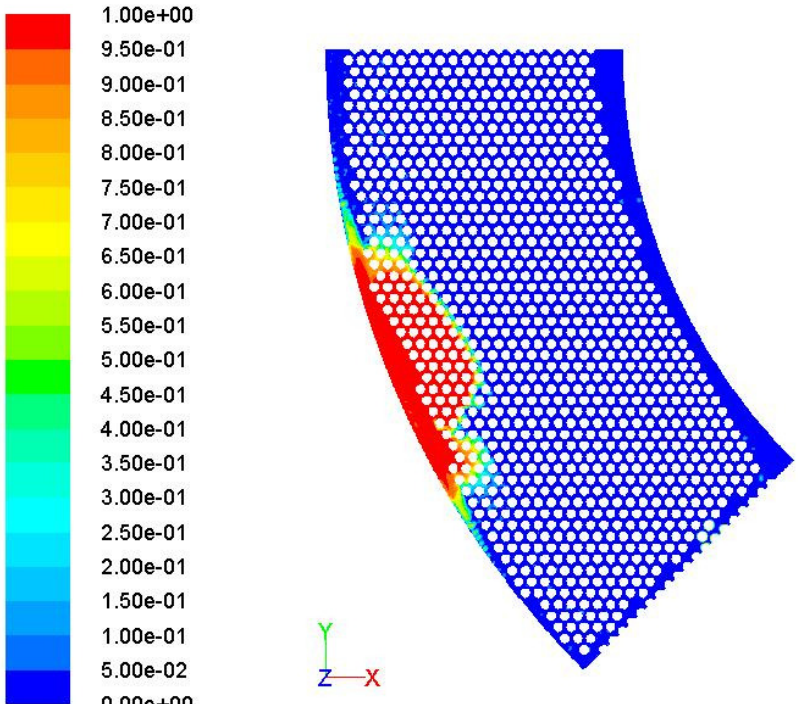

Figure 4.15: Contour of volume fraction plot of 1/8th sector of EOTSG (AFW= 7 l/s)

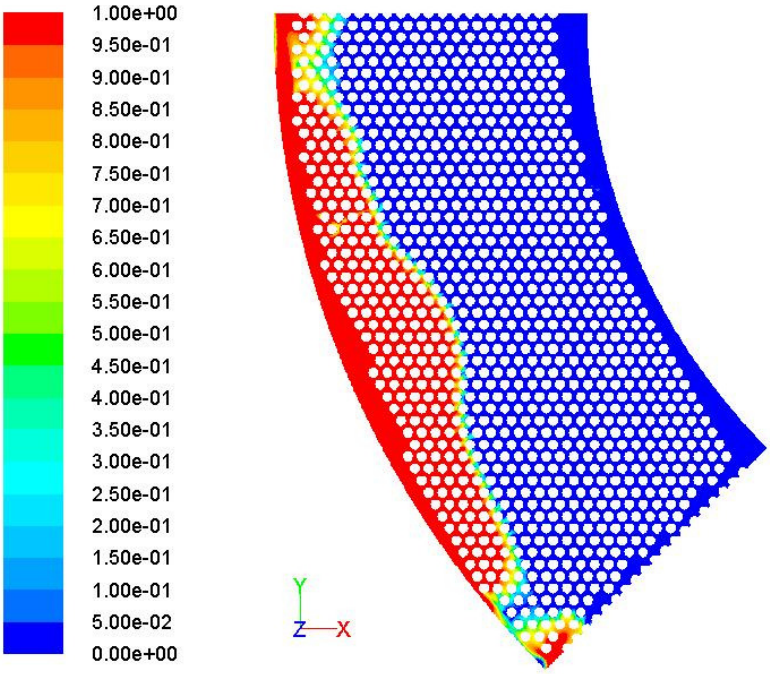

Figure 4.16: Contour of volume fraction plot of 1/8th sector of EOTSG (AFW= 40 l/s)

Table 4.3: Data of AFW and percentage of tubes wetted from computational model of 1/8th sector of the EOTSG

AFW Flow rate(l/s)	Total No. of wetted tubes	No. of Broached holes wetted	% of Total No. of wetted tubes	% of Total No. of Broached holes wetted
7	87	20	4.48%	1.03%
22.5	162	72	8.35%	3.71%
40	248	119	12.78%	6.13%
65	318	175	16.38%	9.02%

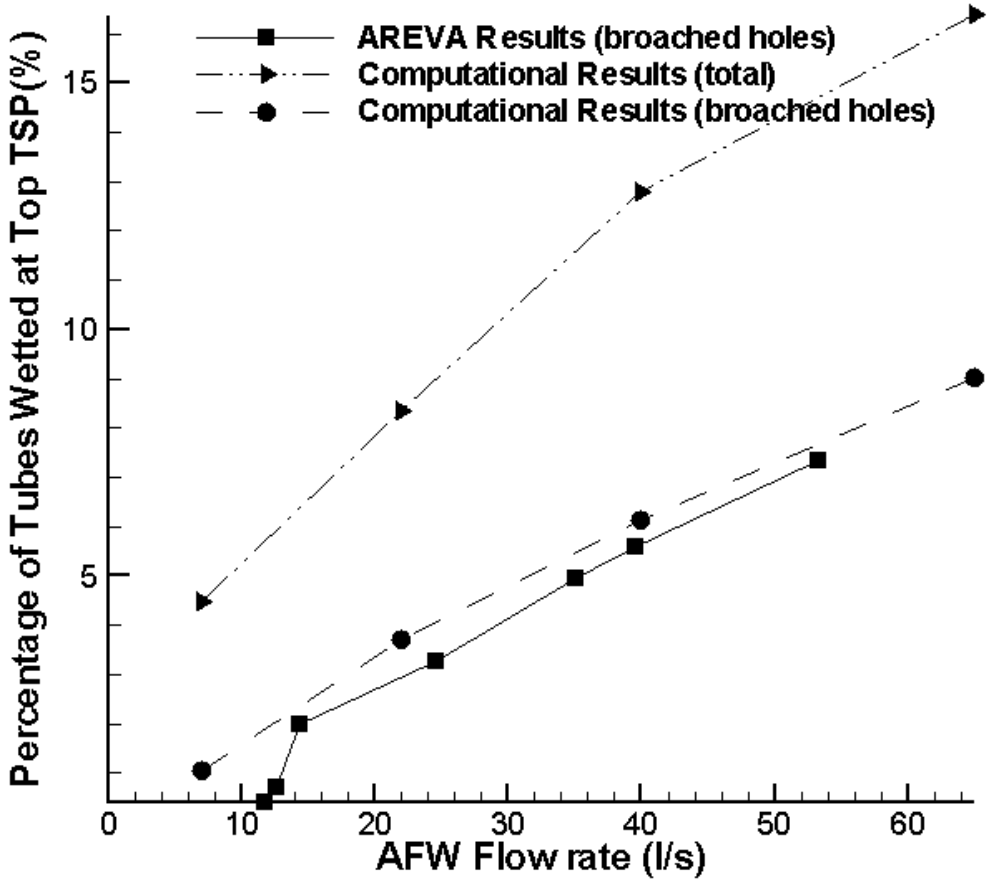

Figure 4.17: Plot comparing results of the % of tubes wetted versus AFW flow rate

Further analysis was carried out to investigate the flexibility of the model with the change in the loss coefficients of the broached holes. Table 4.4 summarizes the data obtained

with the different loss coefficients for an AFW flow rate of 22 l/s. With a higher loss coefficient there is more resistance to leakage flow which encourages the buildup of fluid and thus more tubes are wetted. And with lower loss coefficients there is less resistance to flow and leakage causing less number of tubes to be wetted. The VOF plots are shown in Figures 4.18, 4.19, 4.20 and 4.21. The plots show that when the loss coefficients of 0.5 and 2.0 are implemented, the numbers of tubes wetted are about the same. This was also the case for the other two loss coefficients 4.0 and 6.0. Figure 4.20 shows that when a 6.0 loss coefficient is implemented, the penetration distance in the axis of flow is more than when a loss coefficient of 4.0 is applied. But despite the distance the total number of tubes wetted was approximately equal. It also shows that the loss coefficient value 4.0 was a good estimation to quantify the broached hole leakage flow. The percentage of the number of broached holes wet versus AFW flow rate is plotted along with the computational and AREVA data in Figure 4.22. Inspection of the points show the trend that with higher loss coefficients there are more broached hole tubes wetted. The plot also shows that the loss coefficient of 4.0 gave the best agreement with AREVA's data. This concludes the analysis by stating that according to the computational model there would be about 0.5% to 0.6% more tubes wet in the $1/8^{th}$ sector of the EOTSG as compared to data from AREVA for flow rates above 14.5 l/s. For flow rates below this a lower loss coefficient has to be applied at the broached holes to obtain better results. It also shows that complete wetting of the top TSP of the EOTSG is not possible at the maximum flow rates of the AFW.

Table 4.4: Data of AFW and percentage of tubes wetted from computational model of $1/8^{th}$ sector of the EOTSG with varying loss coefficients (AFW flow rate = 22/s)

Loss coefficient value	Total No. of wetted tubes	No. of Broached holes wetted	% of Total No. of wetted tubes	% of Total No. of Broached holes wetted
0.5	98	41	5.049	2.112
2	115	46	5.925	2.370
4	162	72	8.346	3.709
6	169	81	8.707	4.173

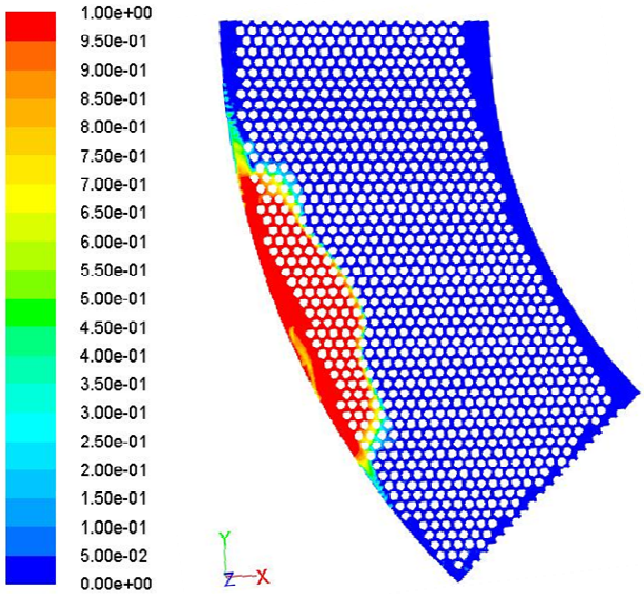

Figure 4.18: Contour of volume fraction plot of 1/8th sector of EOTSG (AFW= 22.5 l/s, $k_{broached}$ = 0.5)

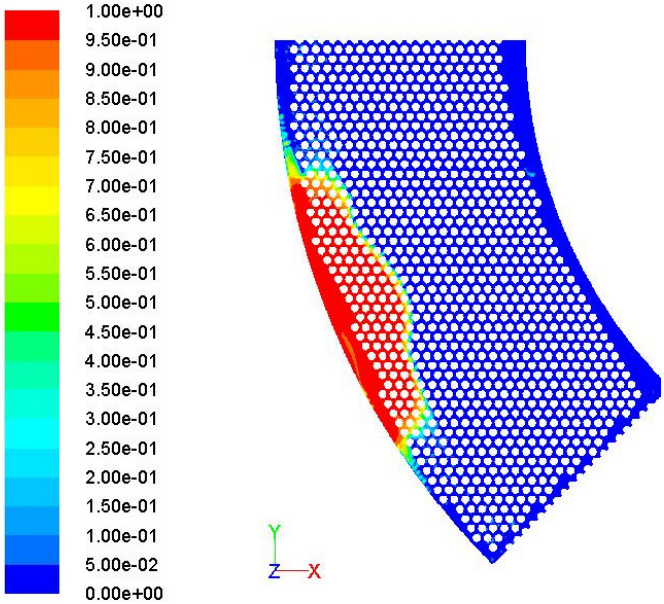

Figure 4.19: Contour of volume fraction plot of 1/8th sector of EOTSG (AFW= 22.5 l/s, $k_{broached}$ = 2.0)

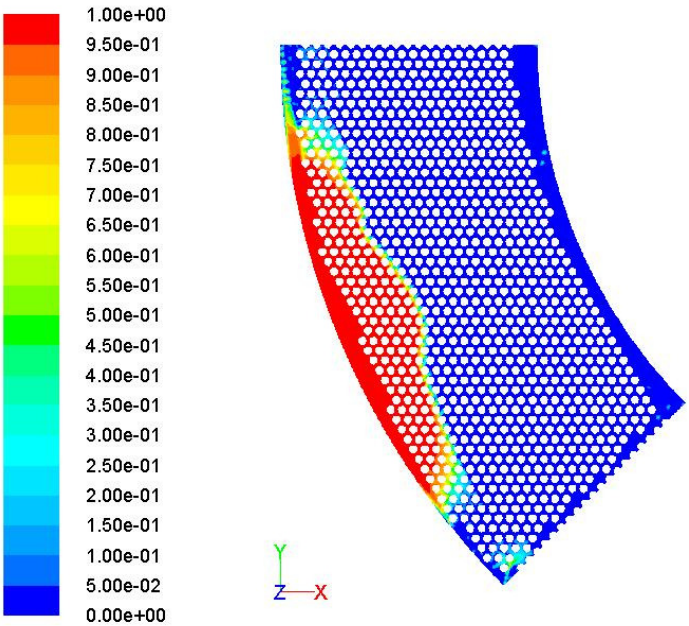

Figure 4.20: Contour of volume fraction plot of 1/8th sector of EOTSG (AFW= 22.5 l/s, $k_{broached}$ = 4.0)

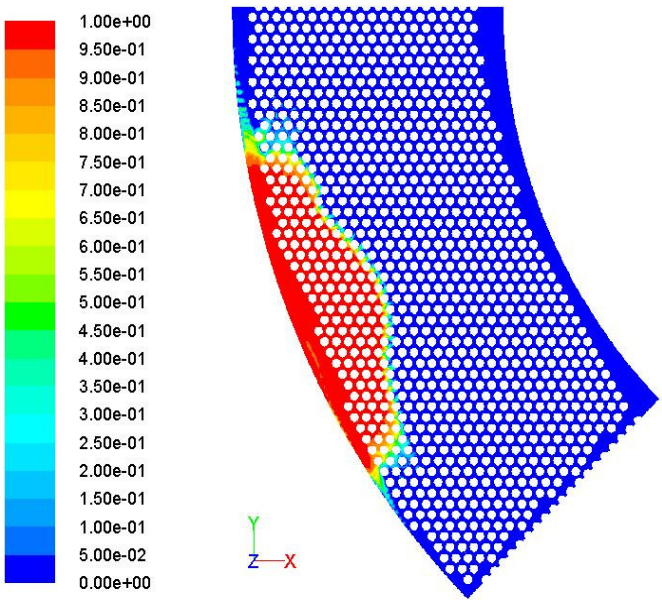

Figure 4.21: Contour of volume fraction plot of 1/8th sector of EOTSG (AFW= 22.5 l/s, $k_{broached}$ = 6.0)

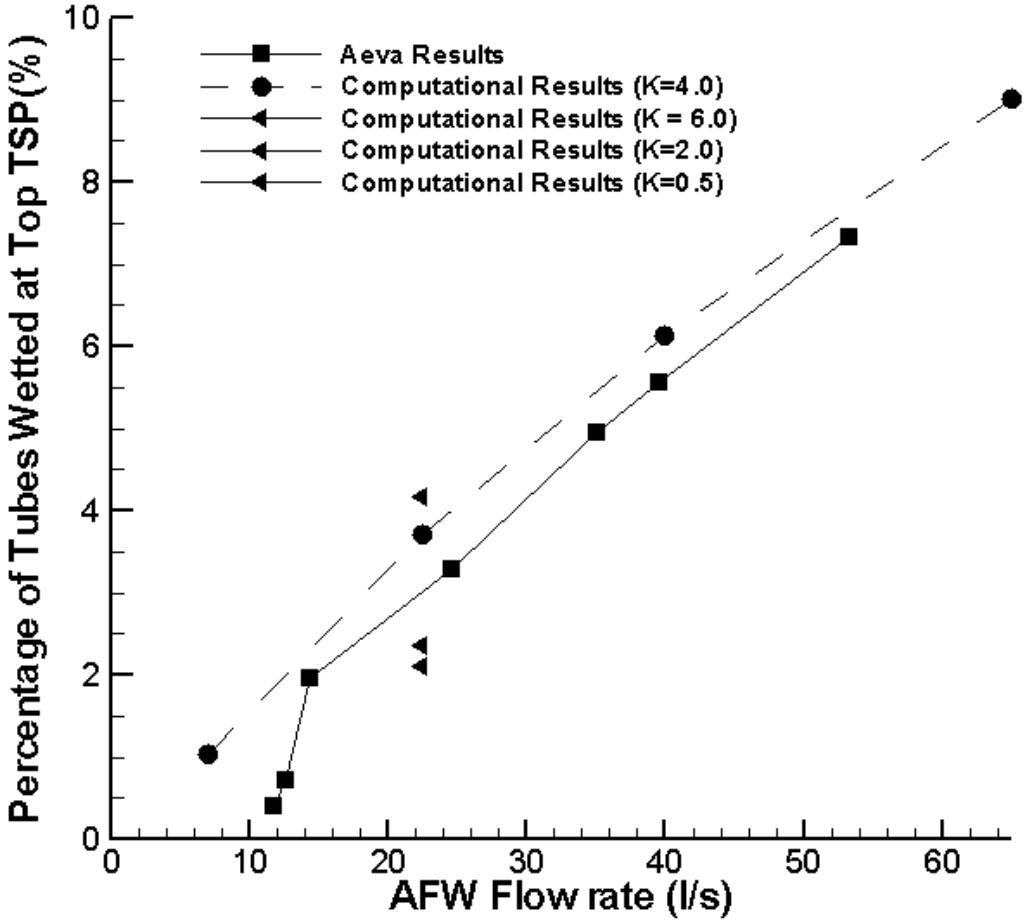

Figure 4.22: Plot comparing data of computational results for various loss coefficients with AREVA results

Chapter 5 SUMMARY AND CONCLUSION

The auxiliary feed water fluid distribution in a 1/8th sector of the EOTSG was investigated using the commercial code, ANSYS FLUENT. In order to perform the fluid analysis, the losses in the bypass leakage flow and broached hole leakage flow were first quantified. Instead of resolving the bypass and leakage flow in the sector of the EOTSG which would be computationally expensive, each of the leakage flows under the respective conditions and geometry were modeled. The loss coefficients of the leakage flows were then implemented using User Defined Functions on the 1/8th sector of the EOTSG computational model. Using this concept, the number of tubes wetted in the sector of the EOTSG for various AFW flow rates was found. Results showed that the computational model predicted 0.5% to 0.6 % more tubes wetted than AREVA's data. With the maximum flow rate of 65 l/s the number of tubes wetted was 318 and the percentage of wetted tubes with broached holes was 8.7 %.

The investigation started with the analysis of the bypass leakage flow between the tube support plate (TSP) and the outer shroud of the EOTSG. Representative computational models were built to obtain the loss coefficients. It was determined that the loss coefficient was a function of the mass flow rate or the flow Reynolds number through the gap and it increased as the Reynolds number increased from 1600 to 3000 for different water heights on the TSP. The experimental and computational loss coefficients agree to within 15% of each other. In contrast, the constant loss coefficient of 1.3 used by AREVA is much higher than that obtained in this study, particularly in the low Reynolds number range. As the Reynolds number approached 3000, the loss coefficients from this study approached the value of 1.3. This value of the loss coefficient was implemented for the bypass flow leakage in the 1/8th sector of EOTSG model.

The research then moved on to the analysis of the broached holes flow through the top TSP plate. Broached hole calculations were performed using a single hole, five holes, and one, two, four and eight rows of broached holes in order to characterize the loss coefficients.

The one hole and five holes computational models were validated with experiments. The computational models showed the presence of voids in the leakage flow through the TSP, which were not observed (visually) in the experiments. With voids, the loss coefficients ranged from 2.0 to 3.0; however, when corrected for the voids, the loss coefficient agreed extremely well with experimental values validating the computational models. The characterization of the broached hole leakage in the one, two and four rows showed that the loss coefficient of the control broached hole increased as the number of rows increased. These results indicate that for the same height of water on the TSP, the resistance to leakage flow increased as the number of tubes increased. These results also indicated that leakage flow through the broached holes was not solely a function of the height of water above the TSP but also the surrounding geometrical topology and the flow characteristics. However when the analysis was done for eight rows it was found that the loss coefficient differed by only 5% of the results from the four rows. This case showed that the loss coefficient after a certain number of rows became constant. From the results it was determined that the loss coefficient asymptotes to an estimated value of 4.0 which was implemented as the leakage flow loss coefficient in the $1/8^{th}$ sector of the EOTSG.

Computational models of $1/8^{th}$ sector of the EOTSG were ran with the respective loss coefficients for the leakage flows. Results showed that as the AFW flow rate increased, the percentage of the number of tubes wetted increased. The data matched with AREVA's analysis for flow rates of 14.5 l/s and higher within 0.5% to 0.6%. It was also deduced that complete wetting of the tubes is not possible at the maximum AFW flow rate of 65 l/s. Further investigation was done on the sensitivity of the model by adjusting the loss coefficient of the broached holes. It was found that as the loss coefficient reduced so did the number of tubes wetted. The results obtained with a loss coefficient of 4.0 showed the closest match to AREVA results.

References:

1. **AREVA NP Inc. Document 02-131136E-08. "Detail of Upper Tube Support Plate (Steam Generator)**

2. **INEL Document "Once Through Steam Generator AFW Flow Distribution and Heat Transfer, "G. E. Mc Creary, T. K. Larson, K. G. Condie, presented at the 1988 ASME winter annual meeting**

3. **AREVA Document 32-9078218-00. "AFW Wetting Model for the EOTSG." AREVA Rev. 012, 4th April 2008**

4. **AREVA NP Inc. Document 32-9023301-001. " TM1-1 EOTSG Secondary Hydraulics"**

5. **INEL Document "Flooding, AFW penetration, and Visual Investigation in Scaled Once Through Steam Generator Facilities, "K. G. Condie, T. K. Larson, and G. E. Mc Creary, prepared for 25th ASME/AICHE National Heat Transfer Conference in Houston, Texas, July 24 – 27, 1988**

6. **"ANSYS FLUENT 12.0 User's Guide (2009)**

Appendix A

UDF Code from ANSYS Online Technical Support

DEFINE_ADJUST function manipulates the variables needed for the calculation of the height of the fluid in each of the broached hole and bypass leakage flow. This UDF has to be directly "hooked" using the "User Defined Function Hooks" option in FLUENT. DEFINE_PROFILE is used to define a custom boundary profile that varies as a function of spatial coordinates based on the height variable from the previous UDF function. The boundary profile needs to be added to the boundary conditions with the appropriate direction and magnitude. The code given below is generic for a broached hole and the bypass flow

```
# include "udf.h"
# include "sg_mphase.h"
# include "mem.h"

real height;.
.
.
.
 real heightby;
 real k =4.0;

DEFINE_ADJUST(Trial,d)
{

Thread **pt;
 Thread *to;
 real vol_fluid;
 .
.
.
real vol_fluidby;
```

Initialize height variables that calculate height of the fluid in the broached hole zone

Initialize vol_fluid variable which calculates volume of fluid occupied in cells in each broached hole zone

```
cell_t c;

 to=Lookup_Thread(d,2);/* bv 1*/

  mp_thread_loop_c(to,d,pt)
  {
   if (FLUID_THREAD_P(*pt))
     {
          Thread *tp = pt[1];
          begin_c_loop(c,tp)
            {
              vol_fluid+=C_VOF(c,tp)*C_VOLUME(c,tp);
                      }
          end_c_loop(c,tp)
            }
   height = vol_fluid/0.045480527;
   printf("height of fluid: %5.5g\n");
  }


to=Lookup_Thread(d,1309);/* BYPASS */
  mp_thread_loop_c(to,d,pt)
  {

   if (FLUID_THREAD_P(*pt))
     {
          Thread *tp = pt[1];
          begin_c_loop(c,tp)
            {
              vol_fluidby+=C_VOF(c,tp)*C_VOLUME(c,tp);
            }
          end_c_loop(c,tp)
            }
   heightby = vol_fluidby/0.03704115;
    }
}
```

Broached hole leakage flow UDF

This UDF code looks up the thread of the zone. It then loops through the pointers that correspond to fluid (pt[1]) in that zone. With the pointers it loops through the number of cells and calculates the cell volume occupied by fluid. By dividing the volume by the cross sectional area the height is obtained

Bypass leakage flow UDF

This UDF code looks up the thread of the bypass zone. It then loops through the pointers that correspond to fluid (pt[1]) in that zone. With the pointers it loops through the number of cells and calculates the cell volume occupied by fluid. By dividing the volume by the cross sectional area the height is obtained

```
DEFINE_PROFILE(proflievelocity, thread, position) /* inlet x velocity = name of the x
velocity */
{
real z[ND_ND]; /* this will hold the position vector */

face_t f; /* f = all the cell faces on the boundary*/
begin_f_loop(f,thread)
{
F_CENTROID(z, f, thread);

F_PROFILE(f, thread, position) =sqrt((2.0*9.81*height)/k);
}
end_f_loop(f, thread)
}
```

DEFINE_PROFILE (Broached hole)

The UDF DEFINE_PROFILE places the profile of the velocity needed at the broached hole leakage flow boundary. It does this by looping through the threads of the boundary zone and applying the loss coefficient equation as a profile to calculate the velocity. Please note that the UDF has to be manually hooked to the appropriate boundary zone in FLUENT under the boundary conditions options.

```
DEFINE_PROFILE(proflievelocitybypass, thread, position) /* inlet x velocity = name of the
x velocity */

{
real z[ND_ND]; /* this will hold the position vector */

face_t f; /* f = all the cell faces on the boundary*/
begin_f_loop(f,thread)
{
F_CENTROID(z, f, thread);
 F_PROFILE(f, thread, position) =sqrt((2.0*9.81*heightby)/1.3);
}
end_f_loop(f, thread)
}
```

DEFINE_PROFILE (Bypass)

The UDF DEFINE_PROFILE places the profile of the velocity needed at the bypass hole leakage flow boundary. It does this by looping through the threads of the boundary zone and applying the loss coefficient equation as a profile to calculate the velocity. Please note that the UDF has to be manually hooked to the appropriate boundary zone in FLUENT under the boundary conditions options.